THE UNIVERSITY OF OKLAHOMA

GRADUATE COLLEGE

DURABILITY OF CEMENTITIOUSLY STABILIZED AGGREGATE BASES FOR PAVEMENT APPLICATION

A Dissertation

SUBMITTED TO THE GRADUATE FACULTY

in partial fulfillment of the requirements for the

degree of

Doctor of Philosophy

By

NAJI NAJIB KHOURY
Norman, Oklahoma
2005

DURABILITY OF CEMENTITIOUSLY STABILIZED AGGREGATE BASES
FOR PAVEMENT APPLICATION

A Dissertation APPROVED FOR THE
SCHOOL OF CIVIL ENGINEEIRNG AND ENVIRONMENTAL SCIENCE

BY

Dr. Musharraf M. Zaman _____
(Chair)

Dr. Younane N. Abousleiman _____
(Committee Member)

Dr. Douglas D. Gransberg _____
(Committee Member)

Dr. Joakim G. Laguros _____
(Committee Member)

Dr. Gerald A. Miller _____
(Committee Member)

To My Parents, My Sister, My Brothers and to Her

ACKNOWLEDGEMENTS

I would like to begin by thanking my supervisor, Professor Musharraf M. Zaman, and express to him my deepest appreciation and gratitude for providing help, guidance, patience and support in my quest to complete this research. I am thankful to him for the dedication and effort in reviewing the materials contained in this dissertation. Without his help and active involvement, this work would not have been successful.

I would like to acknowledge Dr. Younane Abousleiman for his motivation that inspired me to continue my graduate studies. I am also thankful to him for his support and technical help in completing my dissertation. I would like to express my appreciation to Dr. Douglas Gransberg for his valuable comments that helped improve the quality of this work and completion of my dissertation. I am indebted to Dr. Joakim Laguros, not only because of his technical help and support, but for the special attention during my student life at the University of Oklahoma. Dr. Miller's commentary has had a significant impact on the quality of my dissertation. I am very thankful to him.

I would also like to thank the School of Civil Engineering and Environmental Science for providing the necessary equipment and materials to pursue this research. I am also grateful to all the Staff at CEES for all their help. Specifically, I am thankful to Mrs. Audre Carter, Mrs. Brand Finch, Mrs. Molly Smith and Mrs. Suzan Williams. Also, special thanks and appreciation go to Mr. Mike Schmitz for his valuable assistance in the laboratory. I also appreciate the help provided by my colleague, Mr. Pranshoo Solanski. I am indebted to Mr. Bill Chissoe for performing all the scanning electron microscopy and energy dispersive spectrometry tests. In addition, the help provided by Mr. Robert Turner to perform the X-ray diffraction is acknowledged.

A special thank you goes to the suppliers of the aggregates and stabilizing agents. The

financial support from the Oklahoma Department of Transportation, the Oklahoma Transportation Center and the Federal Highway Administration is highly appreciated and acknowledged.

I dedicate this work to my mother (Isabelle; Habeebet Albeh), my father (Najib, Habeeb Albe), my lovely sister (Andre) and my bothers (George, Dany and Charbel) who are immense sources of inspiration for me; I deeply appreciate their understanding, support and encouragement that has helped me, immensely, to achieve my goal.

DISCLAIMER

Neither the developers of this work nor the University of Oklahoma assume any legal liability or responsibility for the accuracy, completeness, or usefulness of any information, product or process disclosed in this dissertation.

TABLE OF CONTENTS

LIST OF TABLES

LIST OF FIGURES

LIST OF EQUATIONS

ABSTRACT

Variations in environmental conditions have been recognized by pavement engineers as a major factor affecting pavement performance. These variations, resulting from wet-dry (W-D) or freeze-thaw (F-T) actions, or a combination of these actions, can significantly affect the engineering properties of pavement materials. During the last few decades, more emphasis has been placed on evaluating the durability effect of such actions on the performance of stabilized aggregate bases.

In this study, the effect of durability, namely, W-D and F-T cycles, on the resilient modulus (M_r) of stabilized aggregate bases is examined. A total of four aggregates commonly used in Okalahoma are utilized. Cylindrical specimens are stabilized with cement kiln dust (CKD), class C fly ash (CFA) and fluidized bed ash (FBA), and then cured for 28 days. After curing, specimens are subjected to W-D or F-T cycles prior to testing for M_r. Results show that the changes in M_r values due to W-D or F-T cycles depend on the stabilizing agent properties and physical properties represented by maximum dry density and optimum moisture content.

In addition, the effect of F-T cycles on the flexural behavior of CFA-stabilized aggregate beams is investigated. This study is motivated by the fact that stabilized aggregate bases are subjected to flexural stresses under wheel loading. Thus, the flexural strength (represented by modulus of rupture) becomes another important design parameter in designing a pavement within the mechanistic framework. Beam specimens are prepared by compacting aggregates mixed with CFA and water, and then cured for 1 hour, 3 days and 28 days. After curing, specimens are subjected to F-T cycles and then tested for resilient modulus in flexure (M_{rf}) and modulus of rupture (MOR). It is found that both M_{rf} and MOR exhibit a decrease as F-T cycles increase. Among other benefits,

this study helps enrich the database on the durability of stabilized aggregate bases. Also, the test procedures employed in this study are expected to benefit future studies in this area.

Cementitious stabilization has been extensively used to improve the performance of pavement materials. In the past, emphasis has been placed on observing the macro-manifestation of stabilized pavement materials, but to the author's knowledge, very little effort has been directed toward the micro-manifestation. In this study, selective existing techniques, namely, X-ray diffraction (XRD), scanning electron microscopy (SEM) and energy dispersive spectrometry (EDS), are used to assess the micro-structural development of cementing compounds in stabilized aggregate specimens. Specifically, the reference intensity ratio (RIR) method is employed to semi-quantify the mass percent of minerals and cementing compounds in the mixtures. Results reveal the formation of cementing compounds (due to stabilization) such as ettringite, calcium silicate hydrate (C-S-H), calcium aluminum hydrate (C-A-H) and calcium aluminum silicate hydrate (C-A-S-H), which are responsible for the increase in strength. Findings from this study shed light on the use of semi-quantification techniques in cementitious stabilization. These techniques would provide a better understanding of cementitious reactions related to their short- and long-term roles.

The design of a pavement structure has evolved from the empirical method, namely the AASHTO 1993 design guide, to the mechanistic-empirical approach (AASHTO 2002 Design Guide). In the mechanistic-empirical method, the most commonly used approaches are: (1) multilayer elastic; and (2) finite element. These methods relate the performance of a pavement structure to stresses and strains induced by vehicular loads.

The distribution of these stresses and strains changes when an unbound base layer (conventional pavement structure) is replaced by a stabilized layer. The stabilized layer exhibits some flexural stresses, thus the evaluation of its flexural strength becomes another important design parameter in designing a pavement structure. When flexural stresses exceed the limiting strength, cracks are formed, which may propagate and reach the pavement surface causing damage to the overall pavement structure. To this end, this study encompasses the investigation of the flexural behavior of stabilized aggregate beams using a finite element model based on a smeared crack approach. A commercial finite element software, ABAQUS, is used for this purpose. The smeared crack model is calibrated using tensile strength, biaxial strength and fracture energy test results. The load-deflection curves of CFA-stabilized specimens under a flexure loading are compared with the predicted values obtained from the finite element simulations. Overall, the numerical predictions correlate well with the laboratory results. Thus, the smeared crack model can be useful in predicting the flexural performance of stabilized beams or stabilized bases and can also be used in the mechanistic design of pavements.

CHAPTER

1

INTRODUCTION

1.1 Background and Needs

The demand for pavement networks in the United States is greater than ever, and the conditions of existing roadways are deteriorating due to heavier vehicles and higher traffic volume. According to a Federal Highway Administration report, approximately 34% of America's roads are in poor or mediocre conditions (RIP, 2005). In the last few decades, state and federal transportation agencies and industry have been challenged to build, repair and maintain pavement systems with enhanced longevity and reduced costs. Specifically, efforts have been made to improve the design methodology and to establish techniques for modification of pavement materials (NCHRP, 2004). Cementitious stabilization is considered one of these techniques; it enhances the engineering properties of aggregate base and subgrade layers, which produces structurally sound pavements. However, the enhancement in engineering properties and the field performance of a stabilized granular base in a pavement system are influenced by many factors including seasonal factors such as wet-dry (W-D) and freeze-thaw (F-T) conditions.

Variations in wet-dry and freeze-thaw conditions can have serious detrimental effects on the service life of a pavement system and should be considered in the

design of such a system. The effect of W-D and F-T cycles on the durability of a stabilized aggregate base layer has received very little attention. NCHRP (1992) recognized that the durability of stabilized aggregate bases is important and should be carefully considered in the mixture design process. In addition, Little et al. (2005) note that the durability of cementitiously stabilized materials has not been fully explored. They recommend that additional research be conducted to develop a rapid and reliable test method for assessing the impact of wet-dry and freeze-thaw cycles on stabilized materials.

The present study evaluates the durability effects, namely, W-D and F-T cycles, on the resilient modulus (M_r) of cementitiously stabilized aggregates. The effect of F-T cycles on the behavior of resilient modulus in flexure (M_{rf}) and modulus of rupture (MOR) is also examined, since it is recognized that a stabilized aggregate base is subjected to flexural stresses. Figures 1-1 and 1-2 show the distribution of critical stresses and strains with depth within the cross-section of a pavement with an unbound aggregate base and with a stabilized aggregate base, respectively. NCHRP (1992) recognized such influences and noted that the structural response of a pavement with a stabilized layer is influenced by its flexural strength.

Knowledge gained from the experimental program illustrating the effect of W-D and F-T cycles on the performance of aggregate bases is expected to add useful information to the database on the durability of stabilized aggregate bases that will help establish more realistic and better durability test procedures.

Cementitious stabilization primarily consists of adding by-products such as ashes, cement and kiln dusts to aggregate or soil. In the presence of water, these materials

react to form cementing products that are responsible for the enhancement of strength and stiffness. The degree of enhancement is influenced by many factors such as aggregate or soil type, stabilizing agent type and curing time. Considerable efforts have previously been directed towards examining the macro-manifestation of such influences. However, very limited studies have addressed the micro-structural developments and the mechanisms associated with such cementitious stabilization. A letter posted on the Transportation Research Board website (Little et al., 2005) recognizes the need for fundamental research to understand cementitious reactions/mechanisms, and their short- and long-term roles in the stabilization process.

The present study aims at providing some insight into the performance characteristics (macro/micro-manifestation) and mechanisms of different aggregate bases stabilized with cement kiln dust (CKD), class C fly ash (CFA) and fluidized bed ash (FBA). Specifically, these characteristics and mechanisms are explained by using the X-ray diffractometer (XRD), the scanning electron microscopy (SEM) and the energy-dispersive spectroscopy (EDS) results. The XRD diffractograms are used to semi-quantify the cementitious products using the reference intensity ratio (RIR) method, while micrographs from SEM are used to visually explore the microstructural development of cementing products. Additionally, the EDS micrographs are used to identify the elements in the crystal formations due to stabilization.

Numerical modeling of pavements using the finite element method (FEM) has advanced steadily with the advancement (capability) of computing power. Several

computer programs such as ILLI-PAVE, MICH-PAVE and Kenpave have been developed for analysis of pavements (Huang, 2004). Other FEM programs have also been utilized for analysis of pavements with more realistic constitutive models. Sukumaran et al. (2004) conducted a study to evaluate the fracture mechanisms in a pavement system under moving aircraft loads. Ioannides and Peng (2004) used a finite element program (ABAQUS) to observe the crack growth in concrete slabs for pavement application. The new AASHTO 2002 design guide is suggesting using the finite element approach to analyze conventional flexible pavements. Very little attention, to the author's knowledge, has previously been focused on evaluating the behavior of a pavement structure having a stabilized aggregate base.

The present study aims at modeling a stabilized aggregate base as a simply supported beam using a smeared crack approach. The commercial finite element software, ABAQUS, is used for this purpose. Such work is expected to contribute toward the use of a mechanistic-based approach in the pursuit of a new and better procedure for designing pavements in the 21st century.

1.2 Hypotheses and Objectives

The main hypotheses of this study are:

(1) Engineering properties of limestone, sandstone and rhyolite aggregate bases can be significantly improved by cementitious stabilization using CKD, CFA and FBA.

(2) The cementing products can be semi-quantified using the X-ray diffraction technique.

(3) Repeated wet-dry (W-D) and freeze-thaw (F-T) cycles have deleterious effects on cementitiously stabilized aggregates. The extent of such effects depends on the curing time, the number of F-T and W-D cycles and the type of stabilizing

agent.

The specific objectives of this study are:

(1) Determine the effect of W-D cycles on resilient modulus (M_r) of aggregate bases stabilized with CKD, CFA and FBA.
(2) Determine the effect of F-T cycles on M_r of aggregate bases stabilized with the same stabilizing agents.
(3) Evaluate the effect of F-T cycles on resilient modulus in flexure and modulus of rupture of one selected aggregate stabilized with one additive.
(4) Semi-quantify the cementing compounds, along with other minerals, from the XRD diffractograms using the reference intensity ratio (RIR) technique.
(5) Model the stabilized specimens as simply supported beams using ABAQUS. Compare results from numerical modeling with pertinent laboratory test results.

1.3 Format of this Dissertation

Following the introduction presented in Chapter 1, Chapter 2 entitled "*Influences of Various Cementitious Agents on the Performance of Stabilized Aggregate Bases Subjected to Wet-Dry Cycles"* addresses the effect of W-D cycles on aggregate bases stabilized with CKD, CFA and FBA (Khoury and Zaman, 2005a). Cylindrical specimens were prepared and cured for 28 days prior to testing for M_r. The variation of resilient modulus with the number of W-D cycles was investigated. Regression models correlating the resilient modulus with the level of stresses were developed. Also, a regression model was developed correlating the resilient modulus values with the number of W-D cycles, the ratio of free lime to SAF (SiO_2+Al_2O_3+Fe_2O_3), and the ratio of maximum dry density to optimum moisture content. Statistical tests (t-test and F-test) were also performed to examine the significance of the regression models.

Chapter 3 entitled "*Environmental Effects on Durability of Aggregates Stabilized*

with Cementitious Materials" examines the effect of F-T cycles on cementitiously stabilized aggregates (Khoury and Zaman, 2005b). Cylindrical specimens were molded, cured for 28 days, then subjected to freezing and thawing cycles. The effect of F-T cycles on the resilient modulus values was investigated. Regression models were developed, correlating resilient modulus with level of stresses. The regression models were statistically evaluated for their significance to predict the resilient modulus as a function of stress. Also, a relative comparison between the effect of F-T and W-D cycles on the performance of stabilized aggregate bases is presented.

Chapter 4 addresses the durability, represented by the number of F-T cycles, on the flexural properties of CFA-stabilized aggregate beams (Khoury and Zaman, 2006). Beam specimens were molded and cured for 1 hour, 3 days, or 28 days, prior to subjecting them to 0, 8 and 16 F-T cycles; zero represents specimens not subjected to any F-T cycles. The effect of F-T cycles on M_{rf} and MOR of the stabilized beams was evaluated. Statistical tests, namely, F-test and t-test, were carried out to evaluate the significance of correlation. Also, the variation of resilient modulus in flexure with the stress ratio was examined. The effect of two different freeze-thaw laboratory procedures was also explored.

Chapter 5 is devoted to examining the performance of stabilized aggregate bases, namely, Meridian and Hanson, using X-ray diffraction, scanning electron microscopy, and energy dispersive spectroscopy techniques (Khoury and Zaman, 2005c). The microstructural developments were observed by using the aforementioned methods. The reference intensity ratio (RIR) method was used to semi-quantify the mass percent of minerals and cementing products in the mixtures.

The variation of the sum of cementing compounds (SCC), due to stabilization, with the unconfined compressive strength and curing time are presented.

Chapter 6 is related to modeling a stabilized beam under flexural loading (Khoury and Zaman, 2005d). A smeared crack model that is generally used for modeling concrete was used. The model was calibrated for a CFA-stabilized aggregate base. Laboratory tests, namely, uniaxial strength, biaxial strength, indirect tensile strength and fracture energy were conducted. These tests were performed on 3-day and 28-day cured specimens. A summary of these results is presented. Also, numerical results from the ABAQUS simulation are presented and compared with pertinent laboratory results.

In Chapter 7, the conclusions of this dissertation and recommendations for future research are presented.

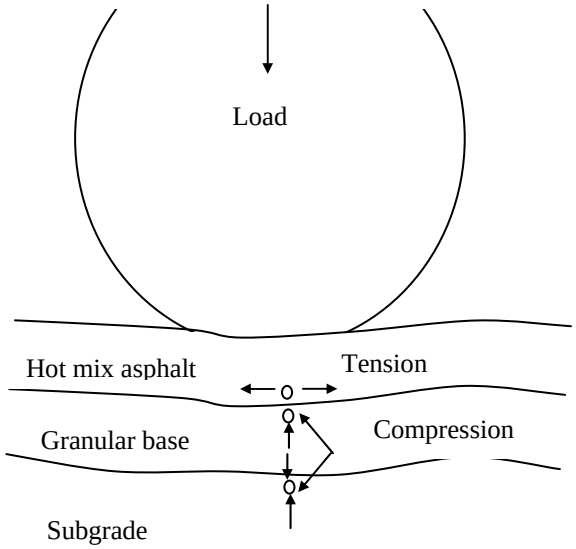

Figure 1-1 Critical tensile and compressive stresses and strains in flexible pavements with an unbound granular base (after Huang, 2004)

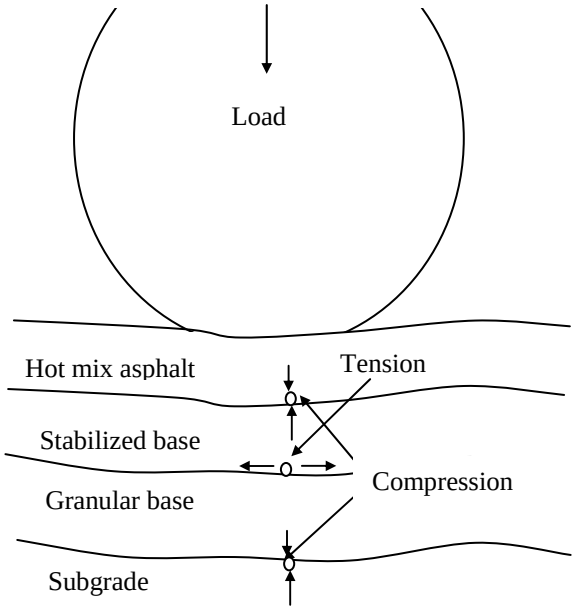

Figure 1-2 Critical tensile and compressive stresses and strains in flexible pavements with a stabilized granular base (after Sobhan, 1997)

CHAPTER

2

INFLUENCES OF VARIOUS CEMENTITIOUS AGENTS ON THE PERFORMANCE OF STABILIZED AGGREGATE BASES SUBJECTED TO WET-DRY CYCLES

2.1 Introduction

Variations in climatic conditions have been recognized by pavement engineers as a major factor affecting pavement performance. These variations, resulting from wet-dry (W-D) and freeze-thaw (F-T) actions, or a combination of these actions have been presented in a number of previous studies (Khoury and Zaman, 2002; Zaman et al., 1999; Berg, 1998; Nunan and Humphrey, 1990) and have been emphasized by others (AASHTO, 2005; Little et al., 2005). The influence of these actions on a pavement structure indicates possible changes in the engineering properties of pavement materials. To this extent, several studies have been undertaken to evaluate the performance of pavement materials under these actions. Specifically, during the last few decades, more emphasis has been placed by transportation agencies and researchers on better understanding the behavior of stabilized aggregate bases and subgrade soils under wet-dry and freeze-thaw cycles. This research area, however, is still not fully explored and additional studies are needed. This need is illustrated in a paper entitled "Millennium paper: Cementitious Materials," posted on the Transportation Research Board (TRB) website. The paper highlights the importance

of additional studies to establish a rapid test to assess the impact of durability, namely, wet-dry (W-D) and freeze-thaw (F-T) cycles on stabilized materials (Little et al., 2005).

The research study presented herein focuses on the durability of aggregate bases stabilized with 15% cement kiln dust (CKD), 10% class C fly ash (CFA) and 10% fluidized bed ash (FBA). Specifically, the influence of W-D cycles on resilient modulus (M_r) is evaluated. Also, the effect of stabilizing agents on M_r is presented.

2.2 Literature review

A review of previous studies reveals no widely acceptable laboratory procedure to evaluate the effect of W-D action on stabilized aggregate materials. Also, it is evident that only limited studies, to the author's knowledge, have addressed the performance of stabilized aggregate base materials under this action.

Among the laboratory procedures, the ASTM D 559 test method is the only standardized American Society for Testing Materials (ASTM) procedure for soil-cement specimens. This test procedure consists of placing a 7-day soil-cement cured specimen in a water bath at room temperature for five hours, then placing it in an oven at a temperature of 71^{o}C (160^{o}F) for 42 hours. The evaluation of W-D cycles is determined by degradation of specimens and their weight loss. Kalankamary and Davidson (1963) reported that evaluating the durability based on the weight loss is overly severe, and it does not simulate the field conditions.

The ASTM test procedure has been used by many researchers, while others employed new and different test methods. For example, Khoury and Zaman (2002) investigated the effect of W-D cycles on resilient modulus, unconfined compressive

strength and modulus of elasticity of a CFA-stabilized low quality aggregate commonly used as a pavement base in Oklahoma. In their study, a new W-D cycle-based laboratory procedure was employed. It consisted of placing 3-day and 28-day cured specimens in an oven having a temperature of 71^{o}C (160^{o}F) for 24 hours, and then submerging them in potable water for 24 hours at room temperature. At the end of each specified cycle, specimens were tested only for M_r and unconfined compressive strength (UCS). Specimens were subjected to up to 30 W-D cycles. Results showed that the mean M_r values of 28-day cured specimens increased as W-D cycles increased up to 12. Beyond 12 cycles, M_r values decreased. Wetting-drying actions also increased the M_r of 3-day cured specimens by 55% after 30 cycles. This increase was especially prevalent at lower W-D cycles. It was also observed that the 28-day cured specimens were more vulnerable to substantial reductions in M_r values than the 3-day cured specimens. Measurement of the resilient modulus as a criterion to evaluate the durability of pavement materials could be more representative of the field conditions than other properties such as unconfined compressive strength.

Miller et al. (1999) evaluated the durability of stabilized soils in Oklahoma. Cured specimens were subjected to wet-dry actions in accordance with the ASTM D 559 test method. The UCS was used as a criterion to evaluate the durability rather than using the weight loss. It was found that the strength increased with the number of W-D cycles. Use of UCS as an indicator of durability due to W-D action may not be very appealing because field-loading situations are rarely unconfined; Thompson and Smith (1990) concluded that the UCS is not a good indicator of the actual strength of an in-service granular base subjected to traffic (i.e., moving vehicles).

Nunan and Humphrey (1990) investigated the effect of W-D cycles on aggregate-cement-stabilized materials. In their study, the ASTM D 559 test procedure was used to examine the influence of such cycles. Results showed that stabilized specimens met the durability requirement with a weight loss of less than 14% after 12 cycles of wetting and drying. Use of the ASTM D 559 test method may be considered severe, and it is not a good indicator of the actual conditions in the field, as indicated by Kalankamary and Davidson (1963).

2.3 Materials

The following aggregates are used in the present study: (1) Meridian; (2) Richard Spur; (3) Sawyer, and (4) Hanson. Meridian is a limestone aggregate with an average calcium carbonate ($CaCO_3$) content of approximately 96%, an average magnesium carbonate content of approximately 1%, and an average silica (SiO_2) content of 3%. Geologically, it is white to gray, relatively pure and crystalline aggregate type. Bulk aggregates were collected from the Willis Quarry (currently known as Martin-Marietta) in Marshall County, Oklahoma. Richard Spur, another limestone aggregate, has a lower $CaCO_3$ content than Meridian, approximately 87%, and a higher SiO_2 content of approximately 10%. Bulk aggregates were provided by Dolese Corporation from Comanche County, Oklahoma. The Sawyer aggregate, a sandstone type-aggregate, was collected from Choctaw County, Oklahoma. Sawyer aggregates have a high SiO_2 content of approximately 94%. Hanson is a rhyolite-type aggregate with an average of 65% silica, 12% alumina (Al_2O_3) and 7% ferric oxide (Fe_2O_3). Bulk specimens were collected from Davis, Oklahoma. Los Angeles (LA) abrasion tests were performed on each aggregate in accordance with the ASTM C 131-96 test

method. A total of three tests were performed on each aggregate type, and the average LA values were found to be 34% for Meridian, 26% for Richard Spur, 22% for Sawyer and 18% for Hanson. It is important to note that the LA value is used as an indicator of the relative quality or competence of various sources of aggregates having similar mineral compositions (ASTM C 131-96).

In the present study, three different stabilizing agents, namely, CKD, CFA and FBA were used. CKD was provided by Blue Circle Company from Tulsa, Oklahoma, currently known as Lafarge. It is produced during the process of manufacturing Portland cement. In general, CKD are particulate mixtures of partially calcined and un-reacted raw feed, clinker dust, and fuel ash, enriched with alkali sulfates, halides and other volatiles. The CKD used in this study has an average amount of silica (SiO_2), Alumina (Al_2O_3) and Ferric oxide (Fe_2O_3) (SAF) of approximately 19% by weight. The calcium oxide (CaO) content is 44%, with two to three percent available in free form.

CFA was obtained from Boral Materials Technology, Oologah plant, Oklahoma. It is produced in coal-fired electric utility plants. The SAF for the CFA is approximately 62%, and the average CaO content is approximately 25%. The exact amount of free CaO for the used CFA was not supplied. The literature reveals that the presence of free CaO for CFA is approximately 7% (Majko, 2004; FHWA, 1982).

FBA was provided by the Brazil Creek Minerals, Inc., Fort Smith, Arkansas. FBA is produced form the combustion of low quality and washery coal (Pandey, 1996). FBA has approximately 35% SAF and 38% CaO, of which 18% is available in free form, known as free lime index.

From the aforementioned chemical properties, as shown in Table 2-1, differences between the chemical composition and physical properties among the selected additives are clearly evident. These differences will lead to varied performances of stabilized aggregate bases under W-D cycles.

2.4 Specimen Preparation

Specimens were prepared according to the method described by Khoury (2001) and Khoury and Zaman (2002). The mixture, for each specimen, consists of raw aggregates blended with either 15% CKD, 10% CFA or 10% FBA. These contents were identified by Zaman et al. (1998) as the optimum additive content (OAC) for commonly used aggregate bases in Oklahoma. In their study, the strength gain, modulus gain, and mixing and compaction considerations in the field were used in determining the OAC. The raw aggregates had the median gradation for type A aggregate bases, as recommended by the Oklahoma Department of Transportation Standard Specification for Highway Construction, and the additive content was added according to the dry weight of aggregates. After uniformly blending both aggregates and additives, the equivalent amount of water for optimum moisture content was added and mixed until uniformity. Then, the mixture was compacted in a 15.24 cm by 30.38 cm (6 in. x 12 in.) mold to reach a dry density approximately 98% of maximum dry density (MDD). The OMCs and MDDs for each aggregate type were determined in accordance with the moisture-density test presented in Khoury (2001). A summary of the OMCs and MDDs is presented in Table 2-2. After compaction, stabilized specimens were cured for 28 days in a moist room with a temperature of approximately 21^{o}C (70^{o}F) and a controlled relative humidity of 90% (± 2.5%). After

curing, specimens were subjected to 0, 8, 16 and 30 W-D cycles; zero representing reference control specimens that were not subjected to any W-D cycles.

2.5 W-D cycles

As mentioned earlier, there is no widely accepted laboratory procedure to determine the effect of wet-dry cycles on stabilized aggregate base materials, specifically, on the resilient modulus. Thus, the laboratory procedure reported in Khoury and Zaman (2002) was used in this study. One W-D cycle consisted of placing a specimen in an oven having a temperature of 71^{o}C (160 ^{o}F) for 24 hours, and then submerging it in potable water for 24 hours at room temperature. W-D cycles were applied on stabilized specimens already cured for 28 days. The numbers of W-D cycles considered in this study were 0, 8, 16 and 30. At the end of each specified cycle, specimens were tested for M_r. An approach described in Khoury (2001) was employed, which consisted of using the same specimens again for M_r testing after subjecting them to multiple sequences of W-D cycles; additional details are given in Khoury (2001).

2.6 Laboratory Procedure

The resilient modulus was used in this study to evaluate the performance of stabilized specimens under W-D cycles. The resilient modulus tests were performed in accordance with the test procedure described in Khoury and Zaman (2002). Specimens were loaded using different test sequences, as illustrated in Table 2-3. A haversine-shaped pulse load, having a duration of 0.1 s and a relaxation period of 0.9 s, was utilized to apply the load. The load-deformation response for the last five-cycles, out of the applied number of 50 cycles, as shown in Table 2-3, was recorded

during the test. A 22.7 kN (5000-lb) load cell was used to apply the load, and two LVDTs with a stroke length of 0.508 cm (0.2 inch) were used to measure the vertical deformation. LVDTs were attached to two aluminum clamps mounted on the specimen at a distance of approximately 7.62 cm (3 in.) from both ends of the specimen. Additional details on the accuracy and precision of readings, and the noise associated with the M_r test procedure are given by Khoury and Zaman (2002).

2.7 Presentation and Discussion of Results

Tables 2–4 to 2–14 present the laboratory results of the resilient modulus of the stabilized specimens under W-D cycles, where the average resilient modulus values and the standard deviation are presented. A way to observe the effect of W-D cycles on resilient modulus is to evaluate the changes in M_r values at a specific stress level. Several models have been used to correlate the resilient modulus of pavement materials with stresses. Witczak (2000) reported that 14 models are available for predicting the resilient modulus of unbound pavement materials. The predictor variables used for these models were mainly confining pressure and deviatoric stress (physically and statistically independent variables), and bulk stress and octahedral stress (stress invariants) (Witczak, 2000). Zaman et al. (1998) used the k-θ model (log-log k_1, k_2 θ model) to correlate the M_r values of stabilized aggregate bases. The k-θ model has long been used for unbound granular materials (Witczak, 2000). In this study, a slightly modified model was used to correlate the resilient modulus. The bulk stress, one of the stress invariants, and the confining pressure (one of the physical variables) were used to predict the resilient modulus in the model given below:

$$M_r = k_1 \times k_2^{\sigma_3} \times k_3^{\theta} \quad \textbf{(2-1)}$$

In a logarithmic form, the model can be written as:

$$\log(M_r) = \log(k_1) + \sigma_3 \log(k_2) + \theta \log(k_3) \quad \textbf{(2-2)}$$

This model is similar to the semi-log k_1, k_2, k_3 [(θ, τ) or (σ_3, σ_d)] model reported by Witczak (2000), but it uses (θ,σ_3) instead of [(θ, τ) or (σ_3, σ_d)]. One of the advantages of using the aforementioned semi-log model is that it is rational for values of $\sigma_3 = 0$. The primary goal of using a regressional model is to be able to compare the results for different wet-dry cycles at a given state of stress.

Results from Tables 2–4 to 2–14 were used to determine the model parameters (k_1, k_2 and k_3). A summary of these parameters is presented in Tables 2–15 through 2–25. From these tables, a frequency plot for the coefficient of determination (R^2) was generated, as shown in Figure 2-1, to assess the significance of the regression model in predicting M_r values as a function of stresses. A total of 34 out of 40 established models reveal relatively high R^2 values between 0.8 and 1. From these tables, it is evident that most of the models reveal high values of F-statistic, from which one can conclude that the employed model was statistically significant and could be used in predicting M_r values. The model parameters were used to determine the M_r values at a confining pressure of 104 kPa (15 psi) and a bulk stress of 547.5 kPa (79.5 psi); these stress levels fall within the stress levels used for testing the specimens. The calculated M_r values are subsequently used to assess the influence of wet-dry action.

2.7.1 Meridian aggregate stabilized with CKD and FBA

Tables 2–15 and 2–16 show that M_r values (at the aforementioned stresses) for

both CKD and FBA specimens exhibited a reduction as wet-dry cycles increased to 30 cycles. The percentage decrease, on the other hand, in resilient modulus of FBA-stabilized specimens was lower than the CKD-stabilized specimens. The M_r values for CKD-stabilized specimens subjected to 30 W-D cycles were approximately 55% lower than the corresponding M_r values of stabilized specimens without (not subjected to) any W-D cycles, while the M_r values of FBA-stabilized specimens (at the same stress levels and number of cycles) were approximately 40% lower, respectively, than the corresponding resilient modulus of specimens without any such cycles. One explanation of such a reduction in resilient modulus could be attributed to the reduction in cementitious reaction due to the repeated W-D cycles, and to the increase in moisture content during wetting; this information (moisture content) is not available since the same specimen approach is used.

2.7.2 Richard Spur Aggregate Stabilized with CKD, CFA and FBA

The effect of W-D cycles on the resilient modulus of Richard Spur aggregates stabilized with CKD, CFA and FBA is presented in Tables 2–17, 2–18 and 2–19. A reduction in resilient modulus values with the increase in W-D cycles was observed. The M_r values for CKD specimens decreased from 4,831 MPa (701 ksi) to 3,224 MPa (468 ksi), after 30 W-D cycles. Quantitatively, this reduction in M_r values is approximately 33%. As for CFA- and FBA-stabilized specimens, the percentage reductions are approximately 32% and 36%, respectively. They are slightly different than the corresponding values for CKD (33%) specimens. Although the percentage of reduction is close, FBA specimens had higher modulus than CFA specimens, followed by CKD specimens.

2.7.3 Sawyer Aggregate Stabilized with CKD, CFA and FBA

The resilient modulus results of Sawyer specimens stabilized with CKD, CFA and FBA, and subjected to W-D cycles are summarized in Tables 2–20, 2–21 and 2–22. With the exception of the CKD-stabilized specimens, the M_r values decreased with an increase in the number of cycles. The CKD-stabilized specimens exhibited an increase in M_r values as W-D cycles increased up to 8 cycles, beyond which a reduction was observed. Such behavior may be attributed to the enhancement of pozzolanic reactions during the wetting and drying phase. The behavior of CFA and FBA specimens revealed that W-D cycles led to a decrease in the M_r values, similar to the behavior of the Meridian and Richard Spur specimens. Laboratory observations revealed a major degradation in FBA specimens after 16 cycles; M_r tests could not be performed on these specimens due to excessive degradation at the bottom of these specimens.

2.7.4 Hanson Aggregate Stabilized with CKD and FBA.

Hanson aggregates were only stabilized with CKD and FBA. Specimens were subjected to as many as 30 W-D cycles. A summary of the resilient modulus values is given in Tables 2–23 and 2–24. The resilient modulus of Hanson specimens had the same pattern as the other aggregate specimens, with the exception of the Sawyer specimen stabilized with CKD, which is presented above. In other words, the resilient modulus showed a decrease as the number of W-D cycles increased from zero to 30 cycles; however the percentage decrease varied with the type of additive. For example, the resilient modulus of CKD specimens decreased from 2,853 MPa (414 ksi) to 1,590 MPa (231 ksi), after 30 cycles, while M_r values for FBA specimens

decreased from 3,786 MPa (550 ksi) to 2,305 MPa (335 ksi).

2.7.5 Effect of Stabilizing Agents and Aggregate Type on M_r

From the aforementioned results it is obvious that the resilient modulus of stabilized specimens is influenced by the stabilizing agent properties. A study by NCHRP (1976) reported that the pozzolanic reactivity of fly ash depends on the following four properties: (1) SiO_2 (S), S + A (Al_2O_3), or S + A + F (Fe_2O_3) content; (2) percentage of fly ash passing No. 325 sieve; (3) loss on ignition or carbon content; and (4) alkali contents or the free lime content that will eventually contribute to the alkali content. Another study by Zaman et al. (1998) attributed the increase in resilient modulus and unconfined compressive strength of stabilized specimens to the free lime content available in the stabilizing agents. In this study, the four properties of CKD, CFA and FBA, were used to assess the effect of stabilization and W-D cycles on M_r values. Figure 2-2 depicts the change in M_r of stabilized specimens without W-D cycles with SAF. It is observed that the M_r values exhibited an increase with the SAF values up to 35%, beyond which a negligible change occurred. This is an indication that the amount of SAF up to 35% would contribute to the increase in pozzolanic reactivity, which is responsible for the modulus increase. Additionally, the percent passing U.S. standard No. 325 sieve showed no specific trend with the increase in resilient modulus. For example, CFA specimens with 88.5% (see Table 2-1) had lower resilient modulus than FBA (45% passing No. 325) specimens. It is a sign that such a property is not a good indicator to assess the influence of stabilization on the resilient modulus. No specific trend was observed for the variation of resilient modulus with loss on ignition (LOI). For example, CFA specimens with a lower

average LOI value (0.23) had resilient modulus values lower than FBA (LOI value of 5.34) specimens. The effect of free lime is graphically depicted in Figure 2-3 where M_r values of stabilized specimens without W-D cycles, are plotted with lime. It is clear that the resilient modulus increases with the lime content; however, the percent increase varied from one aggregate to another. For example, the resilient modulus of Hanson increased by approximately 40% as the CaO content increased up to 18%. Richard Spur specimens, on the other hand, exhibited an increase of approximately 110% due to free lime. The resilient modulus values of Meridian and Hanson stabilized with 10% CFA (without W-D cycles) are presented in Table 2-25. It is important to note that the results of Meridian, with 10% CFA, were reproduced from Khoury (2001), while Hanson specimens were tested for this study without any W-D cycles.

Attempts were made to observe the effect of aggregate properties, namely, physical properties and mineralogical properties. The L.A. abrasion property of raw aggregate property showed no specific trend and could not be considered a good indicator in making performance predictions of stabilized aggregate bases. For example, Hanson, a good quality aggregate base with a low L.A. abrasion value of 18%, has lower M_r values compared to Richard Spur which has a relatively higher abrasion value of 26%. Also, the mineralogical properties of the aggregates did not show a specific trend with the variation of resilient modulus. Figure 2-4 shows the variation of resilient modulus of 15% CKD-stabilized Meridian, Richard Spur, Sawyer and Hanson with the mineralogical properties of aggregates; no specific trend can be observed.

Additionally, the physical properties, presented by optimum moisture content and maximum dry density, of the mixture of aggregate and stabilizing agents were used to observe their influence on resilient modulus. Figures 2–5 and 2–6 show the variation of M_r values with the optimum moisture content and maximum dry density of stabilized specimens without W-D cycles. It is clear that a higher maximum dry density and a lower optimum moisture content produce a higher resilient modulus.

From the aforementioned results, it is clear that the SAF, amount of free lime, and physical properties of the mixture were good indicators in predicting the performance of aggregate bases due to stabilization. These properties could also be used to assess the effect of various W-D cycles. A stabilizing agent with high contents of free lime and SAF would perform better than other stabilizing agents with lower values. And, a mixture with a higher maximum dry density and lower optimum moisture content would maintain a higher resilient modulus after a certain number of W-D cycles than a mixture with lower MDD and OMC, as shown in Figures 2–5 and 2–6.

A regression model correlating the variation of resilient modulus with the aforementioned properties and W-D cycles was developed. The regression model employed in this study is shown in the following equation:

$$M_r = A \times B^{WDC} \times C^{CSAFR} \times D^{DMR} \qquad \textbf{(2-3)}$$

where WDC is the number of W-D cycles, CSAFR is the ratio of free lime to SAF (in decimal), DMR is the ratio of maximum dry density (in kN/m^3) to the optimum moisture content (in %), M_r in MPa, and A, B, C and D are model coefficients. The regression analysis yields the following values: A = 825.85, B = 0.985, C = 1.845, D = 1.565. The corresponding R^2 value is 0.64 and the F value is 20 with a $P_r < 0.0001$,

which indicates that the model is considered statistically significant in predicting the variation of M_r values due to stabilization and W-D cycles. A comparison between the predicted M_r values and the actual M_r values is illustrated in Figure 2-7. From this figure, it is evident that the scatters are close to the 45^o line, which shows that such a model could be a good indicator in making performance predictions of resilient modulus due to stabilization and W-D action.

2.8 Concluding remarks

This study was undertaken to investigate the effect of W-D cycles on the resilient modulus of aggregates stabilized with different stabilizing agents. In general, resilient moduli decreased as W-D cycles increased. However, such decreases varied with the type of additive. Conversely, Sawyer aggregates stabilized with CKD exhibited an increase in M_r values as W-D cycles increased, up to 8 cycles; however, beyond this point, a reduction was observed. Changes in M_r values affected by W-D cycles could be attributed to rate or speed of pozzolanic reactions. It was also found that the variation of M_r values correlated better with the lime amount, SAF content, and optimum moisture content and maximum dry density. A regression model was developed to assess the influence of these properties and W-D cycles on M_r changes. The model had a R^2 of 0.64 and F-value of 20, which showed a good indicator in predicting the variation of M_r with free lime content, SAF, optimum moisture content, maximum dry density and W-D cycles.

Table 2-1 Properties of stabilizing agents

Stabilizing Agents Properties			
Compounds	Percentage per weight, (%)		
	CKD	CFA	FBA
$SiO_2 + Al_2O_3 + Fe_2O_3$	19	62	35
Calcium oxide (CaO)	44	25	38
Magnesium oxide (MgO)	1.5	5.4	2.7
Sulphur oxide (SO_3)	2.5	2	19
Calcium carbonate ($CaCO_3$)	64	---	41
Free lime (CaO)	2-3	7	18
Loss on ignition (LOI)	29	0.2	5.3
Percent fineness	---	11.5	55
Additional Properties Actual values			
Specific gravity	2.74	2.69	2.87

Table 2-2 A summary of optimum moisture content and maximum dry density

Aggregate Type	L.A abrasion value	% & type of Additives	OMC (%)	MDD, kN/m^3
Meridian	34	15% CKD	8.8	20.60
Richard Spur	26		6.5	22.27
Sawyer	22		7.7	21.88
Hanson	18		8.7	21.58
Meridian	34	10% CFA	7.0	21.68
Richard Spur	26		5.5	22.42
Sawyer	22		6.4	22.07
Hanson	18		5.7	21.50
Meridian	34	10% FBA	8.0	20.99
Richard Spur	26		4.9	22.68
Sawyer	22		5.7	22.19
Hanson	18		6.5	21.93
OMC: optimum moisture content				
MDD: maximum dry density				

Table 2-3 Loading sequences used in resilient modulus testing

Sequence #	Confining Pressure (kPa) (psi)	Cyclic Deviator Stress (kPa) (psi)	Contact Stress (kPa) (psi)	Number of Cycles
0	138 (20)	103 (15)	27.6 (4)	200-500
1	138 (20)	69 (10)	27.6 (4)	50
2	138 (20)	138 (20)	27.6 (4)	50
3	138 (20)	207 (30)	27.6 (4)	50
4	138 (20)	276 (40)	27.6 (4)	50
5	103 (15)	69 (10)	27.6 (4)	50
6	103 (15)	138 (20)	27.6 (4)	50
7	103 (15)	207 (30)	27.6 (4)	50
8	103 (15)	276 (40)	27.6 (4)	50
9	69 (10)	69 (10)	27.6 (4)	50
10	69 (10)	138 (20)	27.6 (4)	50
11	69 (10)	207 (30)	27.6 (4)	50
12	69 (10)	276 (40)	27.6 (4)	50
13	34 (5)	69 (10)	27.6 (4)	50
14	34 (5)	138 (20)	27.6 (4)	50
15	34 (5)	207 (30)	27.6 (4)	50
16	34 (5)	276 (40)	27.6 (4)	50
17	0 (0)	69 (10)	27.6 (4)	50
18	0 (0)	138 (20)	27.6 (4)	50
19	0 (0)	207 (30)	27.6 (4)	50
20	0 (0)	276 (40)	27.6 (4)	50

Sequence # 0 represents specimen conditioning

Table 2-4 A summary of resilient modulus of 15% CKD-stabilized Meridian specimens

σ_3 (kPa)	σ_d (kPa)	σ_s (kPa)	M_r (MPa)							
			0 W-D cycle	Standard Deviation	8 W-D cycles	Standard Deviation	16 W-D cycles	Standard Deviation	30 W-D cycles	Standard Deviation
138	69	28	1681	154	1299	81	1071	67	935	58
138	138	28	1784	163	1458	91	1183	74	935	58
138	208	28	2210	203	1550	97	1260	79	965	60
138	277	28	2277	209	1721	108	1405	88	1019	64
104	69	28	1652	151	1363	85	1039	65	660	41
104	138	28	1718	157	1364	85	1041	65	742	46
104	208	28	1914	175	1386	87	1081	67	835	52
104	277	28	2152	197	1489	93	1384	86	894	56
69	69	28	1619	148	1272	79	1008	63	624	39
69	138	28	1692	155	1307	82	1018	64	704	44
69	208	28	1849	169	1346	84	1033	65	796	50
69	277	28	2119	194	1403	88	1277	80	868	54
35	69	28	1609	147	1252	78	985	62	603	38
35	138	28	1688	155	1279	80	994	62	682	43
35	208	28	1835	168	1331	83	1006	63	773	48
35	277	28	2368	217	1375	86	1195	75	846	53
0	69	28	1612	148	1229	77	960	60	585	37
0	138	28	1673	153	1260	79	969	61	666	42
0	208	28	1796	165	1315	82	989	62	757	47
0	277	28	2093	192	1358	85	1151	72	838	52

1 psi = 6.89 kPa; 1 ksi = 6.89 MPa

σ_d = Deviator Stress; σ_3 = Confining Pressure

σ_s = Seating Pressure

Table 2-5 A summary of resilient modulus of 10% FBA-stabilized Meridian specimens

σ_3 (kPa)	σ_d (kPa)	σ_s (kPa)	M_r (MPa)							
			0 W-D cycle	Standard Deviation	8 W-D cycles	Standard Deviation	16 W-D cycles	Standard Deviation	30 W-D cycles	Standard Deviation
138	69	28	4500	119	4538	120	4057	107	3493	92
138	138	28	4761	126	5462	145	4511	119	3647	96
138	208	28	5039	133	6157	163	5210	138	4118	109
138	277	28	6290	166	6658	176	5575	148	4870	129
104	69	28	4502	119	3948	104	3531	93	3166	84
104	138	28	4502	119	3951	105	3525	93	2714	72
104	208	28	4732	125	4193	111	3735	99	3001	79
104	277	28	6289	166	4297	114	3861	102	3330	88
69	69	28	4488	119	3581	95	3182	84	2876	76
69	138	28	4619	122	3639	96	3307	87	2532	67
69	208	28	4700	124	3942	104	3550	94	2846	75
69	277	28	6290	166	4174	110	3753	99	3240	86
35	69	28	4445	118	3456	91	3115	82	2820	75
35	138	28	4589	121	3518	93	3183	84	2428	64
35	208	28	4746	126	3824	101	3464	92	2775	73
35	277	28	5620	149	4100	108	3708	98	3202	85
0	69	28	4438	117	3371	89	3022	80	2742	73
0	138	28	4553	120	3427	91	3136	83	2389	63
0	208	28	4726	125	3768	100	3437	91	2753	73
0	277	28	5575	148	4110	109	3696	98	3192	84

1 psi = 6.89 kPa; 1 ksi = 6.89 MPa

σ_d = Deviator Stress; σ_3 = Confining Pressure

σ_s = Seating Pressure

Table 2-6 A summary of resilient modulus of 15% CKD-stabilized Richard Spur specimens

σ_3 (kPa)	σ_d (kPa)	σ_s (kPa)	M_r (MPa)							
			0 W-D cycle	Standard Deviation	8 W-D cycles	Standard Deviation	16 W-D cycles	Standard Deviation	30 W-D cycles	Standard Deviation
138	69	28	4387	274	4062	254	3012	188	3322	207
138	138	28	4636	290	4248	265	3530	220	3315	207
138	208	28	4995	312	4625	289	5466	341	3547	221
138	277	28	5516	344	5003	312	5970	373	3556	222
104	69	28	4318	270	3877	242	3377	211	2632	164
104	138	28	4401	275	3992	249	3017	188	2787	174
104	208	28	4755	297	4357	272	3564	223	3043	190
104	277	28	5121	320	4792	299	2957	185	3300	206
69	69	28	4290	268	3929	245	3250	203	2557	160
69	138	28	4332	271	3931	246	2916	182	2762	172
69	208	28	4671	292	4194	262	3559	222	2993	187
69	277	28	4969	310	4650	290	2941	184	3284	205
35	69	28	3907	244	3648	228	3408	213	2517	157
35	138	28	4084	255	3656	228	3443	215	2765	173
35	208	28	4104	256	3704	231	2971	186	2965	185
35	277	28	4736	296	4210	263	2943	184	3257	203
0	69	28	3968	248	3527	220	3299	206	2453	153
0	138	28	4191	262	3732	233	3334	208	2739	171
0	208	28	4198	262	3763	235	2904	181	2943	184
0	277	28	5148	321	4737	296	2897	181	3239	202

1 psi = 6.89 kPa; 1 ksi = 6.89 MPa

σ_d = Deviator Stress; σ_3 = Confining Pressure

σ_s = Seating Pressure

Table 2-7 A summary of resilient modulus of 10% CFA-stabilized Richard Spur specimens

σ_3 (kPa)	σ_d (kPa)	σ_s (kPa)	M_r (MPa)							
			0 W-D cycle	Standard Deviation	8 W-D cycles	Standard Deviation	16 W-D cycles	Standard Deviation	30 W-D cycles	Standard Deviation
138	69	28	5081	317	4043	252	3576	223	3599	401
138	138	28	5529	345	4632	289	3855	241	3619	403
138	208	28	6199	387	5129	320	4246	265	3705	413
138	277	28	6579	411	6125	383	4391	274	3867	431
104	69	28	5013	313	4042	252	3470	217	3059	341
104	138	28	5049	315	4174	261	3700	231	3406	379
104	208	28	5140	321	4328	270	4193	262	3654	407
104	277	28	5377	336	5200	325	4473	279	3939	439
69	69	28	4893	306	4054	253	3471	217	3108	346
69	138	28	5029	314	4102	256	3767	235	3364	375
69	208	28	5046	315	4222	264	4237	265	3637	405
69	277	28	5274	329	4836	302	4522	282	3913	436
35	69	28	4994	312	4067	254	3418	213	3049	340
35	138	28	5023	314	4211	263	3779	236	3422	381
35	208	28	5050	315	4263	266	4179	261	3711	413
35	277	28	5286	330	4912	307	4475	279	3869	431
0	69	28	4889	305	4047	253	3389	212	2987	333
0	138	28	4974	311	4081	255	3819	238	3338	372
0	208	28	5085	318	4242	265	4067	254	3684	410
0	277	28	5147	321	5180	323	4469	279	3975	443

1 psi = 6.89 kPa; 1 ksi = 6.89 MPa

σ_d = Deviator Stress; σ_3 = Confining Pressure

σ_s = Seating Pressure

Table 2-8 A summary of resilient modulus of 10% FBA-stabilized Richard Spur specimens

σ_3 (kPa)	σ_d (kPa)	σ_s (kPa)	M_r (MPa)							
			0 W-D cycle	Standard Deviation	8 W-D cycles	Standard Deviation	16 W-D cycles	Standard Deviation	30 W-D cycles	Standard Deviation
138	69	28	8691	543	7979	498	5124	320	5461	289
138	138	28	8838	552	8253	515	5984	374	5675	300
138	208	28	9062	566	8658	541	7128	445	6251	331
138	277	28	11070	691	9318	582	9058	566	7617	403
104	69	28	8798	549	7414	463	5174	323	5427	287
104	138	28	8956	559	8253	515	5761	360	5709	302
104	208	28	9404	587	8708	544	7290	455	6247	331
104	277	28	11675	729	9306	581	8780	548	7591	402
69	69	28	8832	552	7601	475	5247	328	5485	290
69	138	28	9120	570	8378	523	5859	366	5685	301
69	208	28	9788	611	8923	557	7304	456	6248	331
69	277	28	11987	749	9321	582	8540	533	7203	381
35	69	28	8880	555	8101	506	5408	338	5454	289
35	138	28	9142	571	8196	512	5971	373	5732	303
35	208	28	9665	604	9101	568	7279	455	6189	327
35	277	28	13030	814	9591	599	8358	522	7435	393
0	69	28	8900	556	8055	503	5473	342	5400	286
0	138	28	9205	575	8307	519	6107	381	5564	294
0	208	28	9803	612	8915	557	8289	518	5894	312
0	277	28	13296	830	9644	602	9448	590	7283	385

1 psi = 6.89 kPa; 1 ksi = 6.89 MPa

σ_d = Deviator Stress; σ_3 = Confining Pressure

σ_s = Seating Pressure

Table 2-9 A summary of resilient modulus of 15% CKD-stabilized Sawyer specimens

σ_3 (kPa)	σ_d (kPa)	σ_s (kPa)	M_r (MPa)							
			0 W-D cycle	Standard Deviation	8 W-D cycles	Standard Deviation	16 W-D cycles	Standard Deviation	30 W-D cycles	Standard Deviation
138	69	28	3218	201	4278	186	3295	144	2812	123
138	138	28	3646	228	4537	198	3612	157	2938	128
138	208	28	4334	271	5232	228	4178	182	3765	164
138	277	28	4820	301	6069	265	4184	182	4355	190
104	69	28	3112	194	4163	181	3346	146	3038	132
104	138	28	3447	215	4354	190	3552	155	2775	121
104	208	28	3943	246	4987	217	4550	198	3465	151
104	277	28	4546	284	5617	245	5002	218	2782	121
69	69	28	3123	195	4202	183	3430	149	2961	129
69	138	28	3408	213	4291	187	3606	157	2721	119
69	208	28	3949	247	4653	203	4953	216	3321	145
69	277	28	4306	269	5374	234	4972	217	2741	119
35	69	28	3141	196	4348	190	3427	149	2665	116
35	138	28	3338	208	4668	203	3598	157	3275	143
35	208	28	4012	251	4754	207	4851	211	2683	117
35	277	28	4134	258	5252	229	5012	218	2714	118
0	69	28	3113	194	4105	179	3590	156	2597	113
0	138	28	3377	211	4638	202	3597	157	3281	143
0	208	28	3888	243	4812	210	4767	208	2660	116
0	277	28	4063	254	5278	230	4798	209	2692	117

1 psi = 6.89 kPa; 1 ksi = 6.89 MPa

σ_d = Deviator Stress; σ_3 = Confining Pressure

σ_s = Seating Pressure

Table 2-10 A summary of resilient modulus of 10% CFA-stabilized Sawyer specimens

σ_3 (kPa)	σ_d (kPa)	σ_s (kPa)	M_r (MPa)							
			0 W-D cycle	Standard Deviation	8 W-D cycles	Standard Deviation	16 W-D cycles	Standard Deviation	30 W-D cycles	Standard Deviation
138	69	28	3872	169	3248	142	2596	113	2291	100
138	138	28	4177	182	3656	159	2898	126	2249	98
138	208	28	4701	205	4535	198	2908	127	2465	107
138	277	28	5751	251	5263	229	3006	131	2537	111
104	69	28	3884	169	3222	140	1901	83	1981	86
104	138	28	3898	170	2965	129	2164	94	1955	85
104	208	28	4001	174	3066	134	2582	113	2089	91
104	277	28	5557	242	3190	139	2936	128	2197	96
69	69	28	3862	168	2934	128	1766	77	1927	84
69	138	28	3892	170	2832	123	2094	91	1914	83
69	208	28	3996	174	2951	129	2483	108	2043	89
69	277	28	5151	225	3145	137	2886	126	2160	94
35	69	28	3762	164	2871	125	1683	73	1872	82
35	138	28	3842	167	2748	120	2043	89	1871	82
35	208	28	3944	172	2924	127	2433	106	1998	87
35	277	28	5110	223	3111	136	2808	122	2126	93
0	69	28	3803	166	2742	120	1537	67	1827	80
0	138	28	3813	166	2712	118	1895	83	1867	81
0	208	28	3838	167	2902	126	2305	100	1977	86
0	277	28	4998	218	3097	135	2709	118	2127	93

1 psi = 6.89 kPa; 1 ksi = 6.89 MPa

σ_d = Deviator Stress; σ_3 = Confining Pressure

σ_s = Seating Pressure

Table 2-11 A summary of resilient modulus of 10% FBA-stabilized Sawyer specimens

σ_3 (kPa)	σ_d (kPa)	σ_s (kPa)	M_r (MPa)					
			0 W-D cycle	Standard Deviation	8 W-D cycles	Standard Deviation	16 W-D cycles	Standard Deviation
138	69	28	4146	181	3091	135	1002	44
138	138	28	4617	201	3358	146	1095	48
138	208	28	4988	217	3745	163	1278	56
138	277	28	5222	228	4055	177	1317	57
104	69	28	4119	180	2953	129	713	31
104	138	28	4306	188	2765	121	781	34
104	208	28	4588	200	2823	123	905	39
104	277	28	5002	218	2836	124	968	42
69	69	28	4113	179	2459	107	665	29
69	138	28	4254	185	2441	106	734	32
69	208	28	4505	196	2551	111	864	38
69	277	28	5344	233	2620	114	956	42
35	69	28	4128	180	2242	98	652	28
35	138	28	4236	185	2145	93	718	31
35	208	28	4541	198	2193	96	841	37
35	277	28	5241	228	2252	98	944	41
0	69	28	4133	180	1890	82	624	27
0	138	28	4204	183	1892	82	708	31
0	208	28	4492	196	1989	87	837	36
0	277	28	5358	234	2091	91	947	41

1 psi = 6.89 kPa; 1 ksi = 6.89 MPa

σ_d = Deviator Stress; σ_3 = Confining Pressure

σ_s = Seating Pressure

Table 2-12 A summary of resilient modulus of 15% CKD-stabilized Hanson specimens

σ_3 (kPa)	σ_d (kPa)	σ_s (kPa)	M_r (MPa)							
			0 W-D cycle	Standard Deviation	8 W-D cycles	Standard Deviation	16 W-D cycles	Standard Deviation	30 W-D cycles	Standard Deviation
138	69	28	2585	161	2179	136	1618	101	1519	95
138	138	28	2767	173	2328	145	1798	112	1672	104
138	208	28	2843	178	2524	158	2102	131	1735	108
138	277	28	3221	201	2752	172	2991	187	1823	114
104	69	28	2601	162	2124	133	1595	100	1468	92
104	138	28	2603	163	2154	134	1638	102	1484	93
104	208	28	2707	169	2155	135	1749	109	1554	97
104	277	28	3140	196	2425	151	2273	142	1574	98
69	69	28	2559	160	2032	127	1565	98	1421	89
69	138	28	2578	161	2049	128	1603	100	1457	91
69	208	28	2640	165	2074	130	1666	104	1478	92
69	277	28	2972	186	2194	137	2201	137	1533	96
35	69	28	2586	162	2014	126	1558	97	1392	87
35	138	28	2596	162	2029	127	1574	98	1435	90
35	208	28	2754	172	2075	130	1656	103	1438	90
35	277	28	3035	190	2193	137	2111	132	1506	94
0	69	28	2557	160	1947	122	1543	96	1373	86
0	138	28	2597	162	1958	122	1550	97	1411	88
0	208	28	2718	170	2020	126	1634	102	1421	89
0	277	28	2996	187	2195	137	2068	129	1458	91

1 psi = 6.89 kPa; 1 ksi = 6.89 MPa

σ_d = Deviator Stress; σ_3 = Confining Pressure

σ_s = Seating Pressure

Table 2-13 A summary of resilient modulus of 10% FBA-stabilized Hanson specimens

σ_3 (kPa)	σ_d (kPa)	σ_s (kPa)	M_r (MPa)					
			0 W-D cycle	Standard Deviation	8 W-D cycles	Standard Deviation	30 W-D cycles	Standard Deviation
138	69	28	3440	215	2902	181	2504	156
138	138	28	3786	236	2924	183	2624	164
138	208	28	4129	258	3060	191	2418	151
138	277	28	4464	279	3193	199	2517	157
104	69	28	3392	212	2496	156	1814	113
104	138	28	3434	214	2595	162	2009	125
104	208	28	3525	220	2917	182	2227	139
104	277	28	3821	239	3180	199	2340	146
69	69	28	3405	213	2364	148	1724	108
69	138	28	3426	214	2549	159	1883	118
69	208	28	3455	216	2881	180	2090	131
69	277	28	3821	239	3160	197	2302	144
35	69	28	3362	210	2382	149	1694	106
35	138	28	3392	212	2530	158	1846	115
35	208	28	3476	217	2885	180	2043	128
35	277	28	3751	234	3205	200	2250	141
0	69	28	3392	212	2437	152	1106	69
0	138	28	3427	214	2658	166	1263	79
0	208	28	3503	219	2945	184	1458	91
0	277	28	3749	234	3278	205	1632	102

1 psi = 6.89 kPa; 1 ksi = 6.89 MPa

σ_d = Deviator Stress; σ_3 = Confining Pressure

σ_s = Seating Pressure

Table 2-14 A summary of resilient modulus of 10% CFA-stabilized specimens of Meridian and Hanson

σ_3 (kPa)	σ_d (kPa)	σ_s (kPa)	M_r (MPa)			
			Meridian		Hanson	
			0 W-D cycle	Standard Deviation	0 W-D cycles	Standard Deviation
138	69	28	3049	128	2836	177
138	138	28	3150	137	2882	180
138	208	28	3611	140	2923	183
138	277	28	3740	159	2958	185
104	69	28	2953	128	2753	172
104	138	28	3055	128	2737	171
104	208	28	3369	134	2882	180
104	277	28	3392	155	2949	184
69	69	28	2820	126	2647	165
69	138	28	2986	127	2578	161
69	208	28	3301	130	2717	170
69	277	28	3380	167	2875	180
35	69	28	2744	145	2495	156
35	138	28	2933	146	2507	157
35	208	28	3279	155	2696	168
35	277	28	3367	171	2802	175
0	69	28	2445	144	2226	139
0	138	28	2886	146	2414	151
0	208	28	3257	153	2603	163
0	277	28	3313	168	2805	175

1 psi = 6.89 kPa; 1 ksi = 6.89 MPa

σ_d = Deviator Stress; σ_3 = Confining Pressure

σ_s = Seating Pressure

Table 2-15 A summary of the statistical analysis of CKD-stabilized Meridian specimens subjected to wet-dry cycles

	W-D cycles	$[M_r = k_1 \times (k_2)^{\sigma_3} \times k_3^{\theta})]$		R^2	Adjusted R^2	F value	P_r	Significant	M_r*
Meridian with 15% CKD	0	k_1	1341	0.87	0.85	56.26	<0.0001	Yes	1987
		k_2	0.99637						
		k_3	1.00141						
	8	k_1	1112	0.80	0.78	34.92	<0.0001	Yes	1444
		k_2	0.99907						
		k_3	1.00065						
	16	k_1	808	0.80	0.77	33.61	<0.0001	Yes	1190
		k_2	0.99808						
		k_3	1.00107						
	30	k_1	510	0.83	0.81	40.82	<0.0001	Yes	878
		k_2	0.99782						
		k_3	1.00141						

* M_r values calculated at σ_3 = 104 kPa and θ = 547.5 kPa

Table 2-16 A summary of the statistical analysis of FBA-stabilized Meridian specimens subjected to wet-dry cycles

	W-D cycles	$[M_r = k_1 \times (k_2)^{\sigma_3} \times k_3^{\theta})]$		R^2	Adjusted R^2	F value	P_r	Significant	M_r*
Meridian with 10% FBA	0	k_1	3655	0.75	0.72	25.85	<0.0001	Yes	5243
		k_2	0.99632						
		k_3	1.00136						
	8	k_1	2813	0.73	0.70	22.91	<0.0001	Yes	4712
		k_2	0.99996						
		k_3	1.00095						
	16	k_1	2566	0.75	0.72	25.18	<0.0001	Yes	4144
		k_2	0.99946						
		k_3	1.00098						
	30	k_1	2189	0.61	0.57	13.36	0.0003	Yes	3419
		k_2	0.99981						
		k_3	1.00085						

* M_r values calculated at σ_3 = 104 kPa and θ = 547.5 kPa

Table 2-17 A summary of the statistical analysis of CKD-stabilized Richard Spur specimens subjected to wet-dry cycles

	W-D cycles	$[M_r = k_1 \times (k_2)^{\sigma}{}_3 \times k_3{}^{\theta})]$		R^2	Adjusted R^2	F value	P_r	Significant	M_r*
Richard Spur with 15% CKD	0	k_1	3497	0.83	0.81	41.58	<0.0001	Yes	4831
		k_2	0.99813						
		k_3	1.00095						
	8	k_1	3055	0.81	0.79	36.87	<0.0001	Yes	4322
		k_2	0.99814						
		k_3	1.00099						
	16	k_1	2754	0.27	0.18	3.09	0.0715	Yes	3647
		k_2	1.00107						
		k_3	1.00031						
	30	k_1	2227	0.80	0.78	34.79	<0.0001	Yes	3224
		k_2	0.99803						
		k_3	1.00105						

* M_r values calculated at σ_3 = 104 kPa and θ = 547.5 kPa

Table 2-18 A summary of the statistical analysis of CFA-stabilized Richard Spur specimens subjected to wet-dry cycles

	W-D cycles	$[M_r = k_1 \times (k_2)^{\sigma}{}_3 \times k_3{}^{\theta})]$		R^2	Adjusted R^2	F value	P_r	Significant	M_r*
Richard Spur 10% CFA	0	k_1	4474	0.57	0.51	11.04	0.0008	Yes	5469
		k_2	0.99946						
		k_3	1.00047						
	8	k_1	3360	0.73	0.69	22.55	<0.0001	Yes	4793
		k_2	0.99736						
		k_3	1.00115						
	16	k_1	3045	0.97	0.97	291.13	<0.0001	Yes	4169
		k_2	0.99632						
		k_3	1.00127						
	30	k_1	2791	0.85	0.84	49.48	<0.0001	Yes	3721
		k_2	0.99724						
		k_3	1.00105						

* M_r values calculated at σ_3 = 104 kPa and θ = 547.5 kPa

Table 2-19 A summary of the statistical analysis of FBA-stabilized Richard Spur specimens subjected to wet-dry cycles

	W-D cycles	$[M_r = k_1 \times (k_2)^{\sigma_3} \times k_3^{\theta})]$		R^2	Adjusted R^2	F value	P_r	Significant	M_r*
Richard Spur 10% FBA	0	k_1	7635	0.77	0.75	28.97	<0.0001	Yes	10136
		k_2	0.99506						
		k_3	1.00146						
	8	k_1	7273	0.93	0.92	106.5	<0.0001	Yes	8814
		k_2	0.99710						
		k_3	1.00090						
	16	k_1	4169	0.96	0.96	210.75	<0.0001	Yes	7220
		k_2	0.99186						
		k_3	1.00256						
	30	k_1	4508	0.89	0.88	71.83	<0.0001	Yes	6510
		k_2	0.99582						
		k_3	1.00147						

* M_r values calculated at σ_3 = 104 kPa and θ = 547.5 kPa

Table 2-20 A summary of the statistical analysis of CKD-stabilized Sawyer specimens subjected to wet-dry cycles

	W-D cycles	$[M_r = k_1 \times (k_2)^{\sigma_3} \times k_3^{\theta})]$		R^2	Adjusted R^2	F value	P_r	Significant	M_r*
Sawyer with 15% CKD	0	k_1	2537	0.95	0.95	168.35	<0.0001	Yes	4027
		k_2	0.99563						
		k_3	1.00168						
	8	k_1	3586	0.88	0.86	60.43	<0.0001	Yes	5037
		k_2	0.99653						
		k_3	1.00128						
	16	k_1	2947	0.84	0.83	45.82	0.0715	Yes	4253
		k_2	0.99389						
		k_3	1.00184						
	30	k_1	2528	0.27	0.19	3.2	0.066	Yes	3165
		k_2	1.00027						
		k_3	1.00036						

* M_r values calculated at σ_3 = 104 kPa and θ = 547.5 kPa

Table 2-21 A summary of the statistical analysis of CFA-stabilized Sawyer specimens subjected to wet-dry cycles

	W-D cycles	$[M_r = k_1 \times (k_2)^{\sigma_3} \times k_3^{\theta})]$		R^2	Adjusted R^2	F value	P_r	Significant	M_r*
Sawyer 10% CFA	0	k_1	3026	0.72	0.68	21.55	<0.0001	Yes	4586
		k_2	0.99646						
		k_3	1.00143						
	8	k_1	2324	0.60	0.55	12.66	<0.0001	Yes	3519
		k_2	1.00002						
		k_3	1.00075						
	16	k_1	1343	0.88	0.87	64.48	<0.0001	Yes	2698
		k_2	0.99584						
		k_3	1.00207						
	30	k_1	1665	0.77	0.74	27.81	<0.0001	Yes	2204
		k_2	0.99937						
		k_3	1.00063						

* M_r values calculated at σ_3 = 104 kPa and θ = 547.5 kPa

Table 2-22 A summary of the statistical analysis of FBA-stabilized Sawyer specimens subjected to wet-dry cycles

	W-D cycles	$[M_r = k_1 \times (k_2)^{\sigma_3} \times k_3^{\theta})]$		R^2	Adjusted R^2	F value	P_r	Significant	M_r*
Sawyer 10% FBA	0	k_1	3579	0.77	0.75	28.97	<0.0001	Yes	4783
		k_2	0.99678						
		k_3	1.00114						
	8	k_1	1777	0.94	0.93	131.45	<0.0001	Yes	3003
		k_2	1.00291						
		k_3	1.00041						
	16	k_1	501	0.96	0.96	210.75	<0.0001	Yes	1002
		k_2	0.99733						
		k_3	1.00177						

* M_r values calculated at σ_3 = 104 kPa and θ = 547.5 kPa

Table 2-23 A summary of the statistical analysis of CKD-stabilized Hanson specimens subjected to wet-dry cycles

	W-D cycles	$[M_r = k_1 \times (k_2)^{\sigma}{}_3 \times k_3{}^{\theta})]$		R^2	Adjusted R^2	F value	P_r	Significant	M_r*
Hanson with 15% CKD	0	k_1	2280	0.77	0.75	29.07	<0.0001	Yes	2853
		k_2	0.99788						
		k_3	1.00081						
	8	k_1	1766	0.80	0.77	32.97	<0.0001	Yes	2305
		k_2	0.99947						
		k_3	1.00059						
	16	k_1	1144	0.75	0.72	24.94	<0.0001	Yes	1996
		k_2	0.99593						
		k_3	1.00179						
	30	k_1	1268	0.83	0.81	42.13	<0.0001	Yes	1590
		k_2	0.99979						
		k_3	1.00045						

* M_r values calculated at σ_3 = 104 kPa and θ = 547.5 kPa

Table 2-24 A summary of the statistical analysis of FBA-stabilized Hanson specimens subjected to wet-dry cycles

	W-D cycles	$[M_r = k_1 \times (k_2)^{\sigma}{}_3 \times k_3{}^{\theta})]$		R^2	Adjusted R^2	F value	P_r	Significant	M_r*
Hanson 10% FBA	0	k_1	3003	0.69	0.65	18.79	<0.0001	Yes	3786
		k_2	0.99886						
		k_3	1.00064						
	8	k_1	2150	0.81	0.79	36.78	<0.0001	Yes	2996
		k_2	0.99678						
		k_3	1.00122						
	30	k_1	1181	0.81	0.79	37.42	<0.0001	Yes	2305
		k_2	1.00040						
		k_3	1.00115						

* M_r values calculated at σ_3 = 104 kPa and θ = 547.5 kPa

Table 2-25 A summary of the statistical analysis of Meridian and Hanson stabilized with 10% CFA without W-D cycles

	Aggregate Type	$[M_r = k_1 \times (k_2)^{\sigma_3} \times k_3^{\theta})]$		R^2	Adjusted R^2	F value	P_r	Significant	M_r*
10% CFA	Meridian	k_1	2393	0.90	0.89	75.46	<0.0001	Yes	3364
		k_2	0.99770						
		k_3	1.00106						
	Hanson	k_1	2252	0.85	0.83	48.56	<0.0001	Yes	2866
		k_2	0.99942						
		k_3	1.00055						

* M_r values calculated at σ_3 = 104 kPa and θ = 547.5 kPa

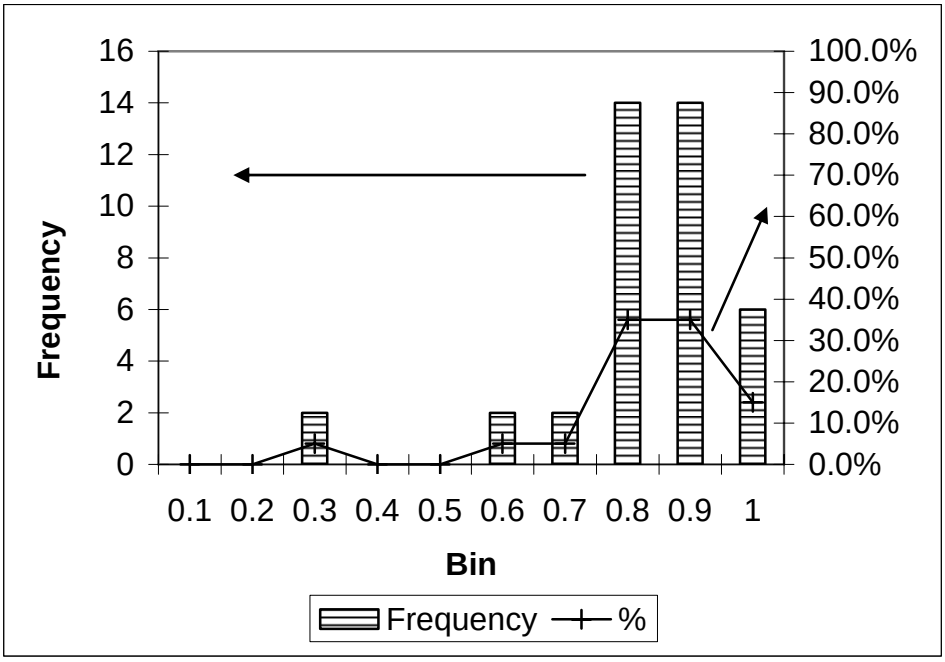

Figure 2-1 Frequency diagram for 40 observations

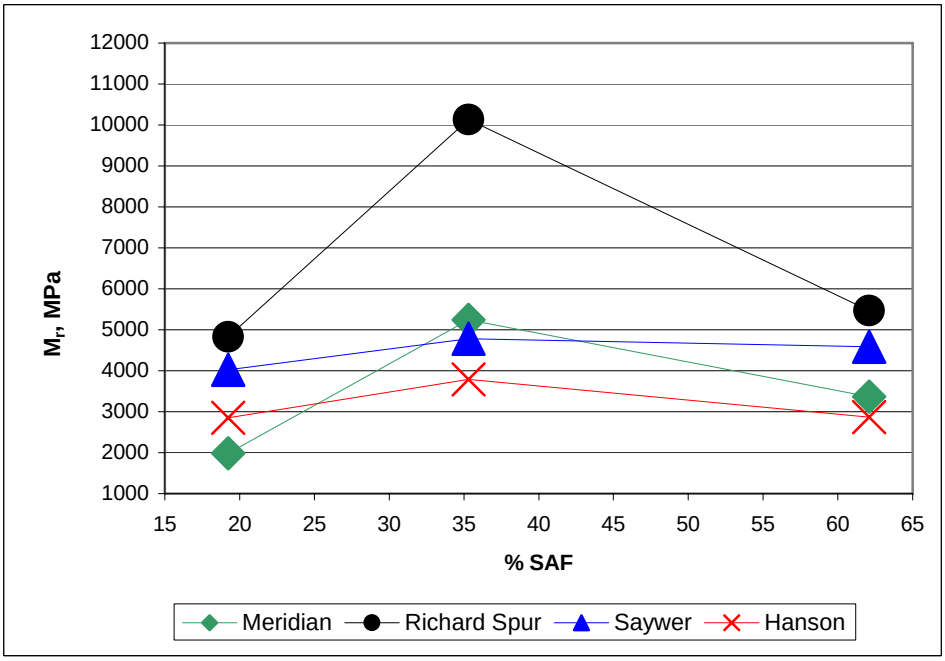

Figure 2-2 Variation of M_r values with SAF content of stabilizing agents

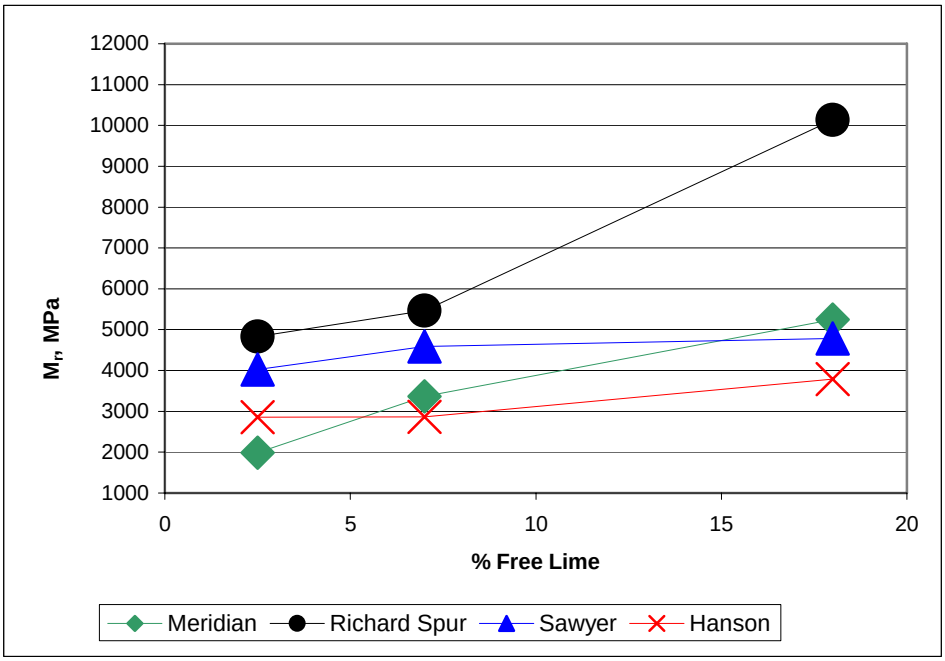

Figure 2-3 Variation of M_r values of stabilized specimens with free lime content of stabilizing agents

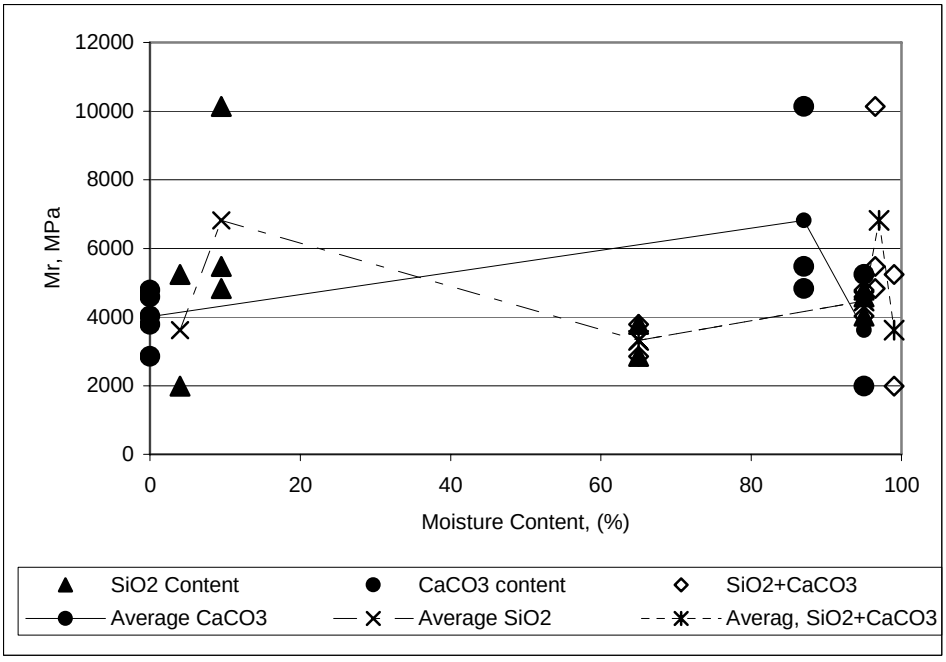

Figure 2-4 Variation of M_r values of 15% CKD specimens with aggregate minerals

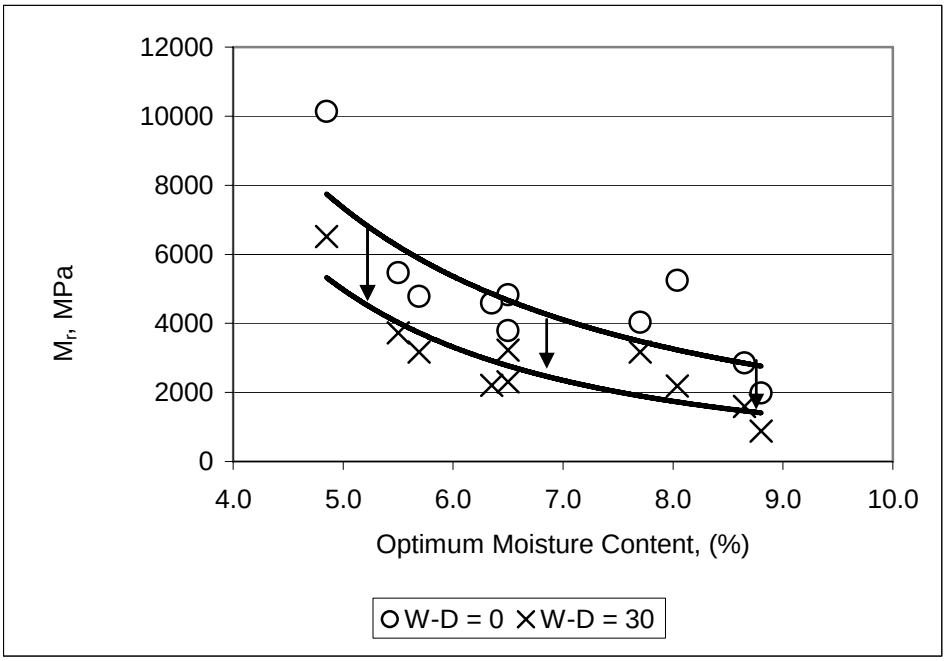

Figure 2-5 Variation of M_r values with OMCs

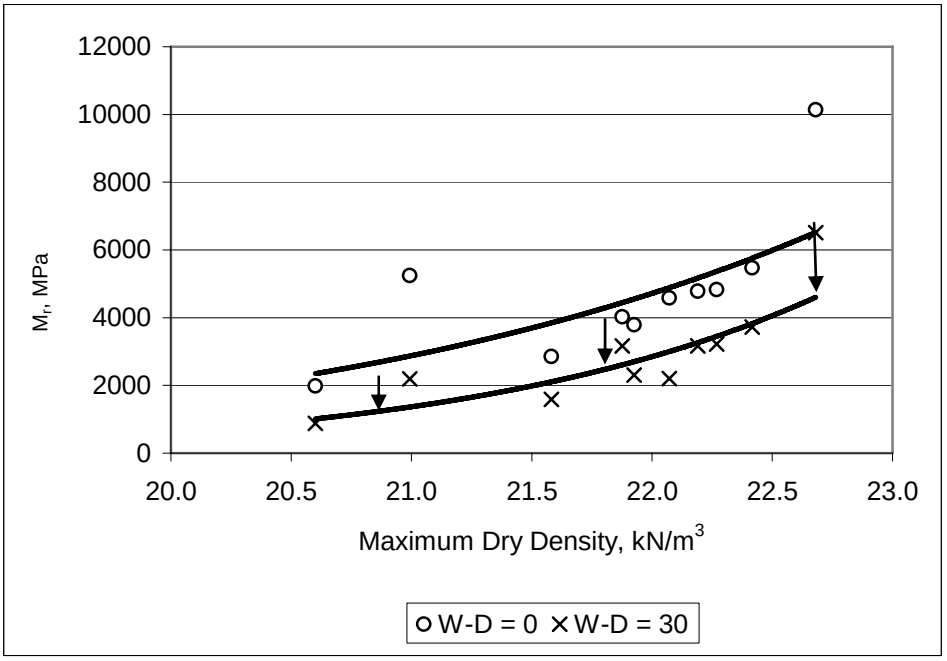

Figure 2-6 Variation of M_r values with MDDs

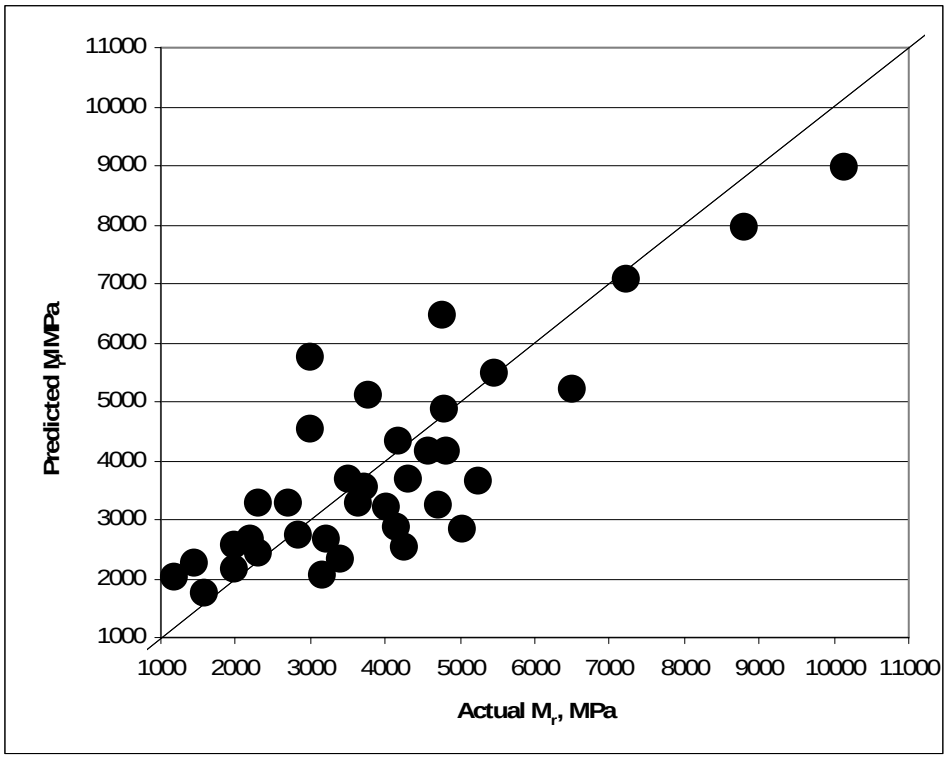

Figure 2-7 A comparison between predicted and actual M_r values

CHAPTER

3

ENVIRONMENTAL EFFECTS ON DURABILITY OF AGGREGATES STABILIZED WITH CEMENTITIOUS MATERIALS

3.1 Introduction

Durability of pavement materials induced by environmental factors, namely, repeated freeze-thaw action, can have a major effect on the performance of a pavement structure. Freeze-thaw action is considered to be as one of the most destructive actions that can induce significant damage to a pavement structure. The extent of the damage depends on many variables such as frost penetration depth, amount of water present during freezing, void space within the domain, number of freeze-thaw cycles, duration of freezing and thawing and type of freeze-thaw cycles. The variation in pavement performance due to seasonal changes indicates possible changes in the engineering properties of pavement material such as resilient modulus. The design and analysis of pavements, therefore, should account for such seasonal effects. NCHRP (1992) recognized the importance of evaluating the durability of stabilized aggregate bases and suggested that such effects be carefully considered in the mixture design. To this end, a bench-scale laboratory study was conducted to evaluate the damage caused by freeze-thaw (F-T) action on aggregates stabilized with different stabilizing agents, namely, cement kiln dust (CKD), class C fly ash (CFA) and fluidized bed ash (FBA).

3.2 Brief Overview of Previous Studies

A study was conducted by Nunan and Humphrey (1990) to evaluate the effect of F-T cycles on a cement-stabilized aggregate base in Maine. Aggregate-cement specimens were prepared using a standard proctor mold. Materials passing a U.S. standard 1.90 cm (0.75 in) sieve and retained on a U.S. standard No. 4 sieve were surface saturated and added to the mixture. After 7 days of curing, specimens were placed in a freezer at –26.1^{o}C (–15^{o}F) for 24 hours, then the specimens were placed in a moist room with a temperature of 21.1^{o}C (70^{o}F) at a relative humidity of 90%, for 23 hours. The specimens were removed from the moist room and tested in accordance with the ASTM D 560 test method. Results showed that specimens with 5% cement had a soil-cement loss less then 14%, which is the durability requirement specified by the ASTM D 560 standard test method. Kalankamary and Davidson (1963) reported that the evaluation of durability by the weight loss as a result of freeze-thaw cycles (ASTM D 560-57) is overly severe, and this test procedure does not simulate the field conditions effectively.

Zaman et al. (1999) conducted an exploratory laboratory study to determine the effect of F-T action on the resilient modulus of a CKD-stabilized low quality aggregate base. Specimens were compacted in a cylindrical split mold having a diameter of 15.24 cm (6 in.) and a height of 30.48 cm (12 in.). A vibratory compaction method was employed in preparing the specimens. After molding, specimens were cured for 7 days before the commencement of F-T cycles. Each F-T cycle consisted of freezing each specimen at –15^{o}C (5^{o}F) for 24 hours, then placing it in a moist room for thawing at 21.6^{o}C (71^{o}F) with 95% relative humidity, for 24

hours. Three different cycle levels, 4, 8 and 12 were considered. At the end of each specified cycle and after the thawing stage, specimens were tested for M_r, followed by the unconfined compressive strength (UCS) test. The M_r tests were conducted according to the AASHTO T 294-94 test method, while the UCS tests were performed in accordance with the AASHTO T 208-82 method. Based on this study, 8 to 12 cycles of freezing and thawing could be considered adequate in investigating the effect of F-T action on the M_r of CKD-stabilized Meridian aggregate. Because resilient modulus is a more appropriate material property in pavement design than UCS, it can be argued that it is a more rational parameter in assessing durability.

In a related study, Khoury (2001) and Zaman and Khoury (2003) evaluated the effect of freezing and thawing on the resilient modulus (M_r) of limestone aggregate base stabilized with CFA. A new laboratory freezing and thawing procedure was employed that consisted of freezing specimens cured for 3 and 28 days at –25^{o}C (-13^{o}F) for 24 hours, and then thawing them at 21.7^{o}C (71^{o}F) with a relative humidity of approximately 90%, for another 24 hours. A rapid freeze-thaw cabinet was used to control temperature and humidity, and the rubber membranes around the specimens were not removed. Results showed that resilient modulus of 28-day cured specimens increased with increasing freezing and thawing cycles up to 12, and then M_r started to decrease. On the other hand, the resilient modulus of 3-day cured specimens increased with F-T cycles up to 30 cycles. It was also found that the UCS and Young's modulus for 3- and 28-day cured specimens increased with increasing F-T cycles. Freezing and thawing cycles produced a negative effect on the resilient modulus of 28-day cured specimens after 12 F-T cycles, while a positive effect on the

M_r values of 3-day cured specimens was observed. This effect is explained in terms of retardation or acceleration of cementitious reactions in a stabilized aggregate specimen. The damage caused by the formation of ice lenses in the pores of stabilized specimens was found to have a negligible effect. The aforementioned F-T test procedure was not severe, as no moisture migration was allowed to and from the specimens due to the membranes around the specimens. This study was also limited to one aggregate and one additive, although it evaluated the effect of curing time on the performance of specimens under freezing and thawing.

3.3 Materials and Sources

The four aggregate base materials: (1) Meridian, (2) Richard Spur, (3) Sawyer, and (4) Hanson, were used to evaluate the influence of F-T cycles on the resilient modulus. Their properties are presented in section 2.3, Chapter 2. Also, cement kiln dust (CKD), class C fly ash (CFA) and fluidized bed ash (FBA) were used. Their properties are presented in section 2.3, and summarized in Table 2-1. As mentioned in the previous chapter, the differences between the chemical composition and physical properties among the selected additives are clearly evident in Table 2-1 and are expected to lead to different performances of stabilized specimens under F-T cycles.

3.4 Specimen Preparation and M_r Test Procedure

Cylindrical specimens were prepared in accordance with the laboratory procedure described in Chapter 2. Specimens were cured for 28 days and then subjected to F-T cycles prior to testing for resilient modulus. The same specimen approach described in Chapter 2 was utilized and consisted of using the specimens again for M_r testing

after subjecting them to multiple sequences of F-T cycles. Resilient modulus tests were performed in accordance with the laboratory test procedure described in Chapter 2.

3.5 F-T Cycles

A freeze-thaw procedure similar to that reported by Khoury (2001) and Zaman and Khoury (2003) was employed in this study. It consisted of freezing the cured specimens at –25^{o}C (-13^{o}F) in a freeze-thaw cabinet for 24 hours, and then thawing at a 21.7^{o}C (71^{o}F) for another 24 hours with a relative humidity of approximately 98%. It is important to mention that the membranes around the specimens were removed during the freezing and thawing to expose specimens to moisture changes. Figure 3-1 is a photograph of stabilized specimens in the rapid F-T cabinet during the freezing and thawing process.

3.6 Presentation and Discussion of Results

One way to observe the influence of F-T action is to evaluate the resilient modulus at a specific stress level, as mentioned in the previous chapter. In this chapter the corresponding M_r values (from Tables 3–1 to 3–10) at a confining pressure, σ_3 = 138 kPa (20 psi), and deviatoric stress, σ_d = 208 kPa (30 psi), were used to assess the effect of F-T cycles. Results from Tables 3–1 through 3–11 were also used to determine the (θ,σ_3) model parameters introduced in Chapter 2. A summary of these parameters and resilient modulus (at σ_3 = 104 kPa, i.e., 20 psi and θ = 547.5 kPa, i.e., 80 psi) are shown in Table 3–12 through Table 3–22. The predicted resilient modulus at the aforementioned stresses were compared to assess whether F-T or W-D cycles have more detrimental effect on the performance of

stabilized aggregate bases.

3.6.1 Meridian Aggregate Stabilized with CKD, CFA and FBA

Table 3-1 presents the resilient modulus values of 15% CKD-stabilized specimens cured for 28 days and subjected to F-T cycles. It is evident that the resilient modulus decreases as F-T cycles increase up to 16. For example, the resilient modulus (at σ_3 = 104 kPa, i.e., 20 psi and θ = 547.5 kPa, i.e., 80 psi) decreases approximately 50% and 80%, at 8 and 16 F-T cycles, respectively. After 16 F-T cycles, specimens started to degrade rapidly and the resilient modulus tests could not be performed at 30 cycles. Figure 3-2 illustrates the severe degradation of specimens stabilized with 15% CKD. It is believed that after 16 F-T cycles the voids within the specimens can not accommodate an increase of moisture content during the thawing phase, and the formation of ice lenses during the freezing phase; therefore, distortion of aggregate structure occurs, specifically within the matrix of fines.

The resilient moduli of 10% CFA-stabilized aggregate specimens under F-T action are summarized in Table 3-2. M_r values decrease with the increase in F-T cycles up to 30. The M_r values (at σ_3 = 104 kPa, i.e., 20 psi and θ = 547.5 kPa, i.e., 80 psi) decreased by approximately 40%, 73% and 81%, at 8, 16 and 30 F-T cycles, respectively. No severe degradation was observed in these specimens. From these results, one can conclude that 30 F-T cycles are not enough to cause any major degradation in the matrix of particles, as seen in CKD-stabilized specimens.

The effect of F-T cycles on the resilient modulus of 10% FBA-stabilized aggregate specimens is presented in Table 3-3. The resilient modulus values decreased as F-T cycles increased up to 30. For instance, the resilient modulus (at σ_3

= 104 kPa, i.e., 20 psi and θ = 547.5 kPa, i.e., 80 psi) decreased from 5,039 MPa (731 ksi) (at zero F-T cycle) to 996 MPa (144 ksi) after 30 cycles of freezing and thawing. Laboratory observations revealed no severe degradation of specimens up to 30 cycles. The existence of no major degradation could be attributed to the fact that the voids in the specimens were not filled with enough water, so the expanding ice, during freezing, did not cause any major damages to the specimens. It is possible that a higher number of F-T cycles may cause major degradation to the specimens, but such data is not currently available. Figure 3-3 shows the average percentage decrease in M_r values of stabilized Meridian aggregates due to F-T action. It is evident that the percentage decrease in resilient modulus of FBA-stabilized specimens is lower than the corresponding CFA-stabilized specimens, followed by CKD-stabilized specimens. For example, the resilient modulus of CKD-stabilized specimens subjected to 16 F-T cycles is approximately 75% lower than the corresponding M_r values of stabilized specimens with no such cycles. The corresponding percentage decrease is 68% and 65% for both CFA- and FBA-stabilized specimens, respectively. Although the percentage decrease in M_r values for CFA- and FBA-stabilized is quite close and could be considered essentially the same for practical reasons, the resilient modulus values for FBA specimens were higher than the corresponding M_r values of the CFA-stabilized specimens. Specifically, the average M_r value of FBA specimens is 2,050 MPa (298 ksi) (at σ_3 = 104 kPa, i.e., 20 psi and θ = 547.5 kPa, i.e., 80 psi), which is approximately 110% higher than the corresponding M_r values of CFA specimens, after 16 F-T cycles. Consequently, the durability of stabilized aggregates is influenced by the type of stabilizing agent used.

3.6.2 Richard Spur Aggregate Stabilized with CKD, CFA and FBA

The effect of F-T cycles on the resilient modulus of Richard Spur (RS) aggregate stabilized with 15% CKD, 10% CFA and 10% FBA are presented in Tables 3–4, 3–5 and 3–6. A decrease in M_r is observed as F-T cycles increase up to 30. The resilient modulus (at σ_3 = 104 kPa, i.e., 20 psi and θ = 547.5 kPa, i.e., 80 psi) of CKD-stabilized specimens after 30 F-T cycles is approximately 90% lower than a comparable specimen with a zero F-T cycle. No severe degradation is observed at 30 cycles, as illustrated in Figure 3-4. The M_r values of CFA specimens exhibited the same trend as CKD-stabilized specimens, under the effect of F-T action. Their M_r values (at σ_3 = 104 kPa, i.e., 20 psi and θ = 547.5 kPa, i.e., 80 psi) decreased from 6,199 MPa (900 ksi) to 957 MPa (139 ksi) as F-T cycles increased from 0 to 30. A similar qualitative trend was observed for the FBA specimens, where the M_r values exhibited a decrease as the number of F-T cycles increases up to 30. The decrease in resilient modulus values can be explained by the increase of moisture content during the thawing phase and the formation of ice lenses within the void space of the specimens. The effect of F-T action on M_r values varies from one stabilizing agent to another, as shown in Figure 3-5, where FBA stabilized specimens have the highest resilient modulus compared to CFA- and CKD-stabilized specimens.

3.6.3 Sawyer Aggregate Stabilized with CKD, CFA and FBA

Tables 3–7, 3–8 and 3–9 summarize the resilient moduli of Sawyer specimens stabilized with 15% CKD, 10% CFA and 10% FBA, respectively, and subjected to various F-T cycles. It is evident that the M_r at a given state of stress decreases with an increase in the number of F-T cycles. Figure 3-6 shows the variation of resilient

modulus (at σ_3 = 104 kPa, i.e., 20 psi and θ = 547.5 kPa, i.e., 80 psi) of Sawyer specimens stabilized with 15% CKD, 10% CFA and 10% FBA. The average resilient modulus (at the aforementioned stresses) of 10% CFA-stabilized specimens subjected to 30 F-T cycles is 1,625 MPa (236 ksi), as compared to 608 MPa (88 ksi), and 769 MPa (112 ksi) for 15% CKD- and 10% FBA-stabilized specimens, respectively. Laboratory observations revealed negligible degradation of specimens. Figure 3-7 shows a photographic view of the 15% CKD-stabilized Sawyer specimens after 30 F-T cycles with no visual degradation evident. From Figure 3-6, one can argue that 10% CFA specimens perform better with Sawyer aggregates than the 10% FBA and 15% CKD specimens. Consequently, one can conclude that the decrease in M_r values, which is an indication of durability, varies with the type of stabilizing agent. The degree of such variation can be explained by the amount of water absorbed during the thawing phase, which varies with the type of stabilizing agent. It is understandable that the more water is absorbed by specimens during the thawing phase, the more distortion is apparent in the specimens during the freezing phase (formation of ice lenses). It is believed that the mastic paste formed as a result of cementitious stabilization clogs the voids, at least partially. The degree of clogging varies from one stabilizing agent to another, and it determines the flow of moisture absorbed during the thawing process.

3.6.4 Hanson Aggregate stabilized with CKD and FBA

Hanson aggregates were stabilized with only CKD and FBA. Specimens were subjected to up to 30 F-T cycles. Summary of the resilient modulus values are given in Tables 3–10 and 3–11. The resilient modulus of Hanson specimens had the same

pattern as the other aggregate specimens. In other words, the resilient modulus showed a decrease as the number of F-T cycles increased from zero to 30.

3.7 Relative Comparison between F-T and W-D Cycles

As mentioned earlier, the regression parameters of (θ,σ_3) model for the resilient modulus of F-T cycles were determined to compare the influence of W-D cycles (from Chapter 2) and F-T cycles on the performance of stabilized aggregate bases. The model parameters, the M_r values, and the statistical analysis are summarized in Tables 3–12 to 3–22. From Tables 3–12 to 3–22, a frequency plot for the coefficient of determination (R^2) was generated, as shown in Figure 3-8. A total of 31 out of 43 established models reveal relatively high R^2 values between 0.8 and 1. From these Tables, it is evident that most of the models reveal high values of F-statistic, from which one can conclude that the employed model was statistically significant and could be used in predicting M_r values. Figure 3-9 shows a relative comparison between the resilient modulus as a result of F-T and W-D cycles. One can conclude that stabilized aggregate bases are more vulnerable to F-T cycles than W-D cycles.

3.8 Concluding Remarks

The effect of F-T action on the resilient modulus of aggregates stabilized with different stabilizing agents, namely, 15% CKD, 10% CFA and 10% FBA was evaluated. Results showed that the resilient modulus decreases as the F-T cycles increase up to 30. Such a decrease could be explained by the amount of water absorbed by the specimens during the thawing process. The more water absorbed, the more the distortion of specimens during the freezing phase due to the formation of ice lenses. It was also found that the degree of damage or distortion due to F-T action

was dependent on the type of stabilizing agent used. The F-T action had a higher effect on the CKD-stabilized specimens for Meridian and Richard Spur aggregates, than CFA and FBA stabilization. On the other hand, Sawyer specimens were found to perform better with CFA compared to CKD and FBA stabilization. Results also showed that F-T cycles had more negative influence on the resilient modulus of stabilized aggregate base than W-D cycles.

Table 3-1 M_r values of 15% CKD-stabilized Meridian aggregate subjected to F-T cycles

σ_3 (kPa)	σ_d (kPa)	σ_s (kPa)	M_r (MPa)					
			0 F-T cycle	Standard Deviation	8 F-T cycles	Standard Deviation	16 F-T cycles	Standard Deviation
138	69	28	1681	154	1026	71	417	57
138	138	28	1784	163	1054	84	429	72
138	208	28	2210	203	1101	96	460	80
138	277	28	2277	209	1125	110	513	88
104	69	28	1652	151	922	85	364	65
104	138	28	1718	157	976	86	432	65
104	208	28	1914	175	992	87	518	64
104	277	28	2152	197	1029	92	564	86
69	69	28	1619	148	903	76	394	61
69	138	28	1692	155	945	81	446	64
69	208	28	1849	169	960	54	530	65
69	277	28	2119	194	1019	87	588	78
35	69	28	1609	147	875	71	402	62
35	138	28	1688	155	927	87	456	62
35	208	28	1835	168	933	82	536	63
35	277	28	2368	217	1003	81	596	71
0	69	28	1612	148	859	75	407	60
0	138	28	1673	153	893	79	457	61
0	208	28	1796	165	918	82	533	59
0	277	28	2093	192	997	81	597	72

1 psi = 6.89 kPa; 1 ksi = 6.89 MPa
σ_d = Deviator Stress; σ_3 = Confining Pressure
σ_s = Seating Pressure

Table 3-2 M_r values of 10% CFA-stabilized Meridian aggregate subjected to F-T cycles

σ_3 (kPa)	σ_d (kPa)	σ_s (kPa)	M_r (MPa)							
			0 F-T cycle	Standard Deviation	8 F-T cycles	Standard Deviation	16 F-T cycles	Standard Deviation	30 F-T cycles	Standard Deviation
138	69	28	3049	119	1861	121	938	106	381	101
138	138	28	3150	126	1925	135	947	119	444	96
138	208	28	3611	133	2161	163	969	138	674	101
138	277	28	3740	166	2221	175	1067	143	437	129
104	69	28	2953	119	1649	101	828	98	336	85
104	138	28	3055	119	1736	105	951	93	448	72
104	208	28	3369	125	2015	110	1115	99	489	82
104	277	28	3392	166	2063	114	1092	109	326	88
69	69	28	2820	119	1741	98	856	84	373	78
69	138	28	2986	122	1847	96	966	89	373	67
69	208	28	3301	124	1911	107	1145	84	503	80
69	277	28	3380	166	1828	109	1141	89	280	86
35	69	28	2744	118	1657	91	850	82	333	78
35	138	28	2933	121	1787	93	969	89	365	65
35	208	28	3279	126	1863	105	1155	92	497	73
35	277	28	3367	149	1629	110	1050	101	454	89
0	69	28	2445	117	1449	89	764	80	257	73
0	138	28	2886	120	1715	89	961	85	334	67
0	208	28	3257	125	1861	101	1162	91	397	75
0	277	28	3313	148	1777	110	1143	101	367	80

1 psi = 6.89 kPa; 1 ksi = 6.89 MPa
σ_d = Deviator Stress; σ_3 = Confining Pressure
σ_s = Seating Pressure

Table 3-3 M_r values of 10% FBA-stabilized Meridian aggregate subjected to F-T cycles

σ_3 (kPa)	σ_d (kPa)	σ_s (kPa)	M_r (MPa)							
			0 F-T cycle	Standard Deviation	8 F-T cycles	Standard Deviation	16 F-T cycles	Standard Deviation	30 F-T cycles	Standard Deviation
138	69	28	4500	119	3067	110	1552	97	791	91
138	138	28	4761	126	3473	135	1718	119	907	96
138	208	28	5039	133	4069	151	2050	138	996	110
138	277	28	6290	166	4320	171	2119	139	1077	129
104	69	28	4502	119	3205	114	1502	104	764	85
104	138	28	4502	119	3493	105	1650	93	843	72
104	208	28	4732	125	3057	111	1728	99	873	84
104	277	28	6289	166	4049	107	1987	107	1051	88
69	69	28	4488	119	3185	95	1582	95	771	77
69	138	28	4619	122	3471	96	1593	87	825	67
69	208	28	4700	124	3082	110	1750	84	868	74
69	277	28	6290	166	3644	98	1905	99	1030	86
35	69	28	4445	118	3181	91	1518	88	747	79
35	138	28	4589	121	2986	94	1581	84	795	64
35	208	28	4746	126	3507	105	1763	82	877	77
35	277	28	5620	149	3878	108	1994	98	1016	85
0	69	28	4438	117	3057	92	1443	85	735	75
0	138	28	4553	120	2940	91	1529	83	764	63
0	208	28	4726	125	3298	104	1616	95	824	89
0	277	28	5575	148	3688	109	1844	98	997	84

1 psi = 6.89 kPa; 1 ksi = 6.89 MPa

σ_d = Deviator Stress; σ_3 = Confining Pressure

σ_s = Seating Pressure

Table 3-4 M_r values of 15% CKD-stabilized Richard Spur aggregate subjected to F-T cycles

σ_3 (kPa)	σ_d (kPa)	σ_s (kPa)	M_r (MPa)							
			0 F-T cycle	Standard Deviation	8 F-T cycles	Standard Deviation	16 F-T cycles	Standard Deviation	30 F-T cycles	Standard Deviation
138	69	28	4387	274	2778	154	1843	188	463	197
138	138	28	4636	290	2759	169	1922	220	511	205
138	208	28	4995	312	3059	189	2168	357	544	213
138	277	28	5516	344	4914	209	2279	373	597	245
104	69	28	4318	270	2711	254	1768	211	417	167
104	138	28	4401	275	2783	278	1758	190	504	187
104	208	28	4755	297	3106	263	1975	223	603	197
104	277	28	5121	320	4992	299	1814	189	668	206
69	69	28	4290	268	2690	245	1710	203	448	165
69	138	28	4332	271	2823	254	1708	172	516	186
69	208	28	4671	292	3076	262	1920	210	612	185
69	277	28	4969	310	4779	281	1787	187	687	205
35	69	28	3907	244	2733	228	1668	213	477	167
35	138	28	4084	255	2862	210	1827	205	541	173
35	208	28	4104	256	3231	231	1675	186	628	169
35	277	28	4736	296	5070	276	1774	181	717	203
0	69	28	3968	248	2713	220	1625	201	476	145
0	138	28	4191	262	2699	213	1787	208	533	171
0	208	28	4198	262	2906	235	1653	186	635	184
0	277	28	5148	321	4516	286	1736	181	719	202

1 psi = 6.89 kPa; 1 ksi = 6.89 MPa

σ_d = Deviator Stress; σ_3 = Confining Pressure

σ_s = Seating Pressure

Table 3-5 M_r values of 10% CFA-stabilized Richard Spur aggregate subjected to F-T cycles

σ_3 (kPa)	σ_d (kPa)	σ_s (kPa)	M_r (MPa)							
			0 F-T cycle	Standard Deviation	8 F-T cycles	Standard Deviation	16 F-T cycles	Standard Deviation	30 F-T cycles	Standard Deviation
138	69	28	5081	317	2907	210	2006	116	881	67
138	138	28	5529	345	2931	231	2336	126	922	76
138	208	28	6199	387	3147	256	2806	133	957	62
138	277	28	6579	411	3376	289	3539	137	1001	67
104	69	28	5013	313	2690	201	1998	109	773	55
104	138	28	5049	315	2853	217	2130	116	876	60
104	208	28	5140	321	3048	225	2312	128	948	65
104	277	28	5377	336	3324	271	3099	135	997	72
69	69	28	4893	306	2597	211	2000	108	794	60
69	138	28	5029	314	2758	213	2096	108	857	62
69	208	28	5046	315	2977	210	2265	132	944	56
69	277	28	5274	329	3199	245	2886	144	994	69
35	69	28	4994	312	2492	212	2001	107	777	57
35	138	28	5023	314	2761	219	2082	118	862	64
35	208	28	5050	315	2951	222	2258	126	935	69
35	277	28	5286	330	3156	245	2911	140	1004	72
0	69	28	4889	305	2471	211	2006	103	778	55
0	138	28	4974	311	2725	207	2087	119	878	65
0	208	28	5085	318	2912	221	2269	103	951	68
0	277	28	5147	321	3125	270	2887	140	1012	74

1 psi = 6.89 kPa; 1 ksi = 6.89 MPa

σ_d = Deviator Stress; σ_3 = Confining Pressure

σ_s = Seating Pressure

Table 3-6 M_r values of 10% FBA-stabilized Richard Spur aggregate subjected to F-T cycles

σ_3 (kPa)	σ_d (kPa)	σ_s (kPa)	M_r (MPa)							
			0 F-T cycle	Standard Deviation	8 F-T cycles	Standard Deviation	16 F-T cycles	Standard Deviation	30 F-T cycles	Standard Deviation
138	69	28	8691	543	5181	332	2968	213	1704	96
138	138	28	8838	552	5233	354	3262	259	1882	102
138	208	28	9062	566	5361	350	3494	309	2084	105
138	277	28	11070	691	5406	378	3711	377	2259	134
104	69	28	8798	549	4645	310	2863	213	1534	96
104	138	28	8956	559	4731	344	2908	234	1594	110
104	208	28	9404	587	7406	363	2920	290	1630	110
104	277	28	11675	729	6523	378	3037	345	2396	124
69	69	28	8832	552	5127	316	2963	218	1455	97
69	138	28	9120	570	5424	359	2732	244	1393	119
69	208	28	9788	611	6169	371	2827	319	1501	110
69	277	28	11987	749	6602	388	2807	356	1559	127
35	69	28	8880	555	5140	330	2852	235	1398	98
35	138	28	9142	571	5502	341	2740	249	1359	101
35	208	28	9665	604	5697	369	2725	293	1460	109
35	277	28	13030	814	6657	399	2749	348	1531	131
0	69	28	8900	556	5271	325	2745	228	1362	99
0	138	28	9205	575	5520	346	2666	255	1318	98
0	208	28	9803	612	6276	361	2673	345	1448	110
0	277	28	13296	830	6731	402	2697	393	1524	128

1 psi = 6.89 kPa; 1 ksi = 6.89 MPa

σ_d = Deviator Stress; σ_3 = Confining Pressure

σ_s = Seating Pressure

Table 3-7 M_r values of 15% CKD-stabilized Sawyer aggregate subjected to F-T cycles

σ_3 (kPa)	σ_d (kPa)	σ_s (kPa)	M_r (MPa)							
			0 F-T cycle	Standard Deviation	8 F-T cycles	Standard Deviation	16 F-T cycles	Standard Deviation	30 F-T cycles	Standard Deviation
138	69	28	3218	201	2166	168	1403	128	568	54
138	138	28	3646	228	2458	171	1480	138	592	51
138	208	28	4334	271	2641	207	1511	166	608	73
138	277	28	4820	301	2894	223	1617	170	677	74
104	69	28	3112	194	2175	165	1166	139	488	59
104	138	28	3447	215	2260	164	1293	143	512	54
104	208	28	3943	246	2563	198	1500	189	600	67
104	277	28	4546	284	2842	214	1668	191	677	50
69	69	28	3123	195	2177	167	1193	142	476	57
69	138	28	3408	213	2208	168	1314	150	526	53
69	208	28	3949	247	2522	184	1517	187	622	59
69	277	28	4306	269	2778	194	1701	188	680	53
35	69	28	3141	196	2184	172	1176	142	474	52
35	138	28	3338	208	2211	176	1295	149	518	53
35	208	28	4012	251	2527	188	1509	182	609	52
35	277	28	4134	258	2762	191	1701	191	708	55
0	69	28	3113	194	2211	163	1158	149	469	50
0	138	28	3377	211	2247	191	1280	159	512	61
0	208	28	3888	243	2515	191	1501	189	604	50
0	277	28	4063	254	2532	209	1699	189	679	52

1 psi = 6.89 kPa; 1 ksi = 6.89 MPa

σ_d = Deviator Stress; σ_3 = Confining Pressure

σ_s = Seating Pressure

Table 3-8 M_r values of 10% CFA-stabilized Sawyer aggregate subjected to F-T cycle

σ_3 (kPa)	σ_d (kPa)	σ_s (kPa)	M_r (MPa)							
			0 F-T cycle	Standard Deviation	8 F-T cycles	Standard Deviation	16 F-T cycles	Standard Deviation	30 F-T cycles	Standard Deviation
138	69	28	3872	169	3754	158	2743	124	1476	69
138	138	28	4177	182	3786	191	2989	139	1548	65
138	208	28	4701	205	3980	224	3161	139	1625	72
138	277	28	5751	251	4103	252	3298	144	1773	74
104	69	28	3884	169	3145	162	2472	91	1207	58
104	138	28	3898	170	3506	155	2789	104	1362	57
104	208	28	4001	174	3899	174	3088	124	1517	61
104	277	28	5557	242	4440	167	3329	141	1665	76
69	69	28	3862	168	3109	153	2556	85	1165	56
69	138	28	3892	170	3539	145	2773	91	1256	56
69	208	28	3996	174	3897	167	3083	108	1393	65
69	277	28	5151	225	4186	176	3335	126	1511	63
35	69	28	3762	164	3115	150	2549	67	896	54
35	138	28	3842	167	3387	144	2814	89	868	59
35	208	28	3944	172	3874	200	3088	106	1042	58
35	277	28	5110	223	4154	163	3326	110	1200	57
0	69	28	3803	166	2991	143	2549	67	661	53
0	138	28	3813	166	3532	154	2842	83	727	54
0	208	28	3838	167	3907	152	3116	105	784	51
0	277	28	4998	218	4237	162	3339	118	960	73

1 psi = 6.89 kPa; 1 ksi = 6.89 MPa

σ_d = Deviator Stress; σ_3 = Confining Pressure

σ_s = Seating Pressure

Table 3-9 M_r values of 10% FBA-stabilized Sawyer aggregate subjected to F-T cycle

σ_3 (kPa)	σ_d (kPa)	σ_s (kPa)	M_r (MPa)							
			0 F-T cycle	Standard Deviation	8 F-T cycles	Standard Deviation	16 F-T cycles	Standard Deviation	30 F-T cycles	Standard Deviation
138	69	28	4146	181	4825	289	1469	87	722	54
138	138	28	4617	201	4312	303	1603	105	816	48
138	208	28	4988	217	3563	316	1583	91	769	67
138	277	28	5222	228	3162	354	1462	115	703	87
104	69	28	4119	180	3011	257	1313	78	535	31
104	138	28	4306	188	2803	256	1310	80	554	34
104	208	28	4588	200	2952	246	1415	79	592	58
104	277	28	5002	218	3078	259	1482	74	640	54
69	69	28	4113	179	2822	214	1270	58	467	29
69	138	28	4254	185	2715	213	1308	64	524	32
69	208	28	4505	196	2922	232	1402	85	580	48
69	277	28	5344	233	3106	250	1507	73	630	65
35	69	28	4128	180	2880	195	1288	69	367	28
35	138	28	4236	185	2689	207	1305	63	434	31
35	208	28	4541	198	2899	191	1389	86	497	49
35	277	28	5241	228	3113	207	1506	82	551	41
0	69	28	4133	180	2812	165	1306	65	240	29
0	138	28	4204	183	2694	205	1310	72	327	31
0	208	28	4492	196	2845	200	1393	83	403	39
0	277	28	5358	234	3126	182	1524	93	467	41

1 psi = 6.89 kPa; 1 ksi = 6.89 MPa

σ_d = Deviator Stress; σ_3 = Confining Pressure

σ_s = Seating Pressure

Table 3-10 M_r values of 15% CKD-stabilized Hanson aggregate subjected to F-T cycles

σ_3 (kPa)	σ_d (kPa)	σ_s (kPa)	M_r (MPa)							
			0 F-T cycle	Standard Deviation	8 F-T cycles	Standard Deviation	16 F-T cycles	Standard Deviation	30 F-T cycles	Standard Deviation
138	69	28	2585	161	1260	107	625	92	228	46
138	138	28	2767	173	1321	94	677	73	265	44
138	208	28	2843	178	1493	103	712	69	285	44
138	277	28	3221	201	1562	123	756	94	312	57
104	69	28	2601	162	1145	105	528	74	217	46
104	138	28	2603	163	1171	96	571	70	242	32
104	208	28	2707	169	1229	96	653	101	284	45
104	277	28	3140	196	1336	98	740	70	317	48
69	69	28	2559	160	1097	91	474	71	201	47
69	138	28	2578	161	1133	101	528	74	237	35
69	208	28	2640	165	1205	93	613	98	277	47
69	277	28	2972	186	1254	107	701	70	315	21
35	69	28	2586	162	1072	90	435	66	207	38
35	138	28	2596	162	1103	91	497	52	234	32
35	208	28	2754	172	1184	89	583	49	275	45
35	277	28	3035	190	1192	98	669	67	314	38
0	69	28	2557	160	1042	98	395	53	195	46
0	138	28	2597	162	1087	87	458	50	231	45
0	208	28	2718	170	1166	102	549	54	272	30
0	277	28	2996	187	1178	102	643	79	315	41

1 psi = 6.89 kPa; 1 ksi = 6.89 MPa

σ_d = Deviator Stress; σ_3 = Confining Pressure

σ_s = Seating Pressure

Table 3-11 M_r values of 10% FBA-stabilized Hanson aggregate subjected to F-T cycles

σ_3 (kPa)	σ_d (kPa)	σ_s (kPa)	M_r (MPa)					
			0 F-T cycle	Standard Deviation	8 F-T cycles	Standard Deviation	30 F-T cycles	Standard Deviation
138	69	28	3440	215	2464	104	1726	68
138	138	28	3786	236	2513	108	1850	61
138	208	28	4129	258	2929	136	2141	77
138	277	28	4464	279	3351	133	2244	71
104	69	28	3392	212	2317	101	1427	84
104	138	28	3434	214	2446	111	1620	93
104	208	28	3525	220	2756	132	1815	72
104	277	28	3821	239	3316	120	1999	78
69	69	28	3405	213	1962	99	1121	96
69	138	28	3426	214	2398	101	1328	68
69	208	28	3455	216	2827	123	1526	94
69	277	28	3821	239	3255	145	1720	85
35	69	28	3362	210	1685	149	967	94
35	138	28	3392	212	1749	169	1017	95
35	208	28	3476	217	2188	150	1229	118
35	277	28	3751	234	2596	150	1420	131
0	69	28	3392	212	1595	142	744	60
0	138	28	3427	214	1693	150	837	89
0	208	28	3503	219	1962	144	911	101
0	277	28	3749	234	2495	150	1125	92

1 psi = 6.89 kPa; 1 ksi = 6.89 MPa

σ_d = Deviator Stress; σ_3 = Confining Pressure

σ_s = Seating Pressure

Table 3-12 A summary of the statistical analysis of CKD-stabilized Meridian specimens subjected to freeze-thaw cycles

	F-T cycles	$[M_r = k_1 \times (k_2)^{\sigma_3} \times k_3^{\theta})]$		R^2	Adjusted R^2	F value	P_r	Significant	M_r*
Meridian with 15% CKD	0	k_1	1341	0.87	0.85	56.26	<0.0001	Yes	1987
		k_2	0.99637						
		k_3	1.00141						
	8	k_1	677	0.90	0.89	74.3	<0.0001	Yes	772
		k_2	1.00047						
		k_3	1.00015						
	16	k_1	152	0.89	0.88	70.13	<0.0001	Yes	162
		k_2	0.99479						
		k_3	1.00111						

* M_r values calculated at σ_3 = 104 kPa and θ = 547.5 kPa

Table 3-13 A summary of the statistical analysis of CFA-stabilized Meridian specimens subjected to freeze-thaw cycles

	F-T cycles	$[M_r = k_1 \times (k_2)^{\sigma_3} \times k_3^{\theta})]$		R^2	Adjusted R^2	F value	P_r	Significant	M_r*
Meridian with 10% CFA	0	k_1	2393	0.90	0.89	25.85	<0.0001	Yes	3364
		k_2	0.99770						
		k_3	1.00106						
	8	k_1	1462	0.68	0.64	17.83	<0.0001	Yes	1949
		k_2	0.99928						
		k_3	1.00066						
	16	k_1	765	0.73	0.70	23.22	<0.0001	Yes	1046
		k_2	0.99584						
		k_3	1.00137						
	30	k_1	293	0.27	0.18	3.11	0.0708	n/a	433
		k_2	0.99953						
		k_3	1.00080						

* M_r values calculated at σ_3 = 104 kPa and θ = 547.5 kPa

Table 3-14 A summary of the statistical analysis of FBA-stabilized Meridian specimens subjected to freeze-thaw cycles

	F-T cycles	$[M_r = k_1 \times (k_2)^{\sigma_3} \times k_3^{\theta})]$		R^2	Adjusted R^2	F value	P_r	Significant	M_r*
Meridian with 10% FBA	0	k_1	3655	0.75	0.73	25.85	<0.0001	Yes	5243
		k_2	0.99632						
		k_3	1.00136						
	8	k_1	2638	0.64	0.60	15.06	0.0002	Yes	3649
		k_2	0.99781						
		k_3	1.00101						
	16	k_1	1252	0.91	0.89	81.69	<0.0001	Yes	1848
		k_2	0.99703						
		k_3	1.00128						
	30	k_1	621	0.93	0.92	105.85	<0.0001	Yes	943
		k_2	0.99658						
		k_3	1.00142						

* M_r values calculated at σ_3 = 104 kPa and θ = 547.5 kPa

Table 3-15 A summary of the statistical analysis of CKD-stabilized Richard Spur specimens subjected to freeze-thaw cycles

	F-T cycles	$[M_r = k_1 \times (k_2)^{\sigma_3} \times k_3^{\theta})]$		R^2	Adjusted R^2	F value	P_r	Significant	M_r*
Richard Spur with 15% CKD	0	k_1	3497	0.83	0.81	41.58	<0.0001	Yes	4831
		k_2	0.99813						
		k_3	1.00095						
	8	k_1	1890	0.75	0.72	25.98	<0.0001	Yes	3595
		k_2	0.99227						
		k_3	1.00265						
	16	k_1	1523	0.64	0.59	14.89	0.0002	Yes	1922
		k_2	0.99999						
		k_3	1.00043						
	30	k_1	402	0.95	0.95	172.43	<0.0001	Yes	583
		k_2	0.99341						
		k_3	1.00194						

* M_r values calculated at σ_3 = 104 kPa and θ = 547.5 kPa

Table 3-16 A summary of the statistical analysis of CFA-stabilized Richard Spur specimens subjected to freeze-thaw cycles

	F-T cycles	$[M_r = k_1 \times (k_2)^{\sigma_3} \times k_3^{\theta})]$		R^2	Adjusted R^2	F value	P_r	Significant	M_r*
Richard Spur 10% CFA	0	k_1	4474	0.57	0.51	11.04	0.0008	Yes	5469
		k_2	0.99946						
		k_3	1.00047						
	8	k_1	2261	0.97	0.96	234.06	<0.0001	Yes	3091
		k_2	0.99773						
		k_3	1.00100						
	16	k_1	1498	0.85	0.84	49.66	<0.0001	Yes	2608
		k_2	0.99492						
		k_3	1.00198						
	30	k_1	712	0.92	0.92	103.78	<0.0001	Yes	948
		k_2	0.99687						
		k_3	1.00112						

* M_r values calculated at σ_3 = 104 kPa and θ = 547.5 kPa

Table 3-17 A summary of the statistical analysis of FBA-stabilized Richard Spur specimens subjected to freeze-thaw cycles

	F-T cycles	$[M_r = k_1 \times (k_2)^{\sigma_3} \times k_3^{\theta})]$		R^2	Adjusted R^2	F value	P_r	Significant	M_r*
Richard Spur 10% FBA	0	k_1	7635	0.77	0.75	28.97	<0.0001	Yes	10136
		k_2	0.99506						
		k_3	1.00146						
	8	k_1	4672	0.63	0.59	14.72	0.0002	Yes	5788
		k_2	0.99570						
		k_3	1.00121						
	16	k_1	2560	0.65	0.61	15.71	<0.0001	Yes	2584
		k_2	0.99917						
		k_3	1.00017						
	30	k_1	1103	0.75	0.73	26.1	<0.0001	Yes	1797
		k_2	0.99969						
		k_3	1.00095						

* M_r values calculated at σ_3 = 104 kPa and θ = 547.5 kPa

Table 3-18 A summary of the statistical analysis of CKD-stabilized Sawyer specimens subjected to freeze-thaw cycles

	F-T cycles	$[M_r = k_1 \times (k_2)^{\sigma_3} \times k_3^{\theta})]$		R^2	Adjusted R^2	F value	P_r	Significant	M_r*
Sawyer with 15% CKD	0	k_1	2537	0.95	0.95	168.35	<0.0001	Yes	4027
		k_2	0.99563						
		k_3	1.00168						
	8	k_1	1867	0.90	0.89	76.6	<0.0001	Yes	2566
		k_2	0.99701						
		k_3	1.00115						
	16	k_1	1012	0.89	0.88	70.19	<0.0001	Yes	1526
		k_2	0.99573						
		k_3	1.00156						
	30	k_1	404	0.27	0.19	3.2	0.066	Yes	616
		k_2	0.99568						
		k_3	1.00159						

* M_r values calculated at σ_3 = 104 kPa and θ = 547.5 kPa

Table 3-19 A summary of the statistical analysis of CFA-stabilized Sawyer specimens subjected to freeze-thaw cycles

	F-T cycles	$[M_r = k_1 \times (k_2)^{\sigma_3} \times k_3^{\theta})]$		R^2	Adjusted R^2	F value	P_r	Significant	M_r*
Sawyer 10% CFA	0	k_1	3026	0.72	0.68	21.55	<0.0001	Yes	4586
		k_2	0.996						
		k_3	1.001						
	8	k_1	2746	0.88	0.86	60.78	<0.0001	Yes	3940
		k_2	0.996						
		k_3	1.001						
	16	k_1	2285	0.88	0.87	64.48	<0.0001	Yes	3099
		k_2	0.997						
		k_3	1.001						
	30	k_1	623	0.77	0.74	27.81	<0.0001	Yes	1493
		k_2	1.001						
		k_3	1.001						

* M_r values calculated at σ_3 = 104 kPa and θ = 547.5 kPa

Table 3-20 A summary of the statistical analysis of FBA-stabilized Sawyer specimens subjected to freeze-thaw cycles

	F-T cycles	$[M_r = k_1 \times (k_2)^{\sigma_3} \times k_3^{\theta})]$		R^2	Adjusted R^2	F value	P_r	Significant	M_r*
Sawyer 10% FBA	0	k_1	3579	0.77	0.75	28.97	<0.0001	Yes	4783
		k_2	0.99678						
		k_3	1.00114						
	8	k_1	2748	0.40	0.33	5.76	0.0123	Yes	3270
		k_2	1.00216						
		k_3	0.99991						
	16	k_1	1204	0.54	0.49	10.17	0.0012	Yes	1465
		k_2	0.99893						
		k_3	1.00056						
	30	k_1	271	0.87	0.86	58.67	<0.0001	Yes	656
		k_2	1.00072						
		k_3	1.00148						

* M_r values calculated at σ_3 = 104 kPa and θ = 547.5 kPa

Table 3-21 A summary of the statistical analysis of CKD-stabilized Hanson specimens subjected to freeze-thaw cycles

	F-T cycles	$[M_r = k_1 \times (k_2)^{\sigma_3} \times k_3^{\theta})]$		R^2	Adjusted R^2	F value	P_r	Significant	M_r*
Hanson with 15% CKD	0	k_1	2280	0.77	0.75	29.07	<0.0001	Yes	2853
		k_2	0.99788						
		k_3	1.00081						
	8	k_1	937	0.86	0.84	51.07	<0.0001	Yes	1303
		k_2	0.99924						
		k_3	1.00075						
	16	k_1	349	0.94	0.94	145.09	<0.0001	Yes	672
		k_2	0.99685						
		k_3	1.00180						
	30	k_1	167	0.96	0.96	237.06	<0.0001	Yes	281
		k_2	0.99467						
		k_3	1.00197						

* M_r values calculated at σ_3 = 104 kPa and θ = 547.5 kPa

Table 3-22 A summary of the statistical analysis of FBA-stabilized Hanson specimens subjected to freeze-thaw cycles

	F-T cycles	$[M_r = k_1 \times (k_2)^{\sigma_3} \times k_3^{\theta})]$		R^2	Adjusted R^2	F value	P_r	Significant	M_r*
Hanson 10% FBA	0	k_1	3003	0.69	0.65	18.79	<0.0001	Yes	3786
		k_2	0.99886						
		k_3	1.00064						
	8	k_1	1275	0.92	0.91	99.98	<0.0001	Yes	2821
		k_2	0.99697						
		k_3	1.00203						
	30	k_1	646	0.81	0.79	37.42	<0.0001	Yes	1784
		k_2	1.00048						
		k_3	1.00177						

* M_r values calculated at σ_3 = 104 kPa and θ = 547.5 kPa

Figure 3-1 Specimens subjected to freeze-thaw cycles using a rapid F-T cabinet

Figure 3-2 Meridian aggregate specimens stabilized with 15% CKD and subjected to 30 F-T cycles; specimens could not be tested due to excessive degradation

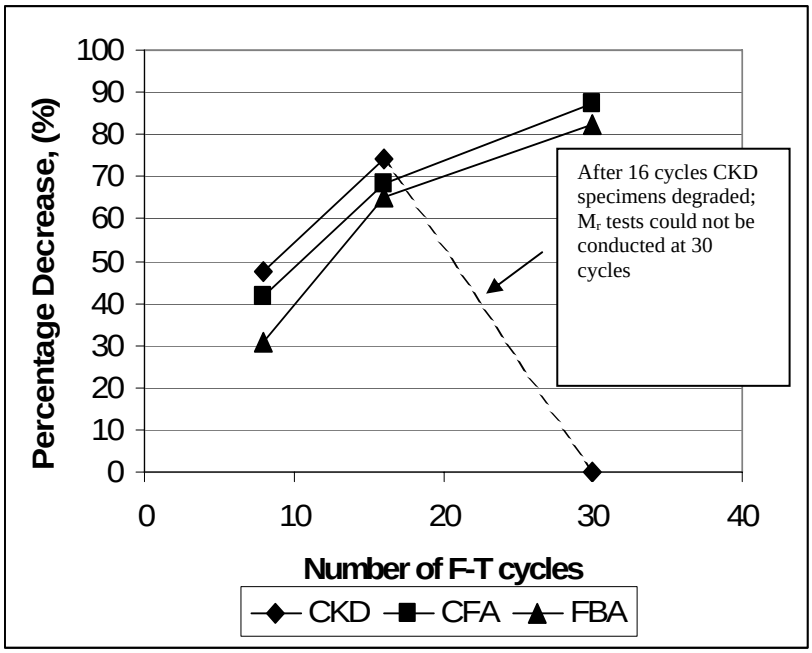

Figure 3-3 Percentage decrease in M_r values of Meridian-stabilized specimens due to F-T cycles

Figure 3-4 Richard Spur aggregate specimens stabilized with 15% CKD and subjected to 30 F-T cycles

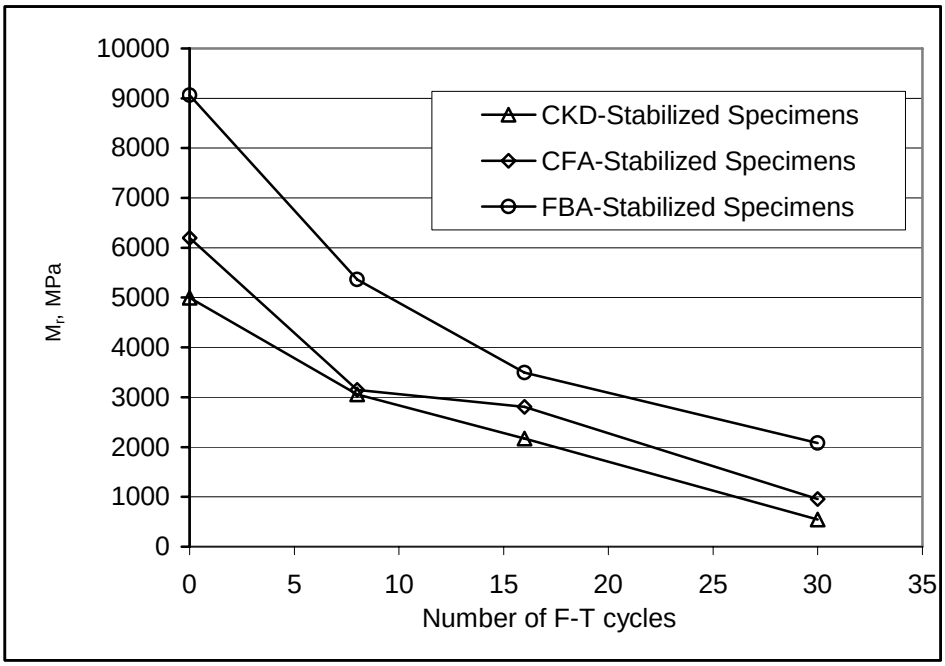

Figure 3-5 Variation of M_r values of Richard Spur-stabilized specimens with F-T cycles (at S_3 = 138 kPa and S_d = 208 kPa)

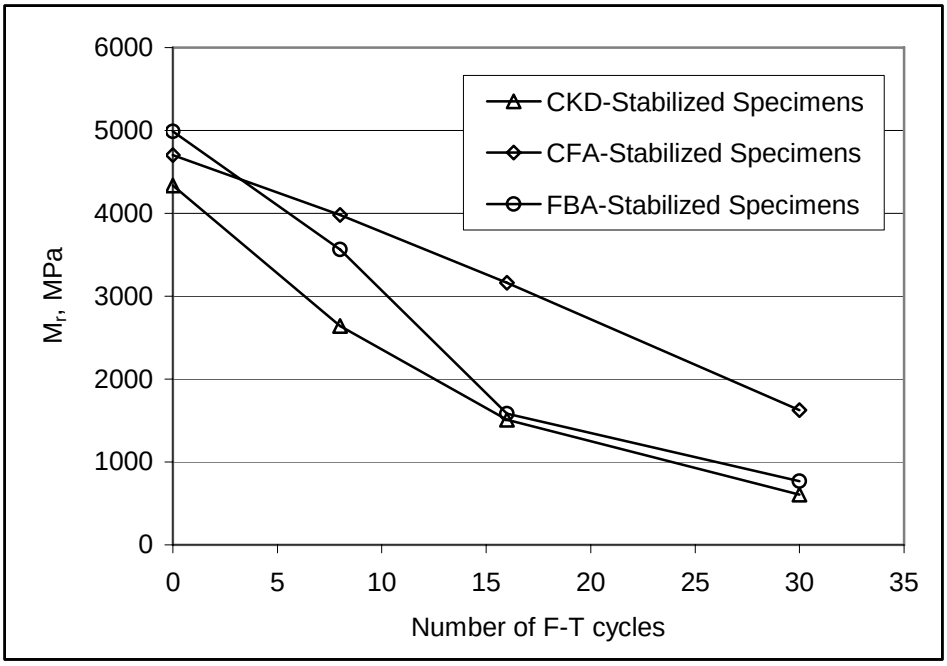

Figure 3-6 Variation of M_r values of Sawyer-stabilized specimens with F-T cycles (at S_3 = 138 kPa and S_d = 208 kPa)

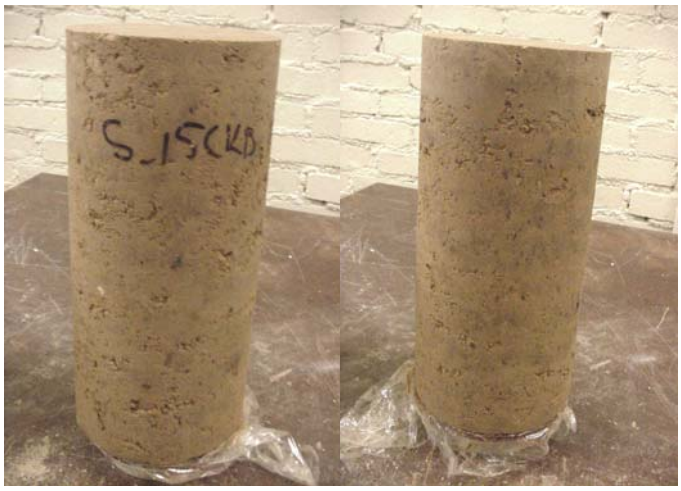

Figure 3-7 Sawyer specimens stabilized with 15% CKD and subjected to 30 F-T cycles

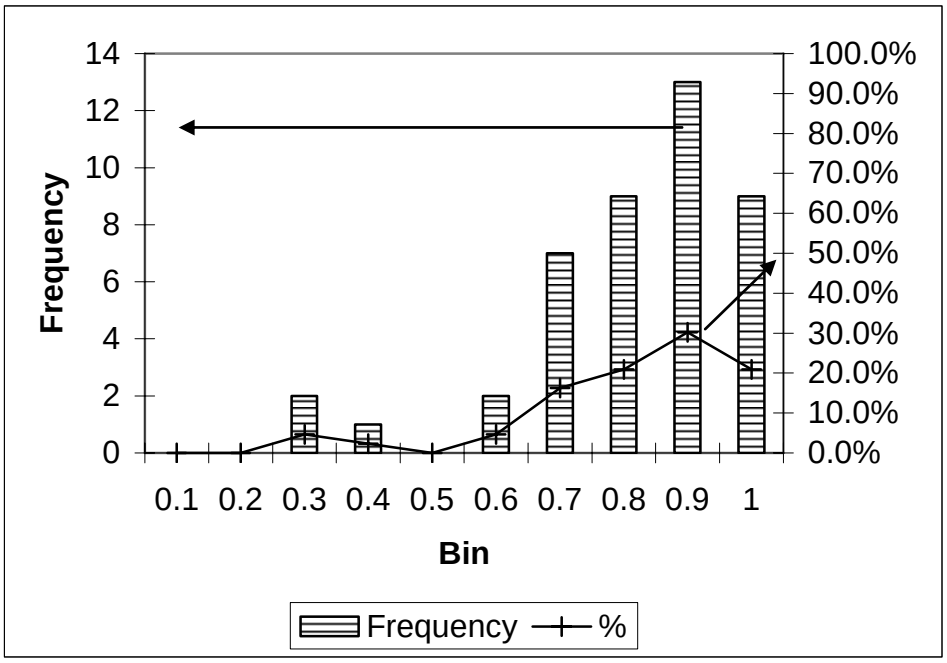

Figure 3-8 Frequency diagram for 43 observations

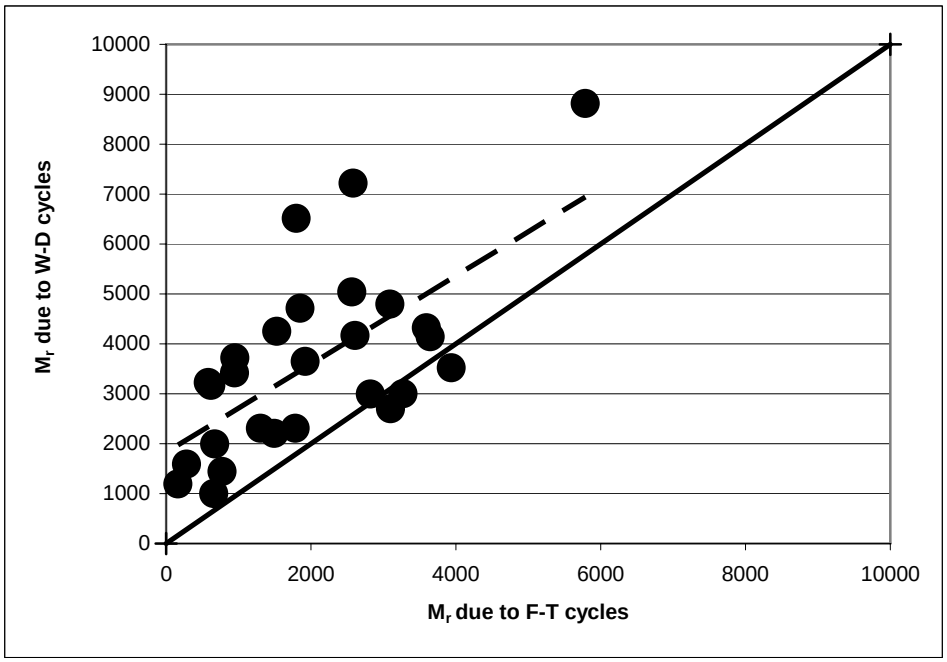

Figure 3-9 A relative comparison between F-T and W-D cycles

CHAPTER

4

DURABILITY EFFECTS ON FLEXURAL BEHAVIOR OF FLY ASH STABILIZED LIMESTONE AGGREGATE

4.1 Introduction

Aggregate base plays an important role in a flexible pavement structure. It provides the necessary support for the surface asphalt concrete (AC) layer and protects the subgrade from overstressing. With the depletion of good quality aggregates, efforts are being made to improve the engineering properties of aggregate base materials by stabilizing them with cementitious agents. When an unbound aggregate base is replaced by a stabilized base, the locations of critical stresses and strains change in the pavement cross-section, from the mechanistic standpoint (Sobhan, 1997; NCHRP, 1992). Thus, the evaluation of engineering properties such as flexural strength and modulus in flexure is important to the successful design of pavements. To this end, several studies have been undertaken to evaluate engineering properties of stabilized bases. For example, Sobhan (1997) evaluated the improvement in flexural strength due to the addition of fibers to recycled aggregates and Portland cement, with or without fly ash. It was reported that aggregates stabilized with cement and fly ash could develop adequate strength to serve as a high quality base course material. In a related study, Khoury et al. (2004) evaluated the flexural strength (or modulus of rupture) and resilient modulus of an aggregate base

stabilized with class C fly ash (CFA). Results showed that stabilized aggregates developed some flexural strength due to cementitious stabilization. Another study by NCHRP (1992) highlighted the importance of incorporating flexural behavior of a high strength stabilized base (HSSB) in pavement design. Stress-strain, strength and fatigue properties were reported. The new AASHTO 2002 Pavement Design Guide (PDG) recommends the modulus of rupture of stabilized materials as an input parameter in flexible pavement design (AASHTO, 2005).

Little attention, however, has been given in the past to the effect of durability, represented by freeze-thaw cycles, on flexural properties of a stabilized base. According to NCHRP (1992), durability of stabilized materials is a vital property that needs to be carefully considered in the pavement design process. As mentioned previously in Chapters 2 and 3, a paper entitled ″Millennium paper: Cementitious Materials,″ posted on the Transportation Research Board website, highlights the importance of establishing a rapid test to assess the impact of durability, namely, wet-dry (W-D) and freeze-thaw (F-T) cycles on stabilized materials (Little et al., 2005). Furthermore, the new PDG highlights the importance of environmental conditions on the performance of both flexible and rigid pavements. Such factors usually influence the underlying layers (base and subgrade), but eventually lead to visible distresses in the pavement surface (AASHTO, 2005).

Several methods are currently available for evaluating the influence of F-T cycles on stabilized pavement materials. The ASTM D 560 test is intended to investigate the durability of compacted soil-cement mixtures. The Iowa freeze-thaw test is similar to the ASTM D 560 method. The ASTM C 593, developed by Dempsey and

Thompson (1973), evaluates the compressive strength of vacuum-saturated specimens. Other test procedures have also been reported (see e.g., Zaman and Khoury, 2003; Berg, 1998). None of these laboratory procedures, however, evaluate the effect of F-T durability on flexural properties. Additional studies are needed to establish acceptable laboratory procedures.

The present study evaluates the effect of F-T cycles on resilient modulus in flexure and flexural strength, as determined by modulus of rupture of stabilized beams that are representative of a stabilized aggregate base under cyclic loading. The effect of curing period on these properties is investigated. Three different curing periods, namely, 1 hour, 3 days and 28 days, are considered. Also, an attempt is made to examine the influence of different F-T procedures on the flexural response of selective specimens.

4.2 Specimen Preparation

Meridian, the aggregate base, and class C fly ash, the stabilizing agent, were used to prepare the specimens; their properties are described in chapter 2. A new laboratory compaction procedure was employed in molding the specimens used in this study. The procedure consisted of the following steps: (1) mixing raw aggregates thoroughly in a mechanical mixer to obtain a uniform mixture; (2) adding a specified amount of CFA (10% of dry weight of aggregate) and mixing thoroughly with the raw aggregate (10% of CFA is considered the optimum additive content as reported by Zaman et al., 1998); (3) adding half of the required water to the aggregate-CFA mixture and mixing thoroughly; (4) adding the remaining water and mixing thoroughly until a uniform mixture was achieved. The resulting mixture used to

prepare one specimen was divided into three parts, each weighing approximately 9.66 kg (21.25 lb), and the specimens were covered to minimize any moisture loss. A split compaction mold was designed and fabricated for this purpose (see Figure 4-1). The mold is 53.34 cm (21 in.) long, 15.24 cm (6 in.) wide and 21.59 cm (8.5 in.) deep. The bottom of the mold consists of two layers. The lower layer is a rectangular plate (53.34 cm x 15.24 cm x 1.91 cm, i.e., 21 in. x 6 in. x ¾ in.) that can be bolted to the rest of the mold. The top layer consists of three removable rectangular plates: one central plate (38.10 cm x 15.24 cm x 1.91 cm, i.e., 15 in. x 6 in. x ¾ in.) and two edge plates (7.62 cm x 15.24 cm x 1.91 cm, i.e., 3 in. x 6 in. x ¾ in.). The central plate (Part A in Figure 4-1) is used to lift the beam once it is extracted from the mold. This method helps reduce any disturbances to the beam specimen while placing it in the freeze-thaw cabinet or placing it in the testing machine. Each specimen was compacted at the optimum moisture content (OMC) (7.0%) and maximum dry density (MDD) (21.7 kN/m^3, i.e., 137.8 pcf).

Each specimen was compacted in three layers. Material for each layer (approximately 9.66 kg, i.e., 21.25 lb) was poured and compacted in the mold by applying pressure with the help of an MTS frame, until the compacted height of each layer was 5.08 cm (2 in.). The average time for preparing a specimen varied between 30 and 45 minutes. Visual observations revealed that the sample preparation method employed here kept the breakage of aggregates during the compaction process to a minimum. No gradation tests on specimens already subjected to compaction were performed.

Following the compaction process, each specimen was wrapped carefully with a

plastic wrap and placed in a humidity chamber for curing over a selected period of time. A rapid freeze-thaw cabinet, having automated control of freezing and thawing, was used as a humidity chamber for curing. The F-T cabinet is capable of maintaining a constant temperature and high relative humidity. Specimens were cured at a constant temperature of approximately 21ºC (70ºF) and a relative humidity of 95% ± 1%. A total of 45 specimens were prepared for this laboratory study, of which 15 were cured for 1 hour, 15 for 3 days, and the remaining 15 for 28 days. The specimens cured for 1 hour were subjected to F-T cycles without being placed in the humidity chamber; preparation of each of these specimens took approximately one hour. After curing, specimens were subjected to a number of selected F-T cycles (0, 8 and 16) prior to testing for flexural strength and modulus in flexure.

4.3 Freeze-Thaw Cycles

Two freeze-thaw procedures were employed in this study. The first procedure (FT-1) consisted of freezing a cured specimen at –25^{o}C (-13^{o}F) in the freeze-thaw cabinet for 24 hours, and then thawing it at 21.7^{o}C (71^{o}F) for another 24 hours at a relative humidity of approximately 98%.

The second procedure (FT-2) used a specially fabricated mold that was designed to place a compacted beam specimen in direct contact with a saturated layer (mold) underneath. The mold was filled with loose aggregate of uniform size (approximately equal to the opening of a No. 10 sieve), as shown photographically in Figure 4-2. Water was fed to these aggregates during the thawing phase, and drained out during the freezing phase so that no heave pressure was built up and exerted on the stabilized beam specimen. The beam specimen and the mold were placed in the F-T cabinet

under the aforementioned temperature and humidity conditions. Efforts were made to keep migration of water from the bottom, by wrapping the mold and the specimen with a plastic wrap. This procedure is believed to better simulate the field condition similar to that of a stabilized base resting on a saturated subgrade. Figure 4-3 shows a photographic view of specimens being subjected to F-T cycles in the freeze-thaw cabinet.

4.4 Resilient Modulus and Flexural Strength Tests

Currently, there is no widely accepted laboratory test procedure to determine the resilient modulus of stabilized beams under flexural loading. Mitchell and Shen (1967) determined the resilient modulus of soil-cement specimens, from both triaxial compression and flexural tests, after 1,000 load repetitions. Sobhan (1997) reported the resilient modulus after subjecting beam specimens to 5% of their fatigue lives. In the present study, the following laboratory resilient modulus test procedure was employed.

The test procedure consisted of applying six stress sequences, as listed in Table 4-1. Each test sequence consisted of a haversine-shaped pulse load having a duration of 0.1 s and a relaxation period of 0.9 s; a total of 100 cycles were applied for each sequence. The load-deformation response was recorded continuously during the cyclic flexure test. A 22.7 kN (5000-lb) load cell was used to apply the load, and two LVDTs with a stroke length of 0.508 cm (0.2 in.) were used to measure the deformation at the midspan of the beam (e.g., 7.62 cm (3 in.) from the centerline of the beam), as illustrated in Figure 4-4.

The elastic or resilient modulus values were calculated from the midspan

deflection using the elastic beam theory for third-point loading, as given by Eq. (4-1) (Sobhan 1997; Huang, 2004):

$$M_{rf} = \frac{23PL^3}{108bh^3\Delta} \qquad \textbf{(4-1)}$$

where M_{rf} is the resilient modulus in flexure, P is the magnitude of repeated load, b is the width of the beam, h is the height of the beam, and Δ is the recoverable cyclic midspan deflection, L is the span length; units that are consistent with the SI system were used in Eq. 4-1. The recoverable deformations from the last five cycles of a 100-cycle sequence were used to calculate the resilient modulus.

The flexural strength test, to evaluate the modulus of rupture, was performed in accordance with the ASTM D 1635-00 test method. As mentioned earlier, a total of 15 specimens were prepared for each curing period. These specimens were divided into three groups. The first group, consisting of five specimens, was subjected to no F-T cycles (i.e., tested directly after curing). The five specimens in the second group were subjected to 8 F-T cycles, and the specimens in the third group were subjected to 16 F-T cycles. The five-replicate specimens were then divided into two sets: (1) the first set consisted of one specimen tested only for modulus of rupture; and (2) the second set consisted of four specimens tested for M_{rf}, and then for modulus of rupture (MOR). The MOR value from the first set was compared to the values in Table 4-1. If the MOR value was within the range of stress, the M_{rf} test was carried out to the sequence with a flexural stress lower than the MOR. If not, the test was carried out to the fifth sequence. This approach was found useful in preventing failure of specimens during the resilient modulus testing. On the other hand, this method did not fully prevent the failure of some specimens during the M_{rf} test, specifically for

those specimens that were only cured for one hour. This is due to the fact the there is always some variability in the strength of specimens for different replicates.

4.5 Effect of F-T Cycles on M_{rf} in Flexure

One way to evaluate the effect of F-T cycles on the M_{rf} values is to observe the changes in M_{rf} values at a specific flexural stress level. The following model was used for this purpose:

$$M_{rf} = M_{rfo} \times A^{F_S} \qquad \textbf{(4-2)}$$

where M_{rf} is the resilient modulus at a given flexural stress (F_S), M_{rfo} (modulus when $F_S = 0$) and A is a model parameter. This model has been used previously in other studies to predict the resilient modulus of pavement materials in flexure. According to Huang (2004), Witczak and Root (1974) used this model to evaluate the dynamic modulus of asphalt using the third-point beam test method. Sobhan (1997) used a similar model to evaluate the resilient modulus in flexure of a stabilized fiber-reinforced pavement base course with recycled aggregates.

The model parameters for all the stabilized beams, with and without any F-T cycles, are summarized in Tables 4–2, 4–3 and 4–4. The models along with their parameters were tested statistically (*t*-test and *F*-test) to observe their statistical significance. Results showed that the regression models and their parameters are sufficient to predict M_{rf} from flexural stress. Tables 4–2, 4–3 and 4–4 also show the predicted values of M_{rf} at a flexural stress of 20.7 kPa (3 psi); F_S of 20.7 kPa (3 psi) was selected because it falls within the stress level applied to specimens.

The results for 1-hour cured specimens showed that the M_{rf} values decreased as F-T cycles increased up to 16. For example, the M_{rf} values are approximately 1,645

MPa (239 ksi), 992 MPa (144 ksi) and 347 MPa (50 ksi), for specimens subjected to 0, 8 and 16 cycles, respectively. Approximately a 79% reduction in the average M_{rf} value of 1-hour cured specimens is noticed as F-T cycles increased from zero to 16. In addition, the actual values, predicted values, and the 95% confidence interval for mean M_{rf} values are plotted in Figure 4-5 in terms of flexural stress and number of F-T cycles. In Figure 4-5, one point is identified as an outlier for specimens subjected to 16 cycles. That point was removed in determining the final regression model parameters. The influence of F-T cycles is also revealed in the degradation of the specimens. Figure 4-6 shows a photographic view of accelerated specimen degradation with increasing F-T cycles. A specimen subjected to 16 F-T cycles has a significantly reduced modulus, and it is more vulnerable to failure. The extent of decrease in modulus and increased degradation is associated with the amount of water available and pore geometry. Laboratory results showed that the moisture content of specimens increased by approximately 2%, after 16 F-T cycles. It is logical to assume that this added moisture saturated more pores, and ice lenses formed in the fine matrix during the freezing cycles, causing destruction in the particle matrix.

Table 4-3 shows that M_{rf} values (at the aforementioned stress level) of 3-day cured specimens exhibited a decrease, as the F-T cycles increased up to 16. The average M_{rf} value decreased from 3,426 MPa (497 ksi) to 720 MPa (104 ksi) as F-T cycles increased to 16. Figure 4-7 also shows the effect of F-T cycles on the resilient modulus. Overall, a reduction in M_{rf} is observed; the percentage of reduction being a function of the number of F-T cycles and flexural stress. Laboratory observations reveal that specimen degradation, after 16 cycles, occurred but was less severe than in

the case of 1-hour cured specimens.

As for 28-day cured specimens, the variations in resilient modulus values are shown in Figure 4-8 and summarized in Table 4-4. From the data in Table 4-4, the average M_{rf} value is approximately 5,248 MPa (762 ksi), compared to 943 MPa (137 ksi) after 16 cycles. Overall, M_{rf} exhibited the same trend as for the cases of 1-hour and 3-day cured specimens. Magnitude-wise, the 28-day cured specimens are less vulnerable to F-T actions, as expected. The average M_{rf} value is 943 MPa (137 ksi), compared to 720 MPa (104 ksi) for specimens cured for 3 days, and 347 MPa (50 ksi) for specimens cured for 1 hour, after 16 F-T cycles. The influence of curing time on the performance of the stabilized beams was also evident through visual observations of specimens.

Figure 4-9 shows a photographic view of specimens cured for 1-hour, 3 days and 28 days, and subjected to 16 F-T cycles. The extent of degradation depends upon the amount of water absorbed by the specimens during the thawing phase, the pressure exerted by the ice lenses within the pores, and the bonding between different particles in the matrix

4.6 Effect of F-T Cycles on Modulus of Rupture

The variation of MOR with the number of F-T cycles is shown in Figure 4-10, where the results for 1-hour, 3-day and 28-day cured specimens are summarized. A summary of the MOR values along with the standard deviation and coefficient of variation is presented in Table 4-5. It can be observed that the modulus of rupture decreased with the F-T cycles, which was consistent with the behavior of M_{rf}. The average moduli of rupture for 1-hour cured specimens subjected to 0, 8 and 16 cycles

are approximately 51 kPa (7.4 psi), 45 kPa (6.5 psi) and 25 kPa (3.6 psi), respectively.

The moduli of rupture for 3-day specimens subjected to 8 and 16 cycles were approximately 45% and 73% lower, respectively, than those for specimens not subjected to any F-T cycles. The average MOR value for 3-day specimens without any freeze-thaw actions was 190 kPa (27.6 psi). Additionally, from Figure 4-10 and Table 4-5 the MOR values for 28-day cured specimens subjected to 0, 8 and 16 cycles are 330 kPa (47.9 psi), 232 kPa (33.6 psi) and 113 kPa (16.4 psi), respectively. Since some specimens exhibited significant degradations due to freeze-thaw actions, significant reductions in modulus of rupture due to F-T actions are expected.

4.7 Correlation between M_{rf} and Stress Ratio

From the aforementioned results, it is evident that resilient modulus varies with the magnitude of the applied cyclic flexural stress. To better illustrate such behavior, the resilient modulus values for all specimens are plotted against the corresponding stress ratios (applied cyclic flexural stress to flexural stress) in Figure 4-11. It is observed that the resilient modulus sharply decreases as the stress ratio increases from approximately 0.1 to 0.6; however, further increase in stress ratio from about 0.6 to 0.95 does not have any significant influence on the resilient moduli. Sobhan (1997) reported similar observations, where the range of stress ratio varied from 0.7 to 0.9. If all data points are considered together to identify a trend, it is evident that M_{rf} decreases with increasing stress ratio, but the R^2 value is rather low, about 0.54.

4.8 Effect of New F-T Procedure

Since no widely accepted laboratory procedure is available, efforts were made in

this study to analyze the effect of different laboratory procedures (FT-1 and FT-2) on the stabilized beams. To this end, two additional specimens were molded according to the method (FT-2) described earlier, cured for 28 days, and subjected to only 8 FT-2 cycles. After 8 FT-2 cycles, excessive degradation was observed in both of these specimens, as shown in Figure 4-12. Neither resilient modulus tests nor strength tests could be performed on these specimens. Laboratory results indicate that the average moisture content increased by approximately 2.3% after 8 FT-2 cycles. This increased moisture was apparently more than enough to cause excessive degradation. From the comparison of results from the FT-1 and FT-2 procedures, the latter procedure, which is similar to what may be experienced in the field, is found to be more destructive.

4.9 Concluding Remarks

The effect of F-T cycles on the flexural properties of a CFA-stabilized Meridian aggregate was examined. Stabilized-beam specimens were molded, cured, and then subjected to different numbers of F-T cycles. After curing, specimens were tested for modulus in flexure and modulus of rupture (MOR). Results revealed that M_{rf} values and MOR decreased as F-T cycles increased from 0 to 16 cycles. The degree of influence of F-T cycles varied with the curing period and the number of F-T cycles. Twenty-eight day cured specimens were found to be less vulnerable to F-T cycles than three-day specimens, followed by 1-hour cured specimens. In addition, the effect of two different F-T cycles procedures was examined. It was found that different F-T procedures produced different effects. The FT-2 procedure, which is believed to better simulate the field condition, caused more damage to 28-day cured

specimens (after eight cycles) compared to FT-1. Also, a variation of M_{rf} with stress ratio was observed, where M_{rf} was found to decrease with increasing stress ratio.

Table 4-1 Loading sequences used in flexural resilient modulus testing

Sequence No.	Cyclic Flexural Stress (kPa)	Cyclic Flexural Stress (psi)	*Contact Stress (kPa)	*Contact Stress (psi)	Number of Cycles
0	24.8	3.6	2.8	0.4	500
1	12.4	1.8	1.4	0.2	100
2	24.8	3.6	2.8	0.4	100
3	37.2	5.4	4.1	0.6	100
4	49.6	7.2	5.5	0.8	100
5	62.0	9	6.9	1	100

* Contact load between the load cell and the beam to insure full contact. The applied load produces a flexure stress (10% of the total applied cyclic stress) reported in the column above, and is known as contact stress in this study.

Table 4-2 Model parameters for 1-hour cured specimens

F-T cycles	Model parameters [$M_{rf} = M_{rfo}(A)^{FS}$)]				R^2	Adjusted R^2	F value	P_r	M_{rf}*
0	M_{rfo}	2097	t value	88.45	0.65	0.61	16.63	0.0028	1645
			Pr	<0.0001					
			95% CL	1724					
				2549					
	A	0.99	t value	-4.08					
			Pr	0.0028					
			95% CL	0.982					
				0.995					
8	M_{rfo}	1375	t value	62.92	0.62	0.58	14.78	0.0039	992
			Pr	<0.0001					
			95% CL	1060					
				1783					
	A	0.98	t value	-3.84					
			Pr	0.0039					
			95% CL	0.976					
				0.994					
16	M_{rfo}	2161	t value	50.19	0.95	0.94	78.12	0.0009	347
			Pr	<0.0001					
			95% CL	1413					
				3305					
	A	0.92	t value	-8.84					
			Pr	0.0009					
			95% CL	0.894					
				1.062					

* Predicted M_{rf} at F_S = 21 kPa (3 psi)

Table 4-3 Model parameters for 3-day cured specimens

F-T cycles	Model parameters [$M_{rf} = M_{rfo}(A)^{FS}$)]				R^2	Adjusted R^2	F value	P_r	M_{rf}*
0	M_{rfo}	4771	t value	35.560	0.476	0.4358	11.81	0.0044	3426
			Pr	0.000					
			95% CL	2852					
				7981					
	A	0.98	t value	-3.440					
			Pr	0.004					
			95% CL	0.975					
				0.994					
8	M_{rfo}	2674	t value	32.600	0.6707	0.6472	28.52	0.0001	1694
			Pr	0.000					
			95% CL	1591					
				4495					
	A	0.98	t value	-5.340					
			Pr	0.000					
			95% CL	0.970					
				0.987					
16	M_{rfo}	1578	t value	26.970	0.6331	0.5965	17.26	0.002	720
			Pr	0.000					
			95% CL	859					
				2899					
	A	0.96	t value	-4.150					
			Pr	0.002					
			95% CL	0.944					
				0.983					

* Predicted M_{rf} at F_S = 21 kPa (3 psi)

Table 4-4 Model parameters for 28-day cured specimens

F-T cycles	Model parameters [$M_{rf} = M_{rfo}(A)^{FS}$)]				R^2	Adjusted R^2	F value	P_r	M_{rf}*
0	M_{rfo}	7528	t value	32.63	0.55	0.51	13.45	0.0037	5248
			Pr	<0.0001					
			95% CL	4123					
				13745					
	A	0.98	t value	-3.67					
			Pr	0.0037					
			95% CL	0.973					
				0.993					
8	M_{rfo}	3383	t value	63.95	0.71	0.69	40.91	<0.0001	2330
			Pr	<0.0001					
			95% CL	2587					
				4423					
	A	0.98	t value	-6.40					
			Pr	<0.0001					
			95% CL	0.977					
				0.988					
16	M_{rfo}	1309	t value	69.63	0.75	0.73	44.01	<0.0001	943
			Pr	<0.0001					
			95% CL	1051					
				1631					
	A	0.98	t value	-6.63					
			Pr	<0.0001					
			95% CL	0.980					
				0.989					

* Predicted M_{rf} at F_S = 21 kPa (3 psi)

Table 4-5 A summary of MOR values

Curing Time	Number of F-T Cycles	MOR_{avg} (kPa)	*Stdev*	*COV*
1 hour	0	51	7.2	14
	8	45	5.9	13
	16	25	1.6	7
3 Days	0	190	42.0	22
	8	103	15.2	15
	16	51	5.7	11
28 Days	0	330	46.6	14
	8	232	21.6	9
	16	113	12.8	11

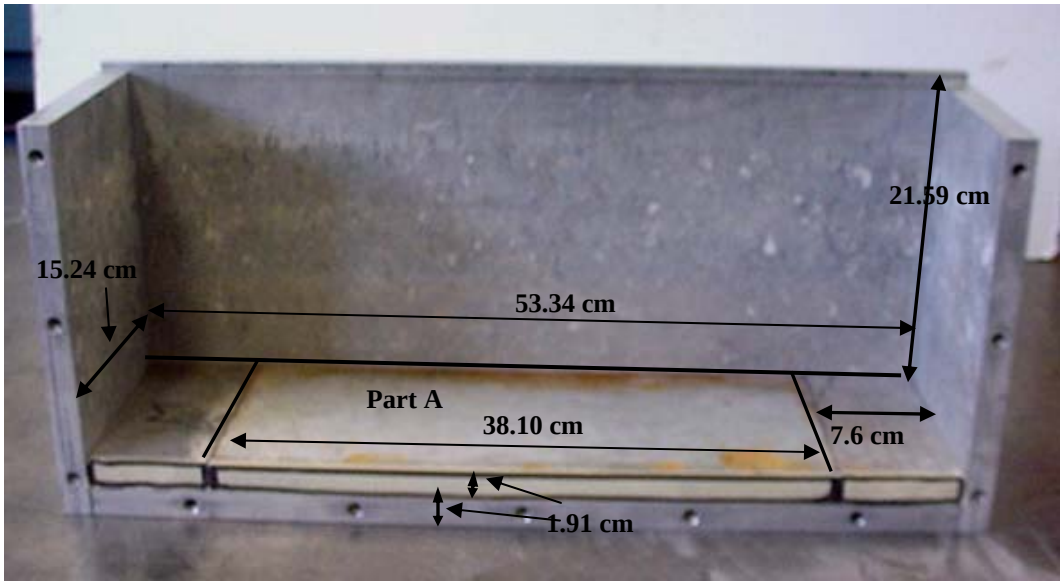

Figure 4-1 Photograph showing the sample preparation mold

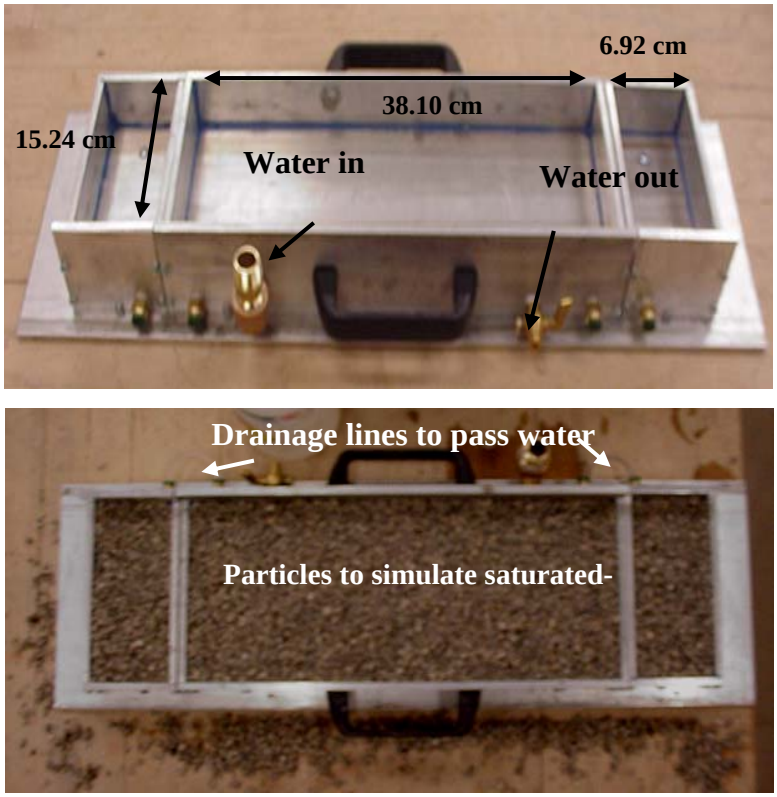

Figure 4-2 Photographic view showing the assembly of the manufactured mold for FT-2 procedure

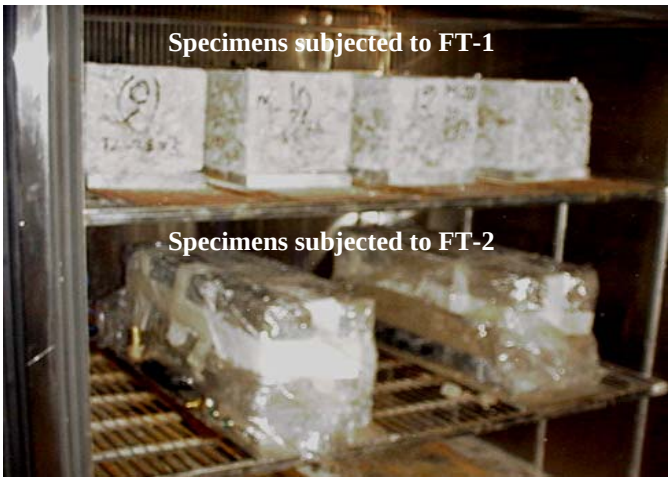

Figure 4-3 Specimens subjected to FT-1 and FT-2 procedures

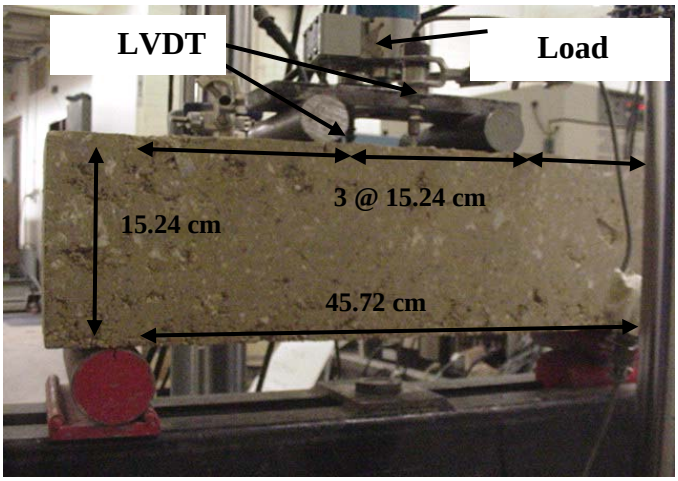

Figure 4-4 Testing setup for resilient modulus and flexural strength

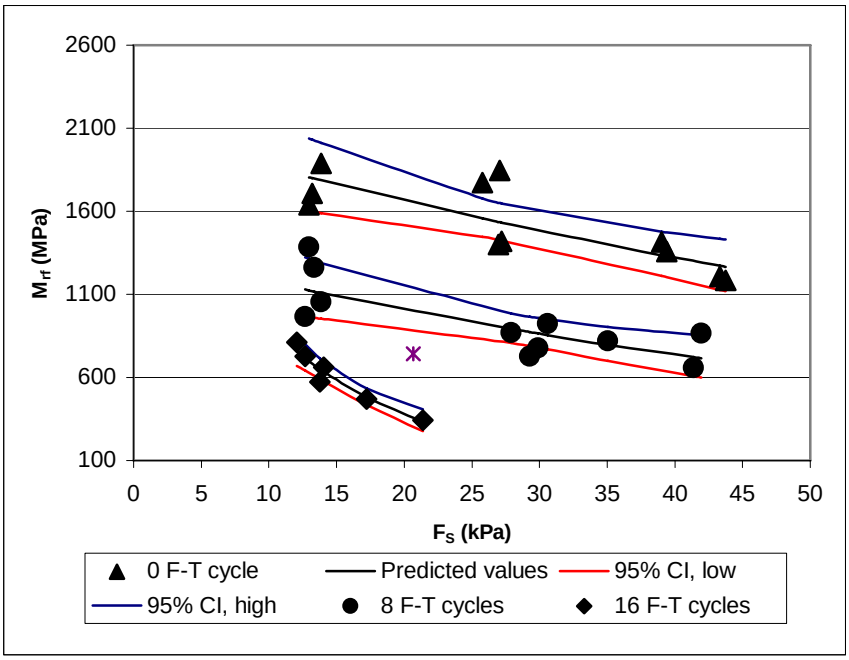

Figure 4-5 Variation of resilient modulus in flexure with cyclic flexural stress and F-T cycles for 1-hour cured specimens (FT-1 procedure).

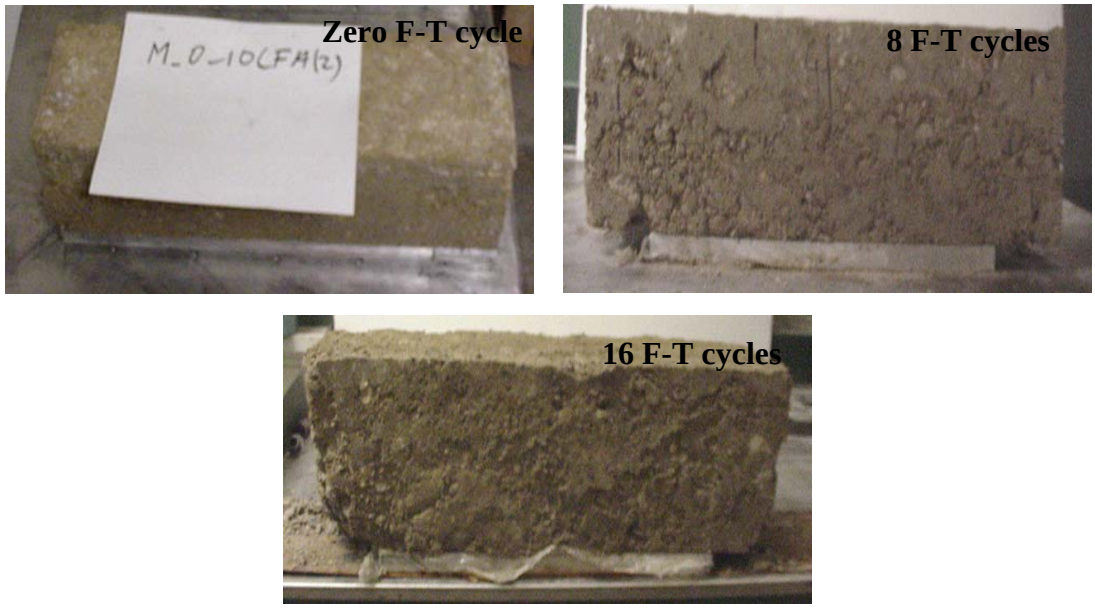

Figure 4-6 Photograph showing 1 hour stabilized specimens subjected to 0, 8 and 16 F-T cycles (FT-1 procedure).

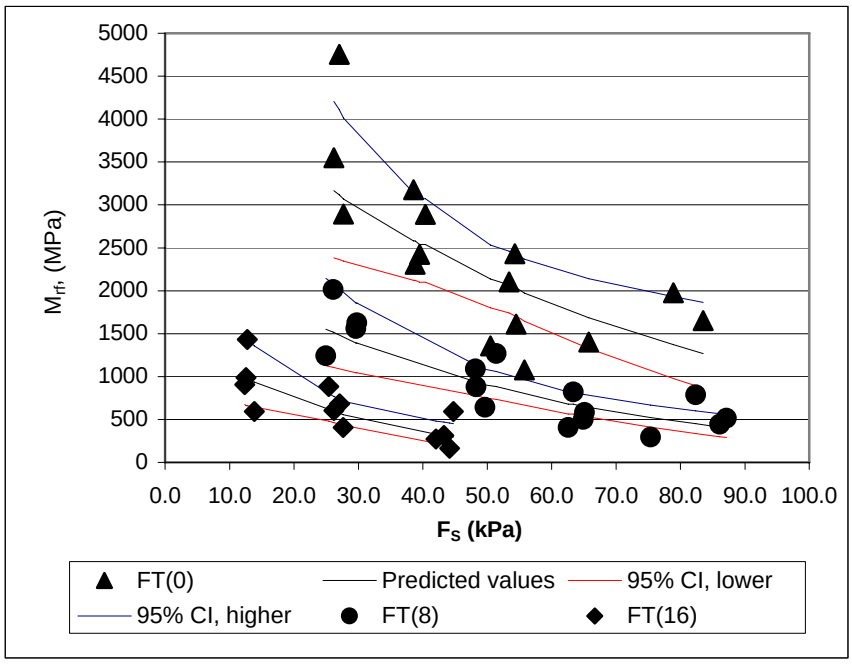

Figure 4-7 Variation of resilient modulus in flexure with cyclic flexural stress and F-T cycles for 3-day cured specimens (FT-1 procedure).

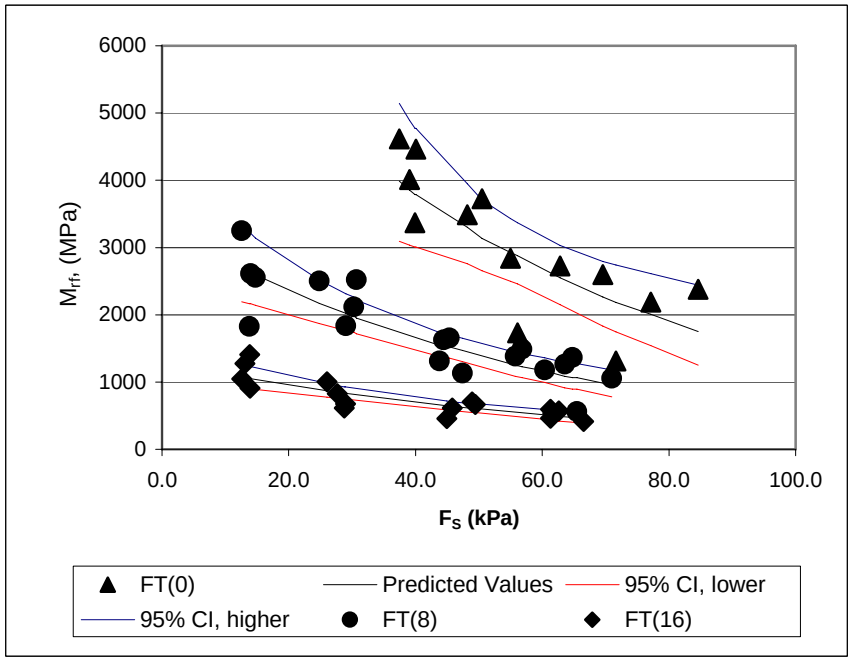

Figure 4-8 Variation of resilient modulus in flexure with cyclic flexural stress and F-T cycles for 28-day cured specimens (FT-1 procedure).

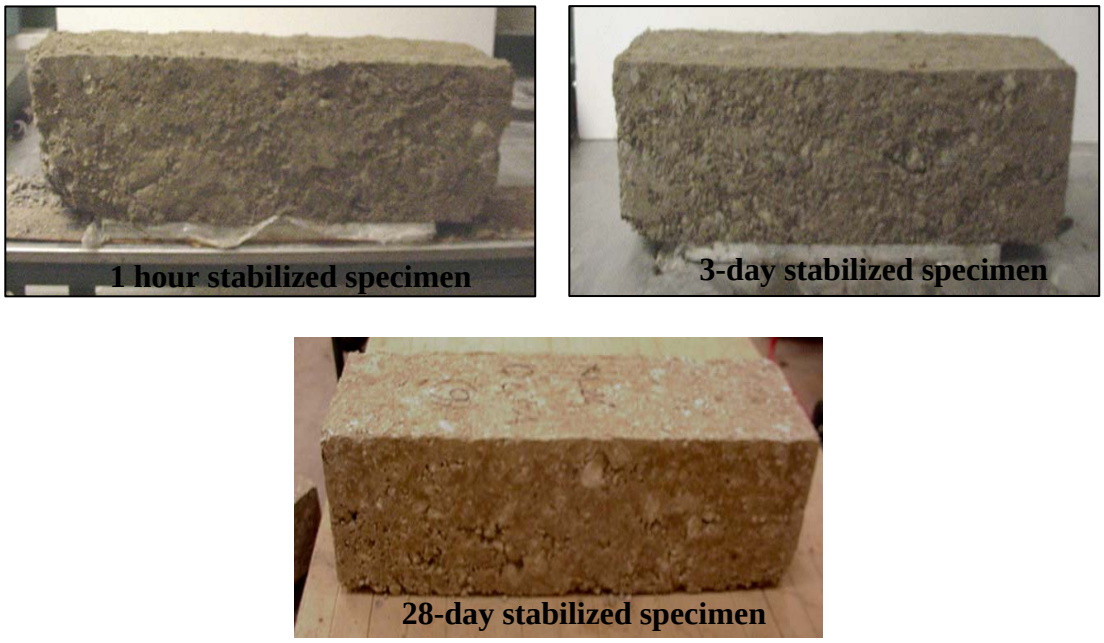

Figure 4-9 Degradation of 1-hour, 3-day and 28-day cured stabilized beams after 16 F-T cycles (FT-1 procedure).

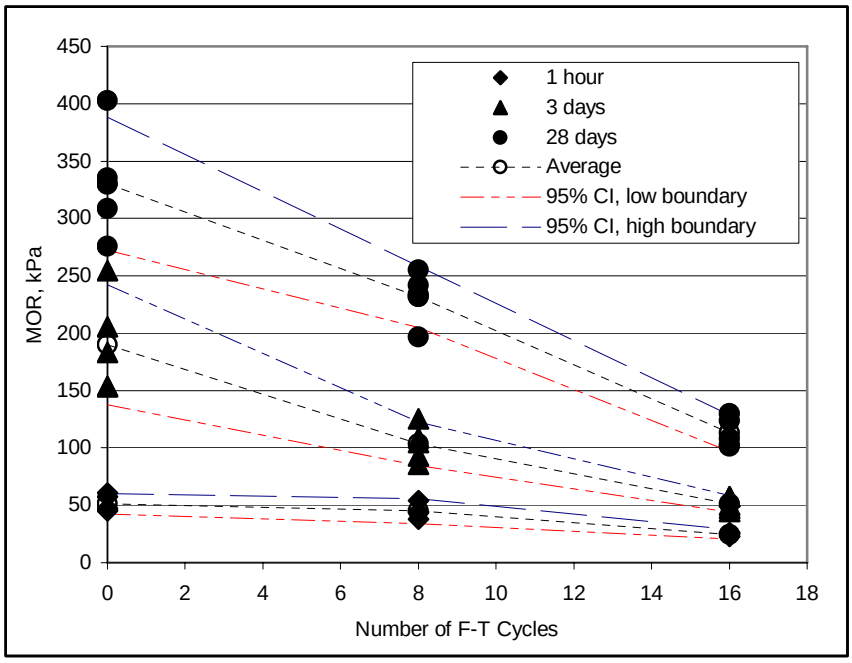

Figure 4-10 Variation of modulus of rupture with F-T cycles for 1-hour, 3-day and 28 day cured specimens

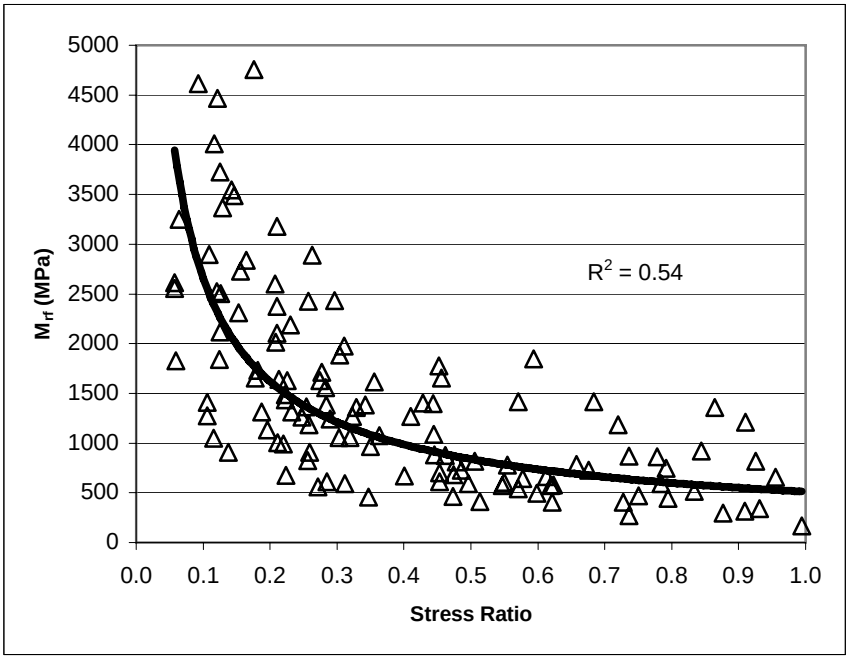

Figure 4-11 Variation of M_{rf} with stress ratio

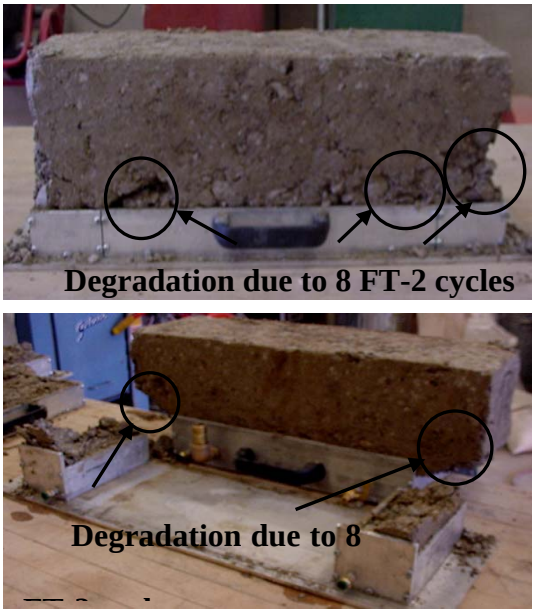

Figure 4-12 Stabilized specimens subjected to 8 FT-2 cycles

CHAPTER

5

SEMI-QUANTIFICATION OF CEMENTING PRODUCTS OF STABILIZED AGGREGATE BASES USING X-RAY DIFFRACTION TECHNIQUE

5.1 Introduction

Cementitious stabilization has been extensively used to improve the performance of subgrade and base layers in pavement application. It consists of mixing stabilizing agents such as fly ash and cement kiln dust with aggregate or soil. In the presence of water, these agents react to form cementitious compounds that are responsible for the amelioration of engineering properties such as strength and stiffness. Several studies have been conducted in the past to evaluate the performance of cementitiously stabilized aggregates or soils in pavement construction. For example, Nunan and Humphrey (1990) conducted field and laboratory tests to evaluate the performance of existing stabilization projects in Maine. Various stabilizing mixtures (e.g. soil-cement and lime-fly ash) were employed to observe their applicability in stabilizing poor quality aggregates. In the study, the macro-manifestation of stabilization represented by unconfined compressive strength (UCS) and resilient modulus was evaluated. No efforts were made to examine the micro-structural developments of the cementing products responsible for an improvement in properties.

Khalid (1993) conducted a laboratory study to evaluate the resilient modulus and strength of cement-stabilized base courses. In that study, the modulus and strength

were the main parameters to assess the influence of cement-stabilization. No laboratory tests were conducted to identify the cementing compounds responsible for the degree of improvement.

In a related study, Baghdadi et al. (1995) conducted laboratory tests to observe the performance of Dune sand treated with various amounts of cement kiln dust (CKD). Compacted specimens were cured for 7, 28 and 90 days, and then tested for unconfined compression, California bearing ratio and split tension. Although, their study added useful data on the behavior of CKD-stabilized sandy materials, it lacked the explanation relative to the cementitious compounds. Identification of such compounds would be helpful in explaining the short- and long-term performance of such materials.

Lav and Lav (2000) studied the micro-structural development of fly ash mixture used as a pavement base material. Unstabilized (plain fly ash) and stabilized specimens (with cement or lime) were prepared and examined with X-ray fluorescence spectrometry (XRF), X-ray diffractometer, thermal analysis (TA) and scanning electron microscopy (SEM) to identify the chemical and phase composition and micro-structural development. Cylindrical specimens were also prepared for identifying the variation in their strengths with curing time. The increase in strength of the stabilized specimens with curing time, and the difference between cement- and lime-stabilized specimens were justified using the aforementioned techniques. Their study highlighted the importance of XRF, XRD, SEM and TA to explain the mechanisms associated with stabilization. In their study, the analysis of the hydration and pozzolanic reaction products was presented. The study, however, did not address

any of the semi-quantification (e.g., reference intensity ratio) or quantification method (e.g., Rietveld) techniques to quantify the cementing products.

Khoury (2001) evaluated the performance of aggregate base stabilized with class C fly ash (CFA). Stabilized specimens were tested for resilient modulus (M_r) and unconfined compressive strength (UCS). No laboratory tests such as X-ray diffraction (XRD), scanning electron microscopy (SEM) and energy dispersive spectroscopy (EDS) were performed to observe the micro-structural developments of the cementitious products responsible for such behavior.

In a recent study, Kim and Siddiki (2003) evaluated the performance of fine grained soils stabilized with lime-kiln dust and lime. In their study only, Atterberg limits, standard Proctor, unconfined compression, CBR, volume stability and resilient modulus tests were performed. No laboratory tests were performed to observe the micro-structural development of cementing products produced due to stabilization.

Wang et al. (2004) used a number of analytical techniques, namely x-ray diffractometry, thermal analysis, scanning electron microscopy and x-ray absorption near edge structure (XANES) to investigate the mineralogy of a soil susceptible to sulfate attack after stabilization. The amounts of gypsum and sulfate were also determined using these techniques. This study highlighted the importance of these techniques in detecting and quantifying compounds in soil stabilization.

Other studies (see e.g., Misra, 1998; Bergeson and Barnes, 1998; Bergesson and Mahrt, 2000; Khoury and Zaman, 2002; Parsons and Kneebone, 2004; Barstis and Metcalf, 2005) have addressed the macro-manifestation of stabilized pavement materials, but no efforts have been directed toward the micro-manifestation.

From the aforementioned review, a need arises to understand the mechanism associated with cementitious stabilization. Such a need is also reflected in the millennium letter by the Cementitious Committee of Transportation Research Board (TRB). The letter is posted on the TRB web site (Little et al., 2005). It notes that fundamental research is needed to understand cementitious reactions and their-short- and long-term roles in the stabilization process. Quantification techniques would address some of these issues and would provide a better understanding of cementitious stabilized materials.

5.2 Overview of cementitious compounds

5.2.1 Hydration of Portland Cement

It is important to understand the chemistry of cement hydration prior to discussing the cementitious reaction associated with fly ashes or lime-pozzolan mixture. The compounds in Portland cement are anhydrous, but when exposed to water these compounds decompose to form hydrated compounds (Lea, 1971). The rate of decomposition depends upon the physical state of the cement compounds and their chemical nature. A summary of the most important reactions and of Portland cement hydration is illustrated in Table 5-1. It is evident that the main Portland cement compounds responsible for hydration are: (1) the calcium silicates (tri-calcium silicate C_3S; and dicalcium silicate C_2S); (2) the calcium aluminates (trecalcium aluminate C_3A); and (3) the tetracalcium aluminoferrite (C_4AF). The calcium silicates react with water to form C-S-H and calcium hydroxide, which is presented in Table 5-1 as reactions 1 and 2. Reactions 3 and 4 require calcium and sufficient sulfate to form ettringite or monosulfoaluminate (Kruger, 1990; Lea, 1971). The last reactions

directly consume calcium hydroxide and therefore, compete with pozzolanic reactions for lime released by hydration of the silicates. Additional information about cement hydration is described by Lea (1971) and Kruger (1990).

5.2.2 Hydration of a Lime-Pozzolan (or Fly ash) Mixture

NCHRP (1976) reported that the reactions that occur when a lime-fly ash mixture is exposed to water to form cementitious materials are complex. These reactions have been reported in several studies. For example, Minnick (1967) presented an illustrative list of reactions. These reactions are illustrated in Table 5-2 (Minnick, 1967; NCHRP, 1976; FHWA, 1982). The major cementing products formed in a lime-fly ash mixtures are probably calcium silicate hydrates, and possibly ettringite, as reported in Minnick (1976), with the possibility of other reactions.

Another study by Kruger (1990) presented the reactions that are likely to take place in lime-pozzolan mixtures. Pozzolan is a siliceous or aluminous-siliceous compound with no cementitious properties, but in the presence of water and lime it reacts to form cementitious compounds. The reactions of pure materials were presented by the following simplified equation:

$$xCH + yS + zH \rightarrow C_x S_y H_{x+z} \qquad \textbf{(5-1)}$$

where CH is calcium hydroxide, S is silica, H is water, and x, y and z are stoichiometric coefficients. The reactions are not limited to silica, but include other cementing products formed by lime, alumina and iron oxide are possible.

It is evident that hydration of Portland cement and reactions of lime-fly ash (pozzolan) produce the same cementitious products. These products are formed due to calcium silicates and calcium aluminates in Portland cement, while free lime (CaO)

is the main compound in a lime-fly ash mixture. Kruger (1990) reported that the primary difference between the pozzolanic reaction and reactions due to cement hydration is the rate at which these reactions occur, but not so much on the composition of hydration products, although these do differ in some cases.

5.3 Objectives

The main objective of this chapter is to identify and semi-quantify the cementitious products of aggregates stabilized with cement kiln dust (CKD), class C fly ash (CFA) and fluidized bed ash (FBA) using different analytical techniques. This will be achieved through the following tasks:

1) Determine the unconfined compressive strength of aggregate bases stabilized with CFA, CKD and FBA.
2) Use X-ray diffraction (XRD), scanning electron microscopy (SEM) and Energy dispersive spectrometry (EDS) on specimens already tested for UCS.
3) Use the reference intensity ratio method to semi-quantify the cementitious products in the stabilized specimens.

5.4 Materials

The only two aggregates used were Meridian and Hanson. As mentioned in Chapter 2, Meridian is a limestone-type aggregate with a high content of calcium carbonate, while Hanson is a rhyolite-type aggregate with a relatively high content of silica. Additional relevant mineralogical and physical properties of these aggregates are given in Chapter 2. The three different stabilizing agents, cement kiln dust (CKD), class C fly ash (CFA) and fluidized bed ash (FBA) were used. The relevant chemical and physical properties are presented in Table 2-1. Differences between the

chemical composition and physical properties among the selected additives are clearly evident. These differences in compounds are expected to lead to differences in the formation of cementing compounds, thus, differences in the strength and performance of stabilized aggregates.

5.5 Specimen Preparation

In this study, the influence of different stabilizing agents on the formation of cementitious compounds due to aggregate stabilization is observed in the fine matrix of the aggregate. The effect of curing time and percentage of additives was also examined. Materials passing the U.S. standard No. 40 sieve were only used for specimen preparation. A modified Harvard miniature method, developed by Khoury et al. (2005), was utilized to prepare specimens. Specimens were compacted at near optimum moisture content (OMC) and approximately 98% maximum dry density (MDD). Proctor tests were performed on the fine matrix (passing U.S. standard No. 40 sieve) mixed with stabilized agents. A summary of both OMCs and MDDs data is presented in Table 5-3. After compaction, specimens were wrapped with a plastic foil and then placed in a desiccator at room temperature (approximately 21^{o}C or 70^{o}F) with a relative humidity of approximately 90%. A summary of the test matrix employed is presented in Table 5-4. The influence of curing time on UCS and micro-structural development of cementitious products is observed on the Meridian aggregate stabilized with different percentages of CFA. Such influence was also examined on the Hanson aggregate but only stabilized with 10% CFA. The effect of different stabilizing agents namely CKD, CFA and FBA, were examined only on the Meridian aggregate.

5.6 Experimental Methods

5.6.1 Unconfined Compressive Strength

After curing, specimens were tested for the unconfined compressive strength (UCS) in accordance with the ASTM D 5102 test method. Specimens were loaded at a constant axial strain of 0.072 cm/min (0.0282 in./min). A dial gauge was used to measure the vertical deformation, and a load ring was used to measure the load. After performing UCS, two out of the three tested replicates were utilized to perform the other laboratory tests (i.e., XRD, SEM and EDS), while the third specimen was only used to determine the moisture content. Each of the two replicates was divided into three portions: (1) Portion 1 was used to determine the moisture content; (2) Portion 2 was used for SEM and EDS; and (3) Portion 3 was used for XRD tests.

5.6.2 Scanning Electron Microscopy and Energy-Dispersive Spectrometry

The SEM technique was employed to qualitatively identify the micro-structural developments in the matrix of the stabilized mix. Portion 2 was oven dried for approximately 24 hours, and then two tiny pieces were mounted on a copper specimen holder and coated with a thin layer of gold palladium to provide surface conductivity. A technics sputter-coater operating under a vacuum of 40 millitorr and 10 mA current was used for coating the specimens. A JEOL JSM 880 scanning electron microscope operating at 15 kV was used to visually observe the coated specimens. The JEOL JSM 880 was fitted with an energy-dispersive X-ray spectrometer (EDS). The EDS was performed on selective specimens where crystals and hydration coating products due to stabilization were identified. The micrographs were taken using EDS2000 software.

5.6.3 X-Ray Diffraction

The X-ray diffraction (XRD) tests were performed using a Rigaku D/Max X-ray diffractometer with bragg-brentano parafocusing geometry, a diffracted beam monochromator, and a conventional copper target X-ray tube set to 40 kV and 30 mA. The measurements were performed from 5^o to 70^o 2θ, with 0.02^o step size and 2 seconds count at each step. Data obtained by the diffractometer were analyzed with Jade 3.1, an X-ray powder diffraction analytical software, developed by the Materials Data, Inc. (Jade, 1999). Portion 3 was oven dried for approximately 24 hours, grounded with a mortar and pestle, and then sieved through a U.S. standard No. 200 sieve. Materials passing through the U.S. standard No. 200 sieve were placed on a specimen holder prior to testing. Generated diffractograms (using the Peaks versus 2θ and d-spacing) were used to identify and semi-quantify the formation of cementitious compounds in the mixture using the reference intensity ratio (RIR).

The RIR method consists of fitting the raw data to a specific profile shape, eliminating the contribution of overlapping peaks, and subtracting the background. This method is a semi-quantitative method which calculates the weight % in the least-square fit of the identified minerals and compounds (Livingston et al., 1998; Jade, 1999; AMIA, 2003). However, the results are only as good as the RIR values. Any profile error due to intensity (%) and positional mismatches in individual powder diffraction file (PDF) lines may influence the accuracy of the final numbers (Jade, 1999). The investigation was intended to shed light on the development of hydration products with time, percentage of additive content, and different aggregate mineralogical characteristics. The RIR method has been used by several studies

(AMIA, 2003; Livingston, et al. 1998) for different applications. According to AMIA (2003) this method is sufficient for many applications, specifically, when it is not possible to obtain pure forms of all components, making it impossible to prepare external calibration curves from standards. Such a method is also considered an alternative when it is not feasible to obtain good structure information for Rietveld analysis.

5.7 Presentation and discussion of results

5.7.1 Unconfined Compressive Strength (Meridian)

The variation of unconfined compressive strength with curing time and percentage of CFA for stabilized Meridian specimens is graphically illustrated in Figure 5-1. The UCS values of raw specimens (no CFA), considered as a baseline, are also presented with curing time in Figure 5-1. UCS values increased with curing time for all percentages of fly ash; however, the degree of increase varies with time and the percentage of CFA. For example, the UCS for 10% CFA increased approximately 25% and 70% as the curing time increased from 1 hour to 3 days and 28 days, respectively. For 25% CFA, the percentage increase is approximately 12% and 48% as curing time increased from 1 hour to 3 days and from 3 days to 28 days, respectively. No additional data is available beyond 28 days; twenty eight days being considered as sufficient criterion for a significant strength gain of stabilized aggregate base. Zaman et al. (1998) reported that a curing period longer than 28 days did not cause any significant increase in UCS values.

From Figure 5-1, it is obvious that stabilized specimens have higher strengths than the raw materials. The magnitude of difference depends on the curing time. It is

an indication that the development of cementitious products with time is responsible for such an increase. For example, the average UCS value of 10% CFA specimens cured for 28 days is approximately 750% higher compared to the corresponding values for raw specimens suggesting that the cementitious reactions are responsible for such an increase. In addition, one can also observe from Figure 5-1 that the 50% CFA specimens have higher UCS values than 25% CFA and 10% CFA. Raw specimens have the lowest UCS values. This is an indication that the more fly ash particles in the mixture, the more the cementing compounds, hence, the higher unconfined compressive strength. Such observation will be better explained using a number of techniques, namely, XRD diffractograms, SEM micrographs and EDS patterns.

The effect of different stabilizing agents was only observed on the Meridian aggregate. A summary of UCS values with stabilizing agents is graphically illustrated in Figure 5-2. Specimens were stabilized with 15% CKD, 10% CFA and 10% FBA. It is evident that the average strength of 10% FBA (1,805 kPa, i.e., 262 psi) is higher than 10% CFA (1,171 kPa, i.e., 170 psi), followed by 15% CKD (861 kPa, i.e., 125 psi). The difference in their strength is primarily due to the difference in chemical properties. Several studies (NCHRP, 1976; FHWA, 1982) have indicated the main factors that influence the pozzolanic reactivity of a lime-fly ash mixture are: (1) percent passing No. 325 sieve; (2) SiO_2, SiO_2+Al_2O_3; (3) loss on ignition; and (4) alkali or free lime contents.

5.7.2 Unconfined Compressive Strength (Hanson)

The variation of unconfined compressive strength with curing time for 10% CFA-

stabilized Hanson specimens is graphically illustrated in Figure 5-3. A similar trend to Meridian specimens was observed. UCS values exhibited an increase of approximately 60% as the curing time increased from 1 hour to 28 days. It is also evident that stabilized specimens have higher strengths than raw specimens. The formation of cementitious compounds is responsible for such an increase, as discussed subsequently.

5.7.3 Scanning Electron Microscopy

The scanning electron microscopy was used to visually observe the micro-structural developments of cementitious products with curing time, stabilization agents, and aggregate type. The hydration products and their degree of formation are expected to vary from one mixture to another. In this study, it was decided to also observe the micro-structure of raw materials.

5.7.3.1 Raw Materials

Figure 5-4 shows the micrographs of cement kiln dust, class C fly ash and fluidized bed ash. Cement kiln dust has oval to spherical particles, while class C fly ash particles are only spherical. Fluidized bed ash particles are amorphous. Figure 5-5 shows the micrographs for raw Meridian and Hanson. These micrographs show these materials prior to mixing with water.

5.7.3.2 Stabilized Specimens (Meridian)

The SEM observations of Meridian aggregate stabilized with 10% CFA and cured for 1 hour, 3 days, and 28 days, are presented in Figure 5-6. As can be seen in Figure 5-6, evidence of hydration of CFA particles is noticeable within the first hour after stabilization. Up to 3 days, only hydration coating around the CFA particles is

observed. However, in the 28-day specimens, crystal formation is noticeable. The formation of hydration coating surrounding the fly ash particles filled the voids resulting in a higher strength compared to raw materials. At 28 days, the crystal formation bonded particles together to produce higher strength than 1 hour or 3 days.

The influence of fly ash percentage (i.e, 10%, 25% and 50%) on the micro-structural development of cementitious products is illustrated in Figures 5–7 and 5–8. It is visually evident that hydration coating around the fly ash particles for 25% and 50% CFA cured for 3 days are formed. It was also found that needle-like hydration products are formed for these percentages of fly ash compared to 10% CFA, at an early curing period (3 days). For 28 days, it is quite obvious that more crystals are formed in the specimens, as depicted in Figure 5-8. From the micrographs, one can conclude that the higher the fly ash amount the more the crystals and thus the higher the strength.

5.7.3.3 Stabilized Specimens (Hanson)

The microstructural development for Hanson specimens were also visually observed and are presented in Figure 5-9. Coating hydration around the fly ash particles was observed for all specimens; however, the mass increased with the curing period. Efforts were made to test additional specimens to identify any crystal formation, but apparently no crystal formation was evident compared to Meridian specimens at a curing period of 28 days. Such observation points to the conclusions that Hanson specimens have lower strength compared to Meridian.

5.7.4 Energy Dispersive Spectroscopy

The crystals were analyzed by EDS to determine their elemental compositions,

since the identification of these elements would help qualitatively specify the type of cementitious products formed due to stabilization. Figures 5–10 to 5–13 show the EDS for specific crystals and hydration products found in selective stabilized specimens. EDS for the selective identified crystals showed the presence of sulfur (S) along with other elements such as Ca and Al, which is an indication of the presence of ettringite or monosulfoaluminate. The hydration coating around the fly ash particles were also analyzed to identify their elemental compounds. The predominant elements were Ca, Al and Si, suggesting the presence of C-S-H, C-A-H and/or the presence of C-A-S-H. The EDS method is not enough to conclude the presence of these compounds. Results from the XRD will also be used to better identify the presence of these compounds.

5.7.5 X-Ray Diffraction

X-ray diffraction analysis was employed in this study to identify and semi-quantify the cementing products in the stabilized specimens. Analyzing the X-ray diffractograms for all the specimens using the peak intensity ratio, and with the help of the identification of major elements in the crystals formation and hydration coating, the following cementitious products are identified in the mixtures.

1) Calcite ($CaCO_3$) is the predominant mineral in Meridian mixes, as shown in Figure 5-14 of 10% CFA stabilized Meridian specimen. In Hanson, however, quartz (SiO_2) is the predominant component (refer to Figure 5-15).
2) Ettringite was more noticeable in Meridian specimens cured for 28 days. Ettringite is a calcium (C) aluminum (A) sulfate (S) hydrate (H) (CASH) type

mineral. No ettringite formation was observed in Hanson specimens. Figure 5-14 shows the presence of ettringite (E) in 10% CFA stabilized Meridian specimen.

3) Also, C-A-S-H type cementing product was also detected in most Meridian and Hanson specimens; however, the intensity is higher in 28 specimens than in 1-hour and 3-day cured specimens. This is consistent with Laguros and Zenieris (1987) that C-A-S-H was detected in CFA-stabilized aggregate base. Figures 5–14 and 5–15 show these minerals represented by Straetlingite (S) and gismondine (G).
4) C_3AH_6 presented by Z in Figure 5-15 was noticeable in Hanson specimens.
5) C-S-H (needle-like Tobermorite) represented by T in Figure 5-14 was only found in the Meridian specimens.

After identifying these products, the RIR method was employed, as explained earlier, for semi-quantifying these products. The least square error (an indicator of the quality of the fit) for the fitting varied between 0.25 and 0.40, which could be partly due to the fact that no in house calibration of RIR for each phases was performed. It could also be related to the method itself. AIMA (2003) reported similar values of least square error of approximately 25% for other applications.

Figure 5-16 shows the variation of the sum of cementing compounds (SCC) (i.e., CA<u>S</u>H, C-S-H type, C-A-H and CASH) values with curing time for both Meridian and Hanson. SCC increased with curing time and had the same qualitative trend as UCS values. The effect of different stabilizing agents on the SCC is shown in Figure 5-17. One can see that FBA has higher SCC values, than CFA followed by CKD. It has the same trend as UCS, and thus one can conclude that the higher the SCC the

higher the strength. In addition, efforts were made to correlate the UCS values with the SCC values, as depicted in Figure 5-18. The unconfined compressive strengths increased approximately linearly with SCC, with a relatively high R^2 value (0.79). Such a correlation would be extremely helpful in better understanding and rationalizing the mechanisms associated with stabilization.

5.8 Concluding remarks

This study was undertaken to investigate the UCS of aggregate bases stabilized with class C fly ash, cement kiln dust, and fluidized bed ash. Such influence was observed on materials passing U.S. standard No. 40 sieve. Specimens were molded at optimum moisture content and maximum dry density. Results showed that the UCS increased with curing time; the percent increase in UCS with increasing curing time from 1 hour to 28 days. It was also found that the higher the fly ash content the higher the UCS values. Moreover, Meridian specimens exhibited higher strength than Hanson specimens. Such behavior was rationalized by using different techniques such EDS, SEM and XRD. From EDS and SEM, it was found that the presence of cementitious compounds was responsible for an increase in strength compared to raw specimens. However, the intensity of crystals, i.e., more numerous, increased with time and the percentage of fly ash. EDS and SEM were used as qualitative techniques to examine the microstructural developments. While XRD was used to both identify and semi-quantify these compounds using the RIR method. Cementing compounds such as ettringite, C-S-H, C-A-H and CASH were identified and the sum of their mass percent (SCC) was plotted with UCS values. The UCS values increased approximately linearly with SCC.

Table 5-1 Primary transformation of Portland cement hydration

1	2 (C_3S) (Tricalcium silicate) + 11 H_2O	= $C_3S_2H_8$ (Calcium Silicate Hydrate) + 3CH (Calcium hydroxide)
2	2(C_2S) (Dicalcium silicate) + 9 H_2O	= $C_3S_2H_8$ (Calcium silicate hydrate) + CH (Calcium hydroxide)
3	(C_3A) (Tricalcium aluminate) + 3($C\underline{S}H_2$) (Gypsum) + 26H_2O	= C6A$\underline{S}H_{12}$ (Ettringite)
4	2(C_3A) (Tricalcium aluminate) + C6A$\underline{S}H_{12}$ (Ettringite) + 4H_20	= 3($C_4A\underline{S}H_{12}$) Calcium monosulphoaluminate
5	(C_3A) (Tricalcium aluminate) + CH (Calcium hydroxide) + 12H_20	= C_4AH_{13} Tetracalcium aluminate hydrate
6	(C_4AF) (Tretracalcium aluminoferrite) + 2CH (Calcium hydroxide) + 10H_20	= C_6AFH_{12} Calcium aluminoferrite

C = CaO; A = Al_2O_3; S= SiO_2; F = Fe_2O_3

Table 5-2 Lime-fly ash (pozzolanic hydration)

$RO + H_2O = R(OH)_2$
$RO + H_2O + CO_2 = R CO_3 + H_2O$
$R(OH)_2 + CO_2 = R CO_3 + H_2O$
$R(OH)_2 + SiO_2 + H_2O = xRO.ySiO_2.zH_2O$
$R(OH)_2 + Al_2O_3 + H_2O = xRO.yAl_2O_3.zH_2O$
$R(OH)_2 + Al_2O_3 + SiO_2 + H_2O = xRO.yAl_2O_3.zSiO_2.wH_2O$
$R(OH)_2 + SO_3 + Al_2O_3 + H_2O = xRO.yAl_2O_3.zRSO_4.wH_2O$
R = Ca or Mg; x, y, z, and w are stoichiometric coefficients

Table 5-3 A summary of OMCs and MDDs

Aggregate Type	Additives type	Percentage	OMC, %	MDD (kN/m^3)
Meridian	Raw	0	12.3	18.7
	CFA	10	12.1	18.8
		25	11.8	19.0
		50	11.3	19.1
	CKD	15	14.7	17.8
	FBA	10	14.2	17.8
Hanson	Raw	0	15.5	17.8
	CFA	10	14.9	18.0

Table 5-4 Test matrix

Aggregate Type	Additives type	Percentage	Curing Period	Number of replicates
Meridian	Raw	0	1 hour	3
			3 days	3
			28 days	3
	CFA	10	1 hour	3
			3 days	3
			28 days	3
		25	1 hour	3
			3 days	3
			28 days	3
		50	1 hour	3
			3 days	3
			28 days	3
	CKD	15	28 days	3
	FBA	10	28 days	3
Hanson	Raw	0	1 hour	3
			3 days	3
			28 days	3
	CFA	10	1 hour	3
			3 days	3
			28 days	3

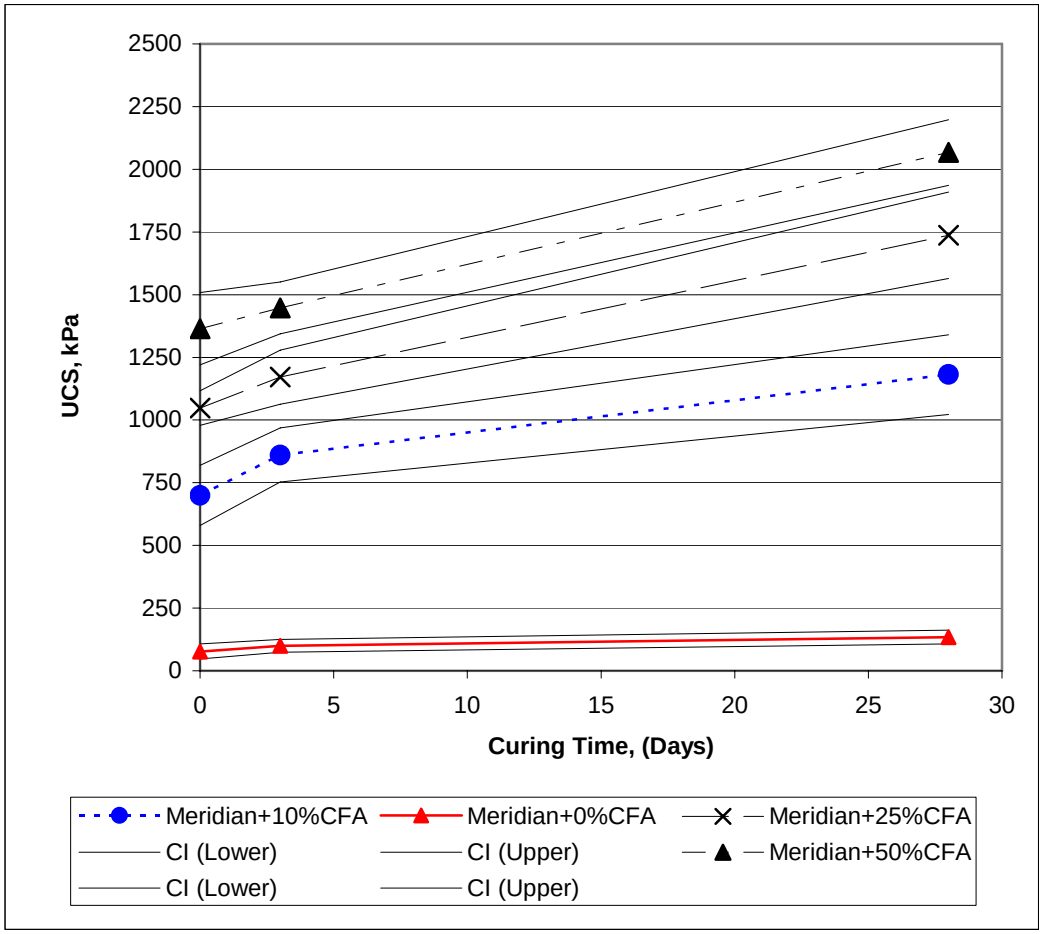

Figure 5-1 Variation of UCS with curing time and percentage of CFA for Meridian aggregate

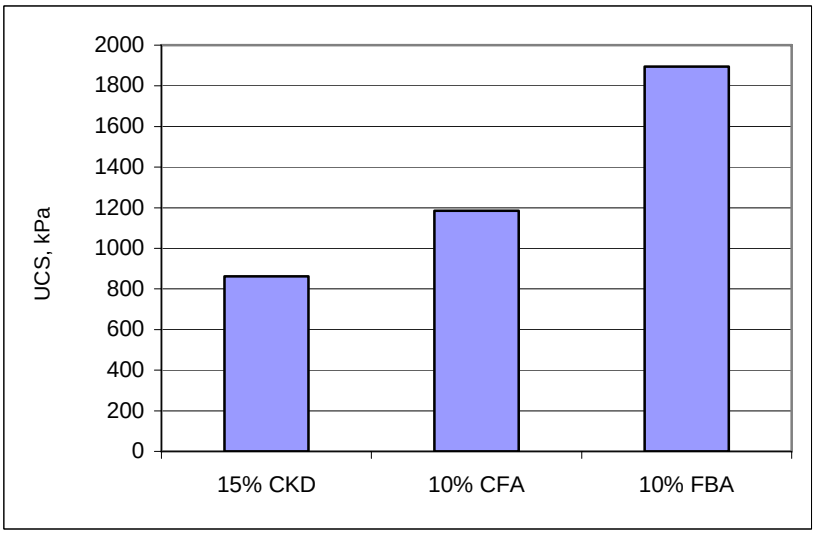

Figure 5-2 Effect of different type of additives on Meridian aggregate

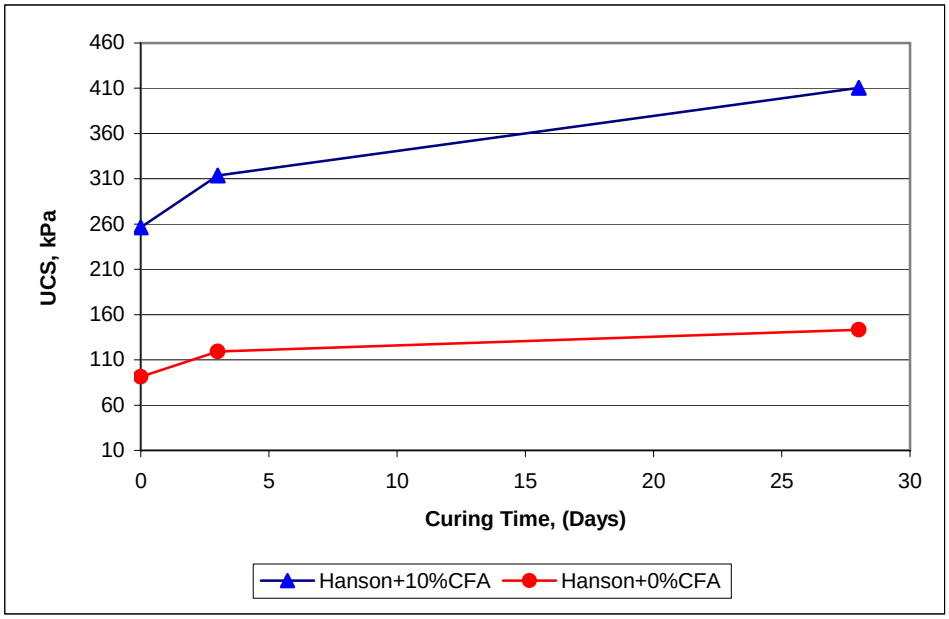

Figure 5-3 Variation of UCS with curing time of 10% CFA-stabilized Hanson and raw specimens

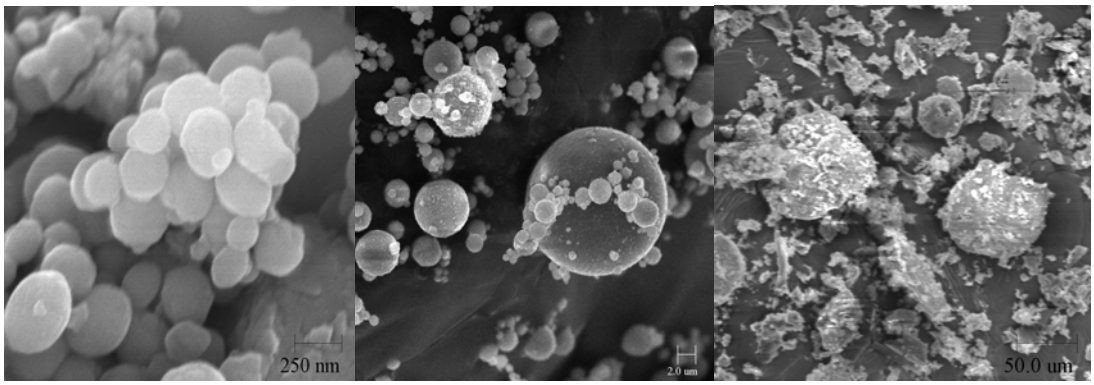

Figure 5-4 SEM micrographs for CKD (left), CFA and FBA

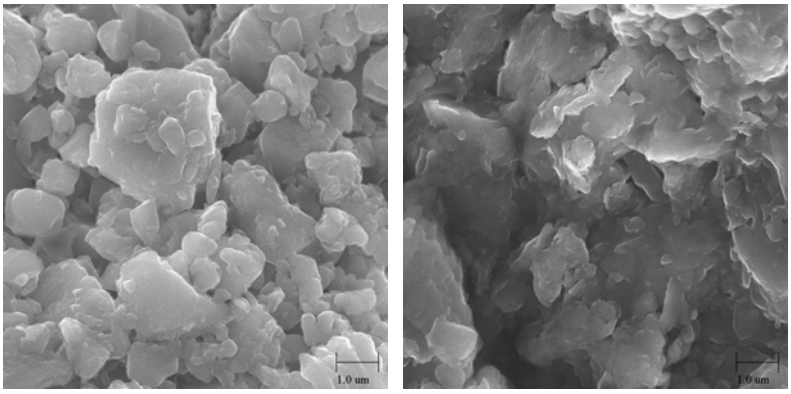

Figure 5-5 SEM micrographs for Meridian (left) and Hanson powder

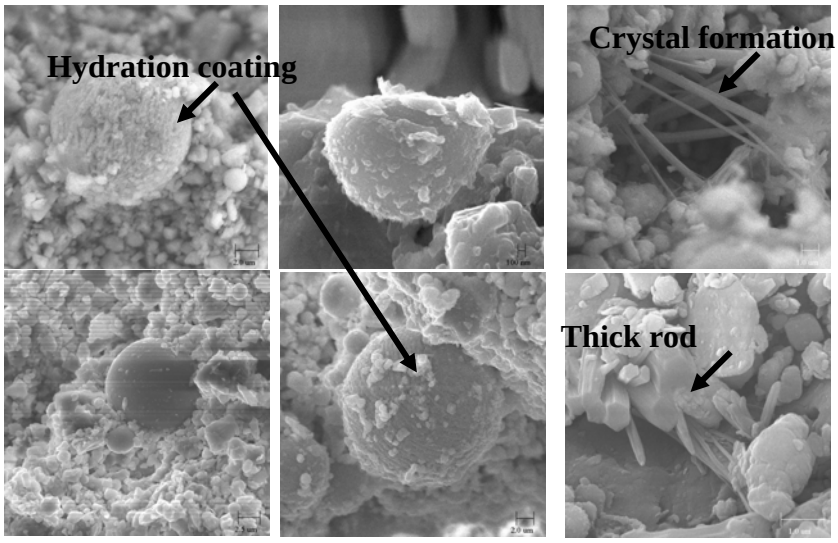

Figure 5-6 SEM micrographs for Meridian stabilized with 10% CFA and cured for 1 hour (left), 3 days and 28 days

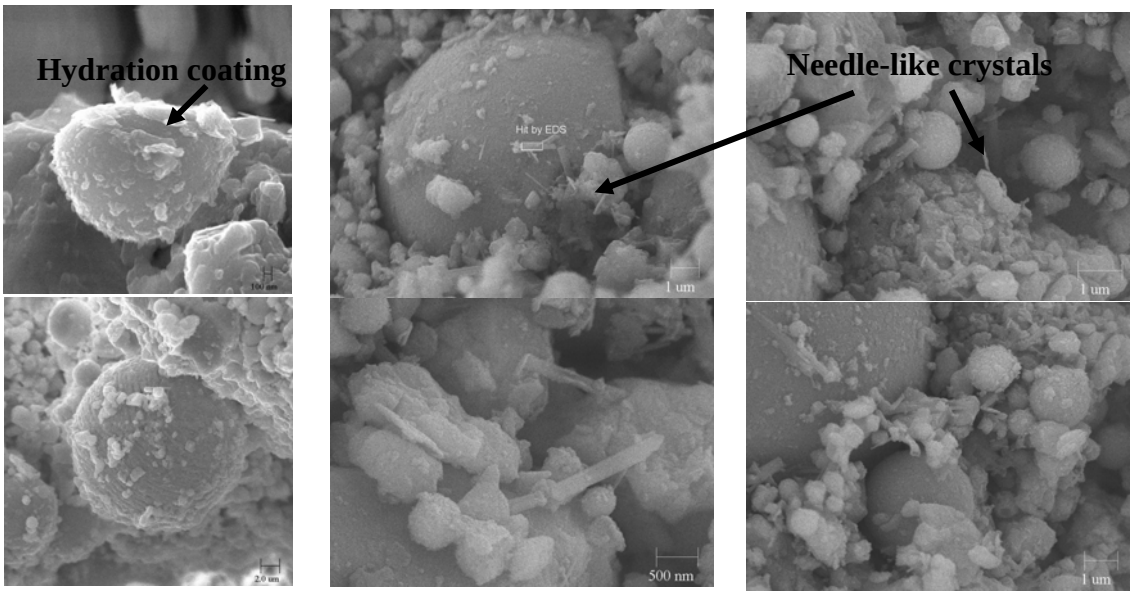

Figure 5-7 SEM micrographs for 3-day Meridian specimens stabilized with 10% (left), 25% and 50% CFA

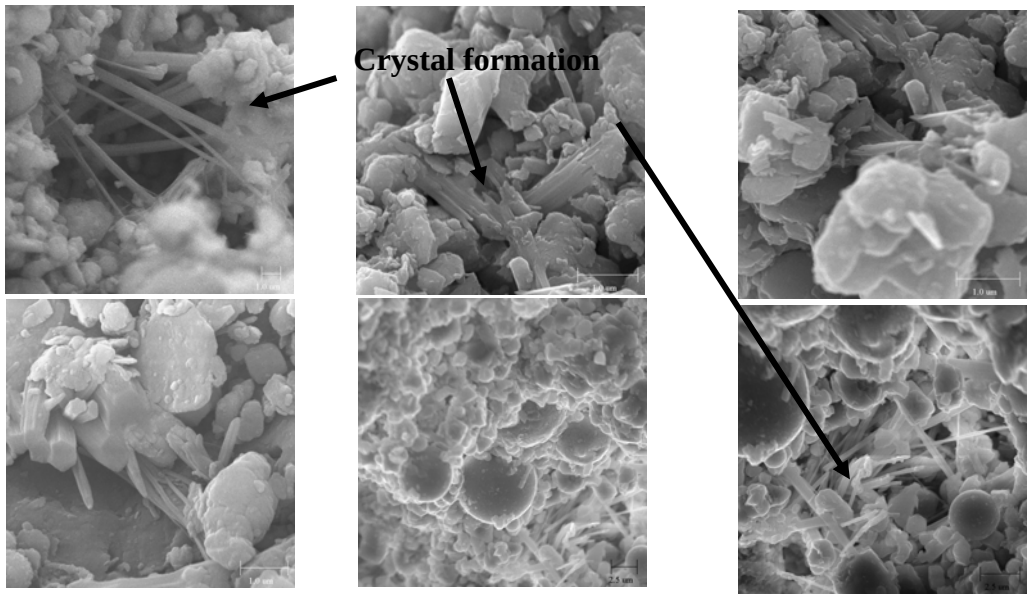

Figure 5-8 SEM micrographs for 28-day Meridian specimens stabilized with 10% (left), 25% and 50% CFA

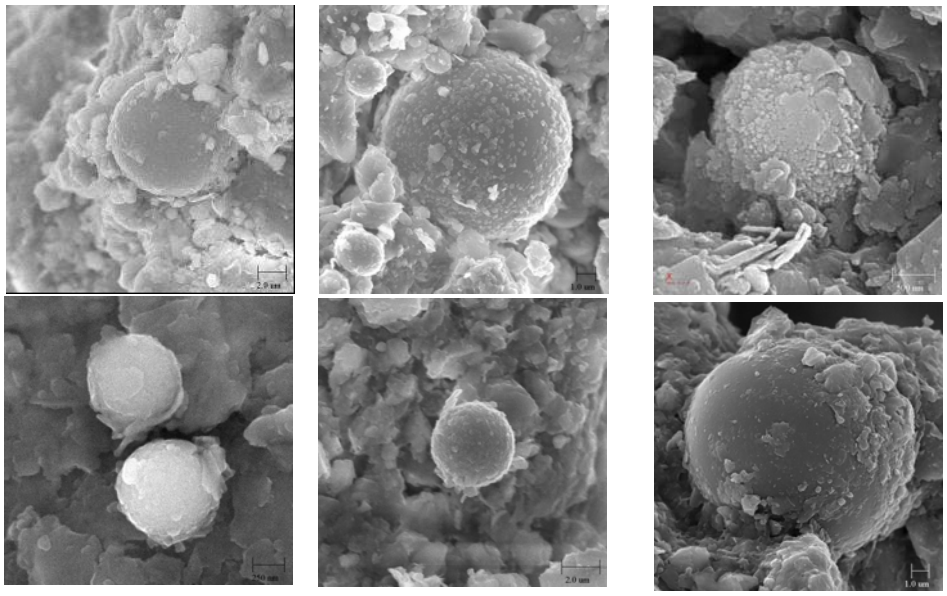

Figure 5-9 SEM micrographs for Hanson stabilized with 10% CFA cured for 1 hour (left), 3 days and 28 days

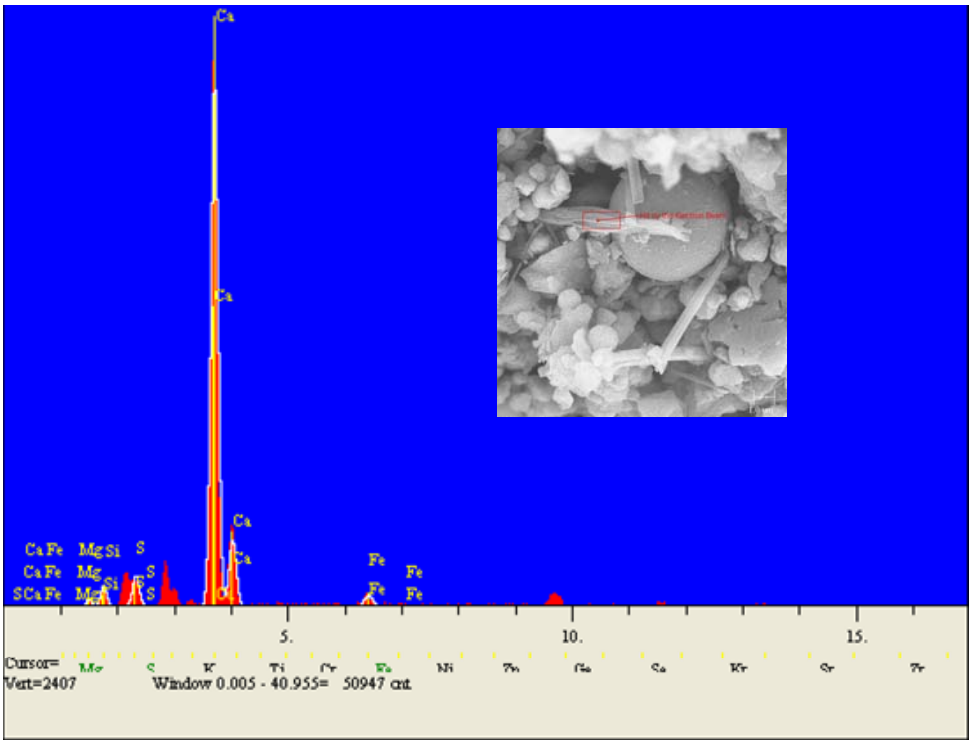

Figure 5-10 EDS for Meridian specimens with crystal formation surrounding the fly ash particle

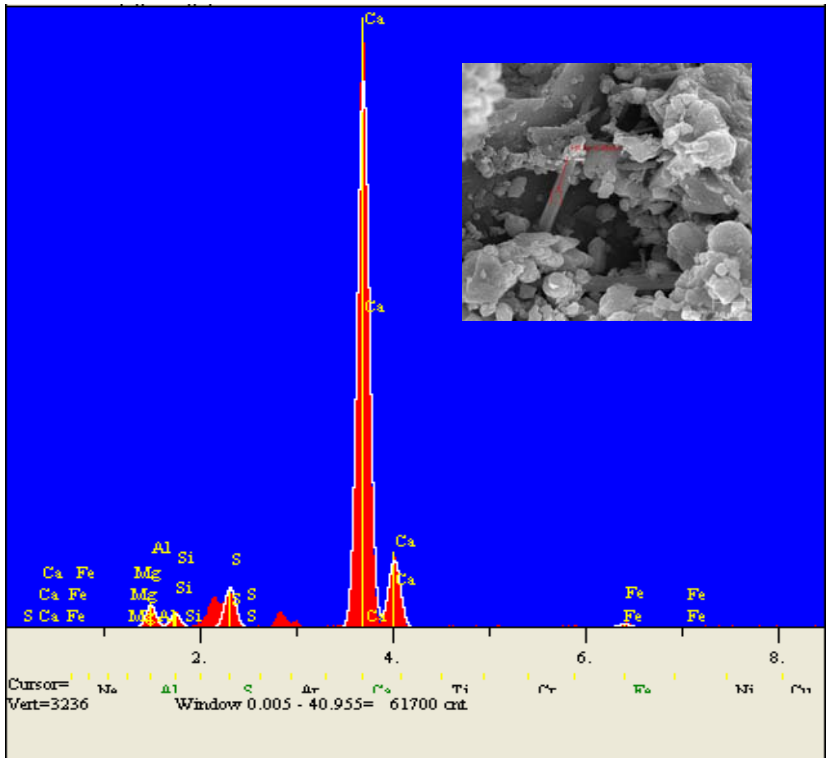

Figure 5-11 EDS for Meridian specimens with crystal hydration

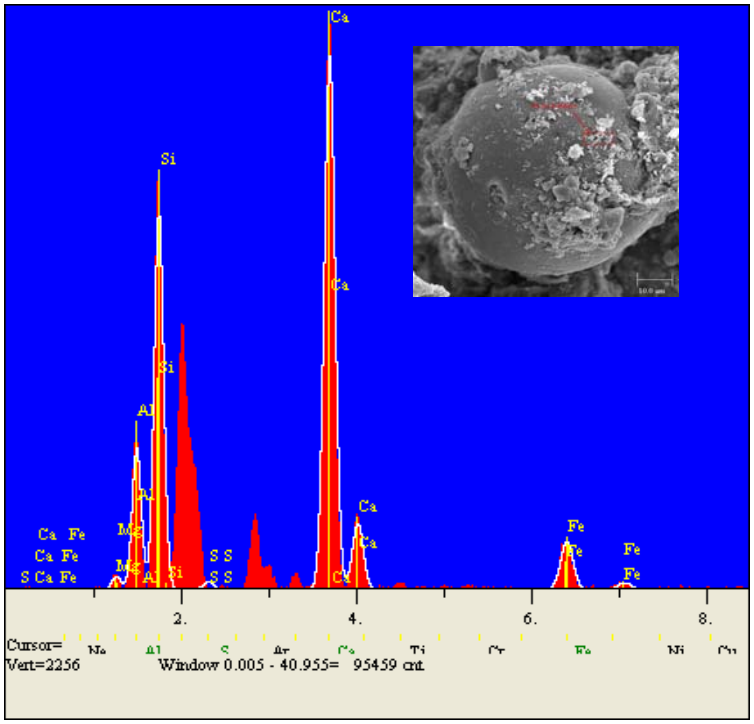

Figure 5-12 EDS for Hanson specimens with coating hydration

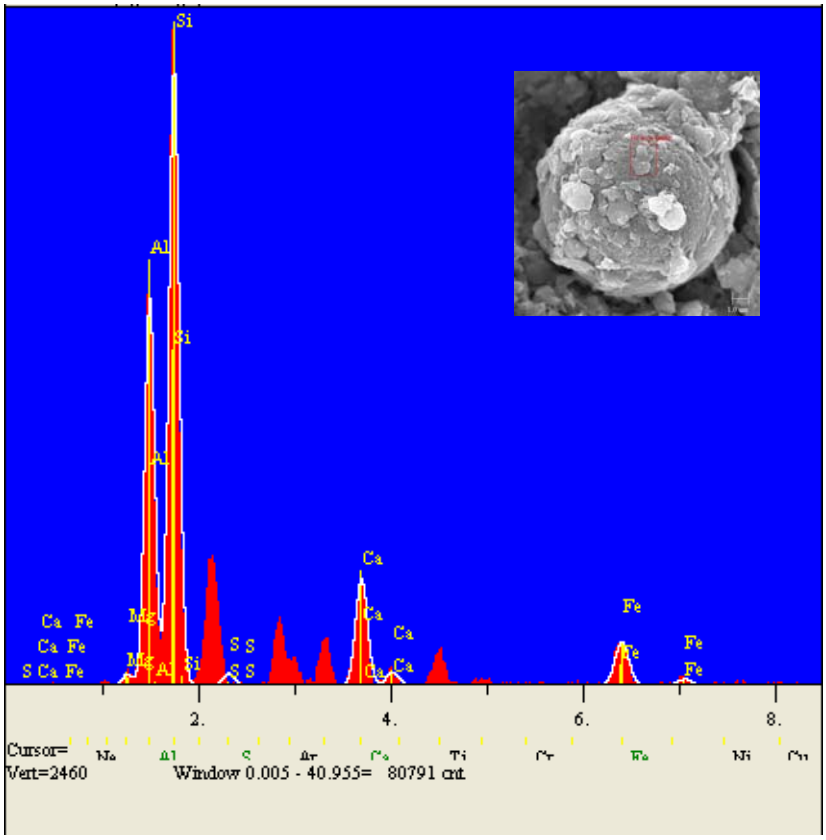

Figure 5-13 EDS for Hanson specimens with coating hydration

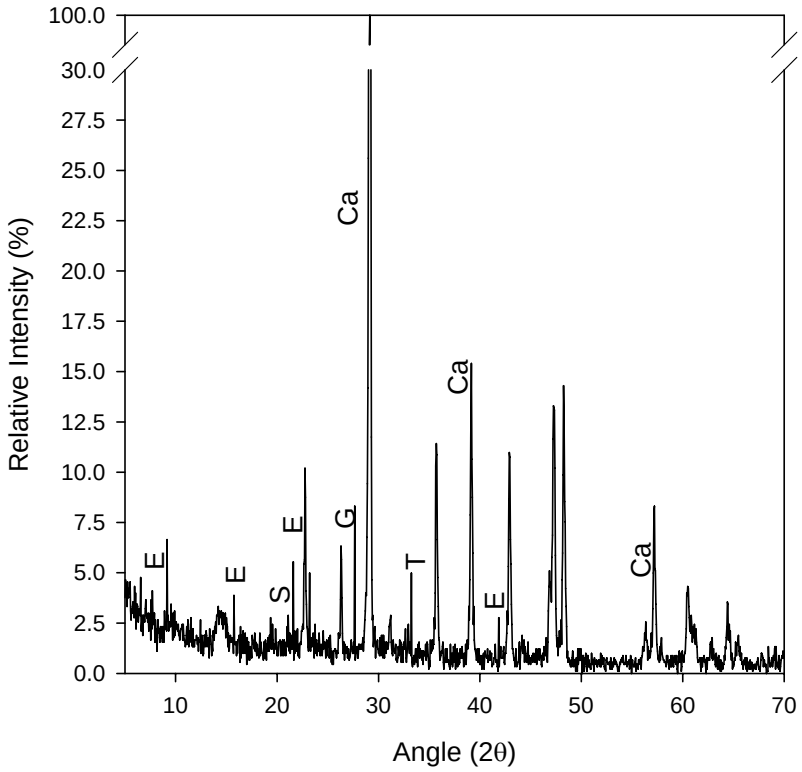

Figure 5-14 Diffractogram of 10% CFA stabilized Meridian specimen cured for 28 days

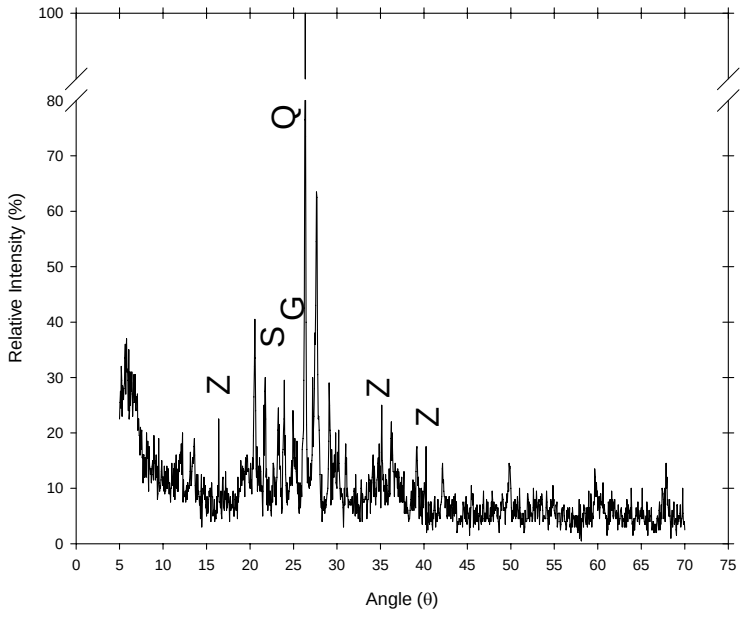

Figure 5-15 Diffractogram of 10% CFA stabilized Hanson specimen cured for 28 days

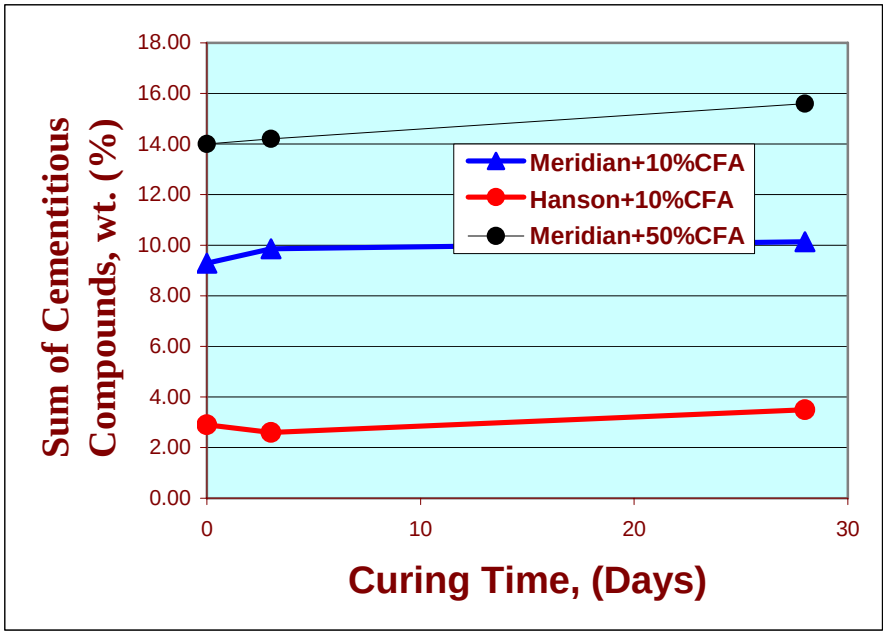

Figure 5-16 Variation of SCC values with curing time

Figure 5-17 Effect of different stabilizing agents on SCC

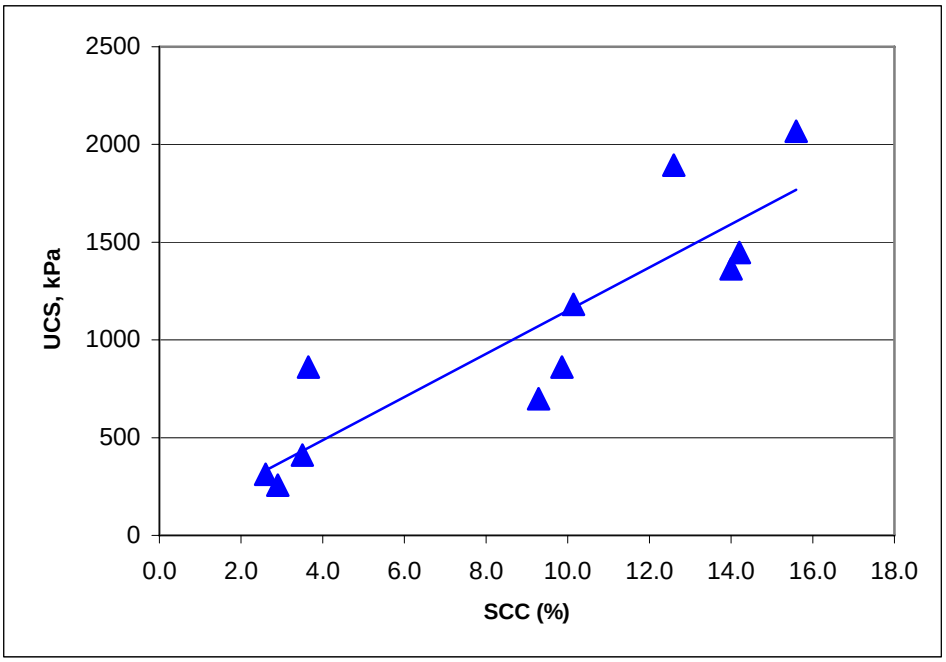

Figure 5-18 Variation of UCS with SCC

CHAPTER

6

FINITE ELEMENT MODELING OF CEMENTITOUSLY STABILIZED UN-NOTCHED BEAMS USING A SMEARED FRACTURE APPROACH

6.1 Introduction

During the past decade, the design of a pavement structure has evolved from an empirical approach, namely, AASHTO 1993 design guide, to a mechanistic-empirical approach (AASHTO 2002 design guide). The empirical method was based primarily on experience and/or observations from laboratory or field tests, while the mechanistic-empirical method relates the pavement response to stresses and strains due to traffic loading, specifically, the tensile strain developed at the bottom of the asphalt concrete (AC) layer and the compressive strain developed at the top of the subgrade layer. These strains are related to the number of allowable load repetitions causing either fatigue or rutting failure in an uncracked pavement, which may not be representative of situations when a crack is induced in the pavement (Tjan, 1998).

Cracks can be caused by the fatigue failure of an asphalt surface or a stabilized base under traffic loading and/or various environmental factors. Cracks generally start at the bottom of the asphalt surface or stabilized base, which may propagate to the surface, under a wheel load (Huang, 2004; Song et al., 2005). A number of studies have been undertaken previously to obtain a better understanding of the cracking mechanisms in an AC pavement structure (Majidzadeh, 1970; Majidzadeh et

al., 1971; Monismith et al., 1971; Lytton et al., 1993; Kim and El Hussein, 1995; Jacobs et al., 1996). These studies, however, were generally limited to experiments, stationary cracks, and to fracture of asphalt concrete. Other studies (Sobhan, 1997; Cavey et al., 1995; NCHRP, 1992) evaluated the field and laboratory properties such as flexural strength and tensile strength of stabilized aggregate bases, without any consideration to numerical modeling. None of these studies in the literature, however, to the author's knowledge, have addressed the fracture mechanics of cementitously stabilized aggregate bases.

Consequently, there is a need to better understand the flexural behavior of a stabilized beam in light of fracture mechanics-based numerical modeling. It is important to note that a design based on either empirical or a mechanistic-empirical approach formulated for an uncracked pavement may not be representative of the actual behavior of a pavement structure with a stabilized base that experiences cracking in the field. The numerical modeling of a stabilized base pursued here is based on the use of fracture energy in pavement analysis. Specifically, a smeared crack model is employed to assess the flexural behavior of un-notched stabilized beams cured for 3 days and 28 days. Finite element predictions are compared with pertinent load-deflection data of 3-day and 28-day cured beams. Meridian aggregate stabilized with 10% CFA was used to mold these beams. Properties of the aggregate and fly ash used are provided in Chapter 2, while Chapter 4 describes in detail the laboratory procedure used for the preparation of these beam specimens.

6.2 Literature review

Cavey et al. (1995) conducted a study, having both field and laboratory

components, to assess the suitability of producing a low-cost pavement base course material from recycled concrete aggregate stabilized with cement. Split tensile, flexural strength, and toughness tests were conducted. Significant enhancement in properties was observed. Another study by NCHRP (1992) highlighted the importance of flexural strength in designing a pavement structure with a stabilized aggregate base. Flexural strength, tensile strength, and compressive strength of stabilized aggregate bases were examined.

According to Ioannides and Peng (2004), many state DOTs and other transportation agencies are actively pursuing a more mechanistic-based design of pavements. Such approaches are expected to improve the design of new pavements in the 21st century. Three issues are important in this respect: (1) failure models; (2) material characterization procedure; and (3) new techniques to account for the stochastic nature of pavement problems. These issues need to be addressed to improve the mechanistic analysis and design procedures. Ioannides and Peng (2004) addressed some of these issues in their work, where a fracture mechanics-based approach was used to predict the structural behavior of a pavement structure. In their study, the Hillerborg's Fictitious Crack Model was used to simulate the crack growth in concrete slabs. ABAQUS was utilized to examine the fracture behavior of the slabs.

Song et al. (2005) employed a cohesive zone model to investigate the fracture behavior of asphalt concrete (AC). The separation and traction response, along the cohesive zone ahead of a crack tip, was modeled by an exponential law by means of a softening cohesive law. The cohesive zone model approach was used to observe the

crack propagation in mode I single-edge and mixed-mode notched beams. Also, the Transportation Research Board's Committee on Flexible Pavement Design (Seeds, 2005) noted that fracture mechanics-based modeling may be next to be used in the future M-E design of pavements.

Wagoner et al. (2005) conducted laboratory tests to select a prospective fracture test for asphalt concrete that complemented the numerical model used for investigating reflective cracking in asphalt concrete overlays. Two series of beam specimens were tested to simulate two different fracture models: (1) with single-edge notch (in the middle), and (2) with offset notch. Mode I represents the tensile opening, and the mixed-mode combines both the tensile opening and the shearing. It was reported that the three-point loading configuration leads to simple testing fixtures and relatively simple stress states during the test. It was also mentioned that modification of the single-edge geometry (with offset notch) can be used to investigate the mixed-mode fracture properties of AC. Such information is vital when studying the mechanisms associated with reflective cracking and thermal behavior of asphalt pavements.

6.3 Fracture Models

A number of fracture models have been used to analyze the fracture behavior of pavement materials, namely, concrete and asphalt. Soares (1997) reported that early attempts to model concrete fracture were generally similar to the analysis of cracks in metals by Griffith (1921) and Irwin (1948). These analyses were based on the linear elastic fracture mechanics theory. Such a model is inappropriate for most concrete structures due to the presence of numerous micro cracks in front of a macroscopic

crack in the fracture process zone, as indicated by Shah and McGarry (1971). As a result, other models, namely, two-parameter model, crack band models, and cohesive zone models, were developed in an attempt to account for the effects of the process zone (Soares, 1997).

Two distinct approaches, namely, discrete crack approach and smeared crack approach, have previously been used to model fracture response within the framework of the finite element method. The discrete approach treats each crack individually and is typically associated with the use of interface elements (Soares, 1997; Ingraffea, 1977; Chen and Saleeb, 1982). The second approach, known as the smeared crack model, was introduced by Rashid (1968). The smeared crack approach assumes that the materials remain as a continuum as it develops cracks. It also assumes an infinite number of parallel fissures across the cracked element. Chen and Saleeb (1982) illustrate an application of this approach for concrete. This approach does not track individual "macro" cracks, but constitutive calculations are performed independently at each integration point of the finite element mesh (ABAQUS, 2005). The presence of cracks enters into these calculations by the way in which the cracks affect the stress and material stiffness of the region surrounding the integration point. As noted by ABAQUS (2005), in general this approach is a preferred choice for modeling concrete if the load-deflection behavior is desired. No specific applications have been reported previously for stabilized aggregates that are similar to concrete but much weaker. In the present study, the smeared approach, available in ABAQUS, is used in modeling un-notched stabilized aggregate beams under flexural loading.

6.4 Finite Element Modeling of Beam Specimens

ABAQUS, which is a general-purpose (1-D, 2-D and 3-D, static or dynamic) finite element code, was employed in this study for modeling stabilized beams. The problem at hand is a simply supported beam under flexural loading. Beam specimens having a length (L) of 53.34 cm (21 in.), a width (w) of 15.24 cm (6 in.) and a depth (d) of 15.24 cm (6 in.) are utilized. Each beam is subjected to a third-point loading (ASTM D 1635-95), as shown in Figure 6-1.

6.4.1 Element type

Several studies (Zaghloul et al., 1995; Pan, 1997; Pirabarooban, 2002) have used eight-noded, linear brick elements (C3D8R) in analyzing problems similar to that under consideration. According to ABAQUS (2005) manuals a minimum of four-noded linear elements (CPS4R) for a 2-D mesh and eight-noded elements (C3D8R) for a 3-D mesh, with a reduced integration scheme, is needed to capture flexural response of a beam. ABAQUS (2005) manuals have used the C3D8R element to illustrate the use of smeared crack approach in idealizing a 3-D reinforced concrete slab. The same element configuration was also used for the analysis of 3-D reinforced concrete structures and 3-D un-reinforced notched concrete beam under 3-point bending. The C3D8R-type element was, therefore, utilized here to model the flexural response of un-notched, cementitiously stabilized aggregate beams under 3-D idealization. Figure 6-2 shows the 3-D finite element mesh of the beam used here along with the boundary conditions. The number of elements in the mesh is 1792. This mesh was considered representative, after examining the effect of different mesh sizes on the overall behavior of the beam.

6.4.2 Model Parameters

6.4.2.1 Stress-Strain Behavior

The smeared crack model requires the stress-strain behavior of plain material under uniaxial compression loading outside the elastic range. In this study, a total of seven cylindrical specimens (15.24 cm x 30.48 cm, i.e., 6 in. x 12 in.) were molded according to the test procedure described by Khoury (2001) and tested to obtain representative stress-strain data for CFA-stabilized aggregate base. Out of the seven specimens, three specimens were cured for 3 days, while the other four were cured for 28 days. The stress-strain curve of each specimen was used to determine the unconfined compressive strength and the plastic strain. Due to the nature of laboratory tests involved and the variability of the test results, as experienced in the present study, it was decided to perform a statistical analysis to check for outliers. The average of all the replicate curves was used as the input stress-strain curve representing the behavior of CFA-stabilized material under uniaxial compression loading. The average stress-strain data thus obtained for 3-day and 28-day cured specimens is presented in Error! Reference source not found..

6.4.2.2 Failure Ratios

The smeared crack model uses a failure surface to determine the initiation of cracking. This failure surface, known as "crack detection surface," is a linear relationship between the effective pressure (first invariant) and the Von Misses stress (ABAQUS, 2005). Defining the crack detection surface requires the determination of the following four failure ratios.

(1) R-1: *Ratio of the ultimate biaxial compressive stress to the ultimate uniaxial compressive stress.*

As per the definition of R-1, biaxial and uniaxial compressive strength values are required to determine this ratio. A total of 8 rectangular specimens (15.24 cm x 15.24 cm x 5.08 cm, i.e., 6 in. x 6 in. x 2 in.) were molded. Four of these specimens were cured for 3 days and the other four for 28 days. After curing, these specimens were tested in accordance with the test procedure described in Kupfer and Gerstle (1973). The test consists of failing the rectangular (plate) specimens at a principal stress ratio (σ_1/σ_2) of 1 in compression. Results showed that the average biaxial strength of 3-day cured specimens is approximately 3,347 kPa (486 psi) with a standard deviation of 951 kPa (138 psi). The 28-day cured specimens had an average biaxial strength of approximately 4,437 kPa (644 psi) with a standard deviation of 1,310 kPa (190 psi). Given the average biaxial strengths and the average uniaxial compressive strength (see Table 6-1) the R-1 value was considered 1.76 for 3-day cured specimens and 1.55 for 28-day cured specimens.

(2) R-2: *Ratio of the uniaxial tensile stress to the ultimate uniaxial compressive stress.*

Determination of R-2 requires both tensile strength and uniaxial compressive strength values. Since it is difficult and tricky to conduct tensile tests on stabilized aggregate specimens, the indirect tensile strength was considered as the tensile strength of the stabilized aggregate. A study by NCHRP (1992) reported that the indirect tensile strength provides a reasonable measure of the tensile strength of stabilized aggregate materials. Indirect tensile strength tests were performed in accordance with the ASTM D 3967 test method on eight specimens of which four were cured for 3 days and the other four for 28 days. Each specimen had a height of approximately 11.58 cm (4.56 in.) and a diameter of approximately 15.24 cm (6 in).

From these test results, the 3-day cured specimens had an average tensile strength of approximately 135 kPa (19.6 psi) (with a standard deviation of 22.74 kPa; 3.3 psi), while the 28-day cured specimens had an average tensile strength of 200 kPa (29 psi) (with a standard deviation of 11 kPa; 1.6 psi). From these results and from the compressive strength test results in Error! Reference source not found., the R-2 values were found to be 0.071 and 0.069 for 3-day and 28-day cured specimens, respectively.

(3) R-3: *Ratio of the magnitude of a principal component of plastic strain at ultimate stress in biaxial compression to the plastic strain at ultimate stress in uniaxial compression.*

Results from the biaxial and uniaxial compression tests, discussed in previous sections, were used to evaluate R-3 for 3- and 28- cured specimens. From the biaxial strength tests, it was found that the average plastic strain of 3-day cured specimens was approximately 0.0031 cm/cm (0.0031 in./in.). The 28-day cured specimens had an average value of 0.0022 cm/cm (0.0031 in./in.). From Error! Reference source not found., it is evident that 3-day cured specimens had an average plastic strain (at ultimate stress, uniaxial compression test) of 0.0014 cm/cm (0.0014 in./in.). For 28-day cured specimens, the corresponding plastic strain is 0.0012 cm/cm (0.0012 in./in.). Given these values, R-3 values were found to be approximately 2.21 for 3-day cured specimens and 1.83 for 28-day cured specimens.

(4) R-4: *Ratio of the tensile principal stress at cracking, in plane stress, when the other principal stress is at ultimate compressive value, to the tensile cracking stress under uniaxial tension.*

Determination of R-4 ratio requires the evaluation of the tensile stress at cracking when the other principal stress is at ultimate. Such property requires the performance of biaxial test, where a tensile stress σ_1 is applied in one direction with a constant σ_2

equal to the ultimate compressive strength in the other direction. Performing such a laboratory test on rectangular specimens of stabilized aggregate materials is quite difficult and may not be feasible. As such, a value of 0.3333 was used to represent the behavior of Meridian aggregate stabilized with 10% CFA. Influence of this parameter on the overall behavior of the beam was examined through a parametric study.

6.4.2.3 Tension-Stiffening (Softening) Curve

The smeared crack model requires the tension-stiffening curve as an input parameter to describe the post-failure behavior after cracking. The tension-stiffening curve is a function of the crack opening, which is considered a material property. In this study, a linear tension softening curve was used to present the behavior of the stabilized aggregate as shown in Figure 6-3. Such a curve can be determined from a direct tension test of a notched specimen, where the tensile strength versus crack opening is determined. Since performing such a test on stabilized aggregate base is not feasible and quite cumbersome, an alternate approach was employed. The approach consists of determining the fracture energy (G_f) of stabilized aggregate base from a three-point bending test of a notched beam, as described in the next section. Given the fracture energy and the tensile strength, the ultimate displacement u_o (at which the postfailure strain softening curve gives a zero stress) can be determined from the following mathematical equation (ABAQUS, 2005; Soares, 1997; and Bazant and Planas, 1998):

$$u_o = 2\frac{G_f}{\sigma_t} \qquad \textbf{(6-1)}$$

where, σ_t is the maximum tensile strength. The procedure to evaluate the tensile strength of the stabilized materials is presented earlier. The procedure for the evaluation of the fracture energy is described below.

6.4.2.3.1 Determination of Fracture Energy

One of the methods to determine the fracture energy is the RILEM laboratory test procedure described by Bazant and Planas (1998). The RILEM method consists of determining the fracture energy, for mode I fracture, from a three-point bending test on a notched beam specimen, as illustrated in Figure 6-4. The load-deflection (P-δ curve) curve is established and used to calculate the energy W_o (area under the P-δ curve) supplied by the load P. Given W_o, the fracture energy is calculated from the following equation:

$$G_f = \frac{(W_o + mg\delta_o)}{A_o} \qquad \textbf{(6-2)}$$

where, $mg\delta_o$ is a correction for the weight of the beam and loading arrangement, δ_o is the deflection at failure, and A_o is the area of the ligament given by the projection of the fracture zone perpendicular to the beam axis, as shown in Figure 6-4. This test method has been previously used by several researchers (Hillerborg, 1985; Soares, 1997; RILEM, 1991).

A total of 5-notched beam specimens were prepared with Meridian aggregate stabilized with 10% CFA, in accordance with the specimen preparation procedure described in Chapter 4. Out of the five specimens, two specimens were cured for 3 days and three for 28 days, prior to testing for G_f. Each beam had a width of 10.16 cm (4 in.), a depth of 15.24 cm (6 in.), a length of 53.34 cm (21 in.), and a notch depth, a_o of 2.54 cm (1 in.), as shown in Figure 6-4. Figure 6-5 shows a photographic

view of the test setup of a notched beam prior to testing for G_f.. Specimens were loaded at a constant displacement rates such that the maximum load was reached in approximately 5 min., as recommended by RILEM test procedure (RILEM, 1991). The load-deflection curves for 3-day and 28-day cured specimens were recorded and are graphically shown in Figures 6-6 and 6-7, respectively. From these figures, W_o and δ_o values were determined and used for calculating G_f, as specified by Eq. 6-2, for 3- and 28-day cured specimens. It was found that the average G_f value for 3-day cured specimens was 0.066 N/cm (0.038 lb/in.), while the 28-day cured specimens had an average G_f value of approximately 0.114 N/cm (0.065 lb/in.). Given these values and the tensile strength (presented in section 6.4.2.2), the ultimate displacements (u_o) (corresponding to a tensile strength of zero, as shown in Figure 6-3) were determined from Eq. 6-1. The average u_o of the 3-day cured specimens was found to be approximately 0.00965 cm (0.0038 in.), while the 28-day cured specimens had an average u_o of 0.01143 cm (0.0045 in.). Figure 6-8 shows a photographic view of crack path during the fracture energy test.

6.4.2.4 Postcracking Shear Retention

The smeared crack model has the option of taking into consideration the effect of postcracking shear retention. The shear retention is specified by the reduction in the shear modulus when cracking takes place. Mathematically, such reduction is presented by ρ G, where G is the elastic shear modulus of the uncracked materials and ρ is a multiplying factor. In this study, the full shear retention approach (shear response is not affected by cracking) was used. It is also important to note that determination of ρ from laboratory experiments is quite difficult and not feasible

since combined tension and shear tests are required.

6.5 Presentation and Discussion of Results

The load-deflection responses obtained from the laboratory results and the numerical simulation of 3-day un-notched stabilized beams are presented in Figure 6-9. In Figure 6-9, the laboratory test results are represented by a range (hatched area); it is a way to exhibit the nature of the variability in the laboratory test results. And, the numerical response of the beam is presented by a single curve, since the average values of all the model parameters defined in the previous sections were used. Figure 6-10 is another way of presenting the results, where the average load-deflection curve from laboratory testing and the numerical prediction are plotted. From Figure 6-9, it is evident that the load-deflection curve (from numerical prediction) falls within the experimental results up to a deflection of 0.01778 cm (0.007 in.), beyond which a lower trend is observed. This trend in the softening zone of the load-deflection curve could be attributed to the softening-tension curve defined for the 3-day cured specimens. A more rapid reduction in stress (as seen in the tension-softening curve) after initial cracking leads to less stiff responses. One can also observe that the maximum load of the beam compares well with the experimental data (Figure 6-10). The maximum load (numerical prediction) is approximately 1,335 N (300 lb) compared to the experimental value of 1,401 N (315 lb).

Results for the 28-day cured specimen are graphically illustrated in Figures 6–11 and 6–12. Figure 6-11 shows the threshold of the experimental results, while Figure 6-12 shows only the average laboratory and the predicted load-deflection curves. The numerical results fall within the range of the experimental test results, as shown in

Figure 6-11. The maximum loads for the 28-day cured specimens from both experimental and numerical-prediction results are fairly close. In terms of magnitude, the peak load from the finite element prediction is approximately 2,255 N (507 lb), which occurred at a deflection value of 0.011 cm (0.0044 in.). Comparatively, the laboratory results show an average peak value of approximately 2,576 N (579 lb) at a deflection of 0.00965 cm (0.0038 in.). Contrary to the 3-day cured specimens, the postcracking behavior of 28-day cured specimens is somewhat stiff compared to the experimental results, as seen in Figure 6-12. Such behavior is expected because of the bias the smeared crack approach introduces in the analysis. The smeared crack approach does not account for the crack propagation, although the crack propagation paths (vertical or curved) are clearly observed in experimental results (see Figure 6-13). Figure 6-13 shows the cracks path in an un-notched beam in the laboratory. This trend cannot be modeled using the smeared crack approach, since the presence of cracks in the smeared approach (as mentioned in previous sections) enters only through the constitutive calculations. Modeling of discrete cracks may provide a better representation of such behavior, but it would be a very complex and rather impractical approach from an application point of view.

From the aforementioned results and observations, it is evident that the smeared crack model can be useful, in an overall sense, in predicting the flexural behavior of stabilized aggregate beams. Implementation of the smeared crack model can be pursued in the development of mechanistic-based pavement design approach. In this regard, results from the present study are in agreement with the sentiment reflected by other studies, (Majidzadeh, 1970; Soares, 1997; Ioannides and Peng, 2004; and Seeds,

2005) concerning the importance of fracture energy approach in pavement analysis and design.

6.6 Concluding Remarks

This study was undertaken to assess the use of the smeared crack approach in predicting the flexural behavior of stabilized aggregate bases. It was observed that, overall, the peak load from the numerical simulation compared fairly well with the experimental results for both 3-day and 28-day cured specimens. On the other hand, the trend in the load-deflection exhibited some differences in the softening zone. For 3-day cured specimens, the postcracking behavior was less stiff than the experimental results, which could be attributed to the faster reduction in the tension-stiffening curves. As for 28-day cured specimens, the postpeak behavior exhibited a stiffer response compared to experimental data. Such behavior is expected and could be explained by the bias introduced when using a smeared crack approach that does not account for crack propagation although this phenomenon is clearly evident in testing. Modeling of discrete cracks may provide a better representation of such behavior, but it will be more complex and rather impractical approach from an application point of view.

Table 6-1 Stress-strain data for 3-Day and 28-Day cured specimens

Strain (in/in)	3-Day Cured Specimens		28-Day Cured Specimens	
	Average Stress (kPa)	Average Stress (psi)	Average Stress (kPa)	Average Stress (psi)
0	1144	166	1621	235
0.0001	1226	178	1801	261
0.0002	1309	190	1967	285
0.0004	1453	211	2257	328
0.0006	1584	230	2491	362
0.0008	1695	246	2671	388
0.001	1785	259	2794	406
0.0012	1853	269	2862	415
0.0014	1902	276	n/a	n/a

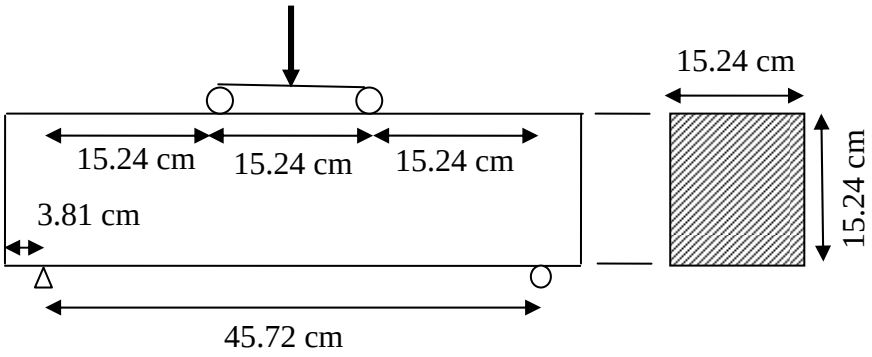

Figure 6-1 Schematic view of an un-notched beam under flexural loading: geometry and dimensions

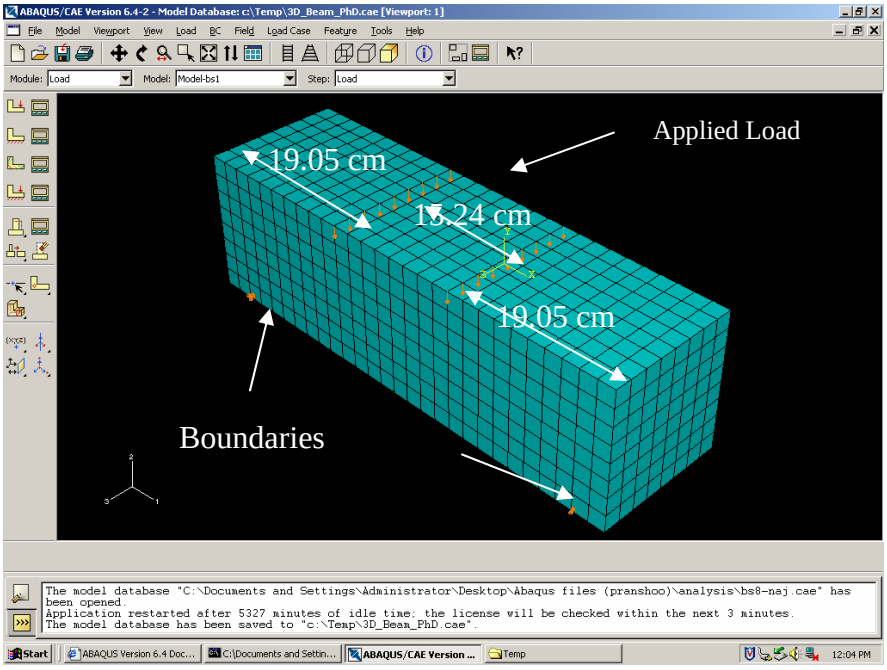

Figure 6-2 3-D finite element mesh used for un-notched beam

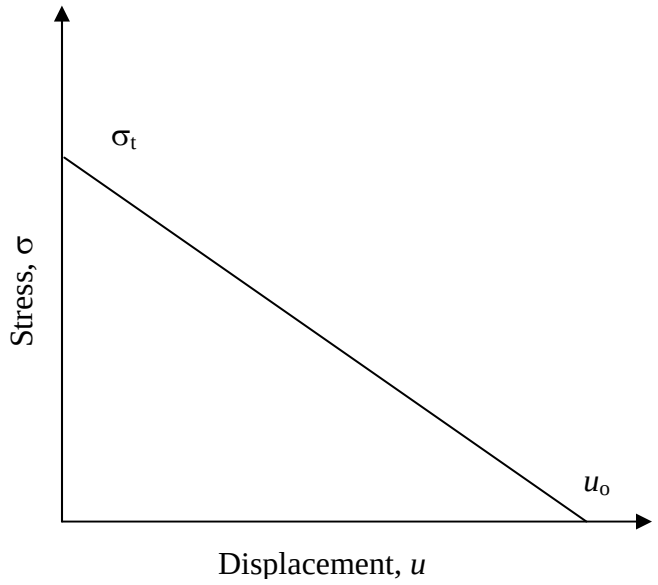

Figure 6-3 Tension-stiffening model used in this study

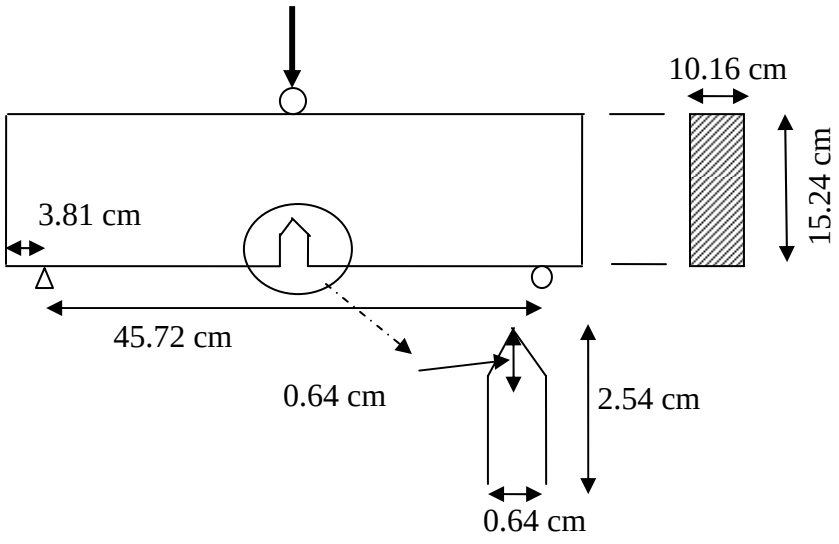

Figure 6-4 Schematic view of a notched-beam for fracture energy test: geometry and dimensions

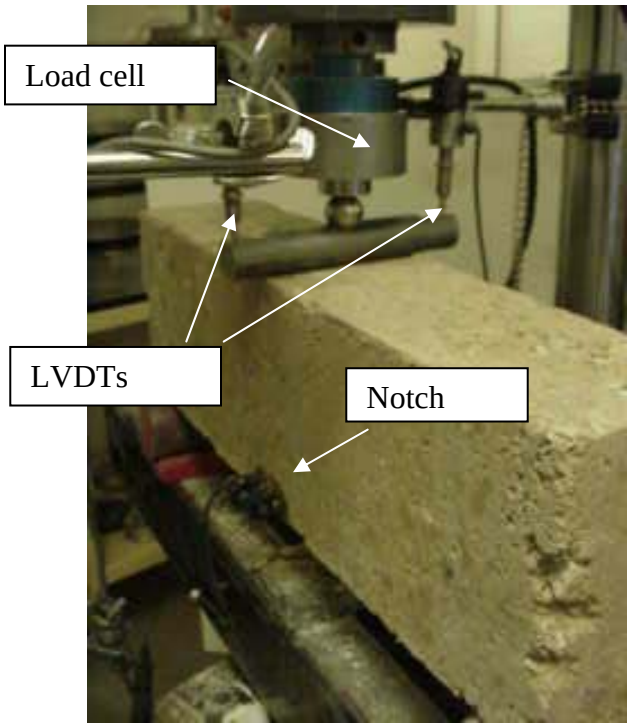

Figure 6-5 Photographic view of a notched beam specimen prior to testing for G_f

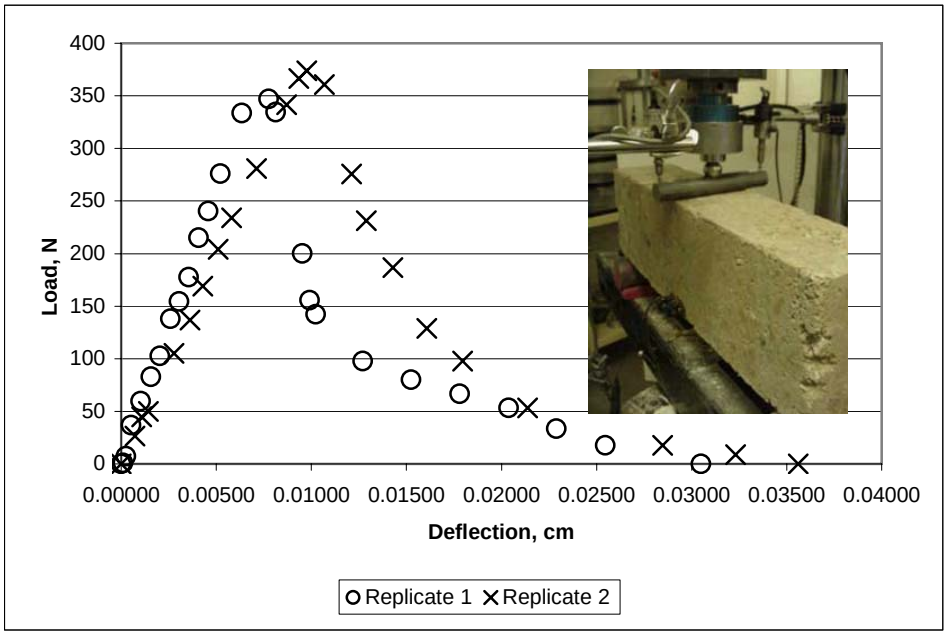

Figure 6-6 Load-deflection curve for 3-day cured specimens

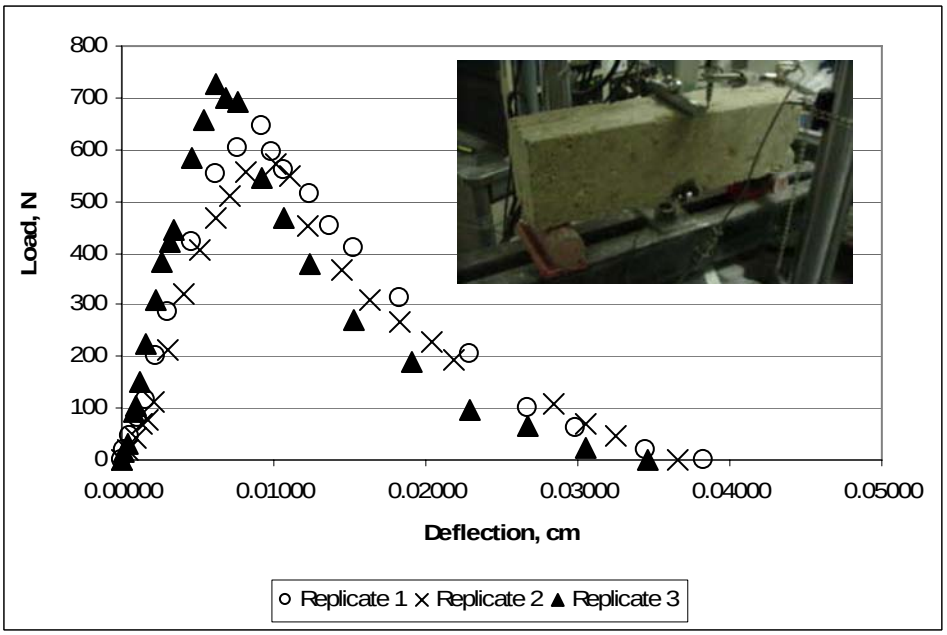

Figure 6-7 Load-deflection curves for 28-day cured specimens

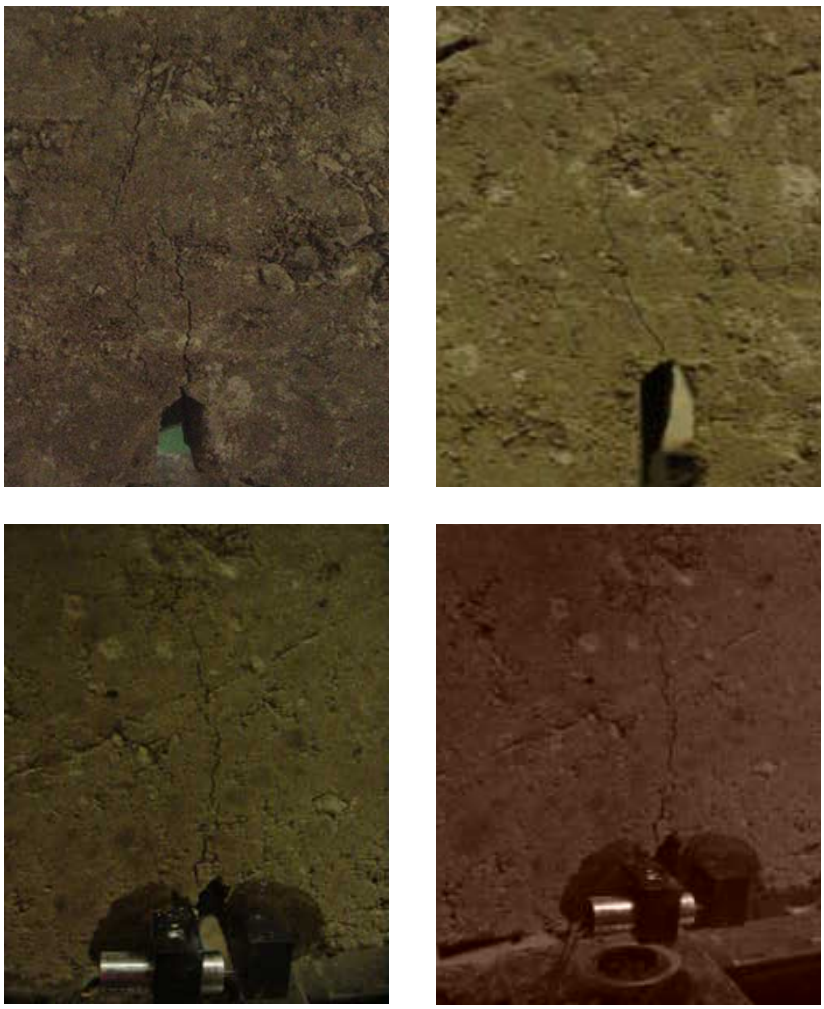

Figure 6-8 Cracks path during the fracture energy test

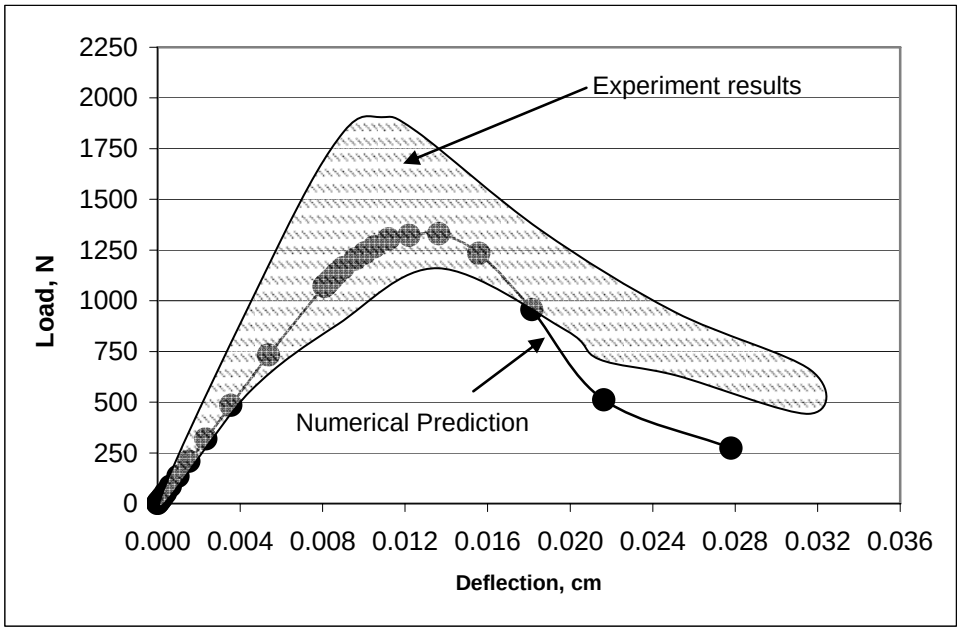

Figure 6-9 Comparison between experimental results and numerical prediction for 3-day cured specimens

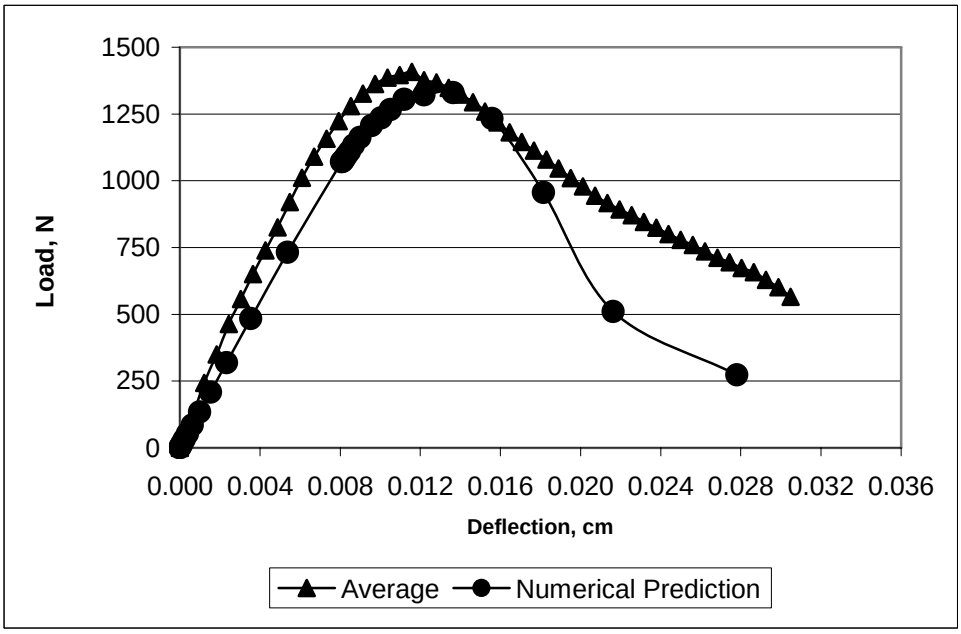

Figure 6-10 Comparison between average experimental results and numerical prediction for 3-day cured specimens

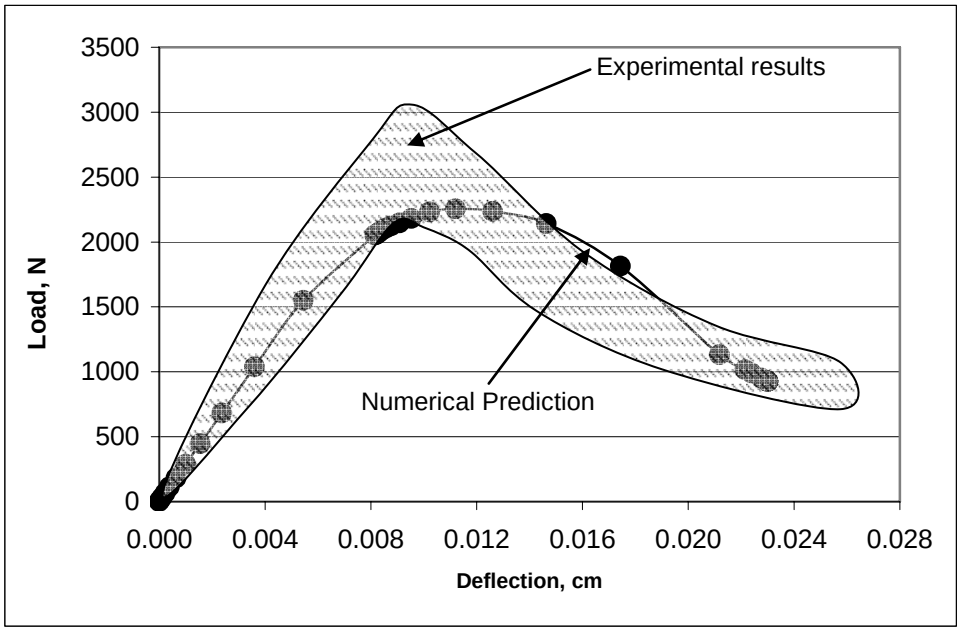

Figure 6-11 Comparison between experimental results and numerical prediction for 28-day cured specimens

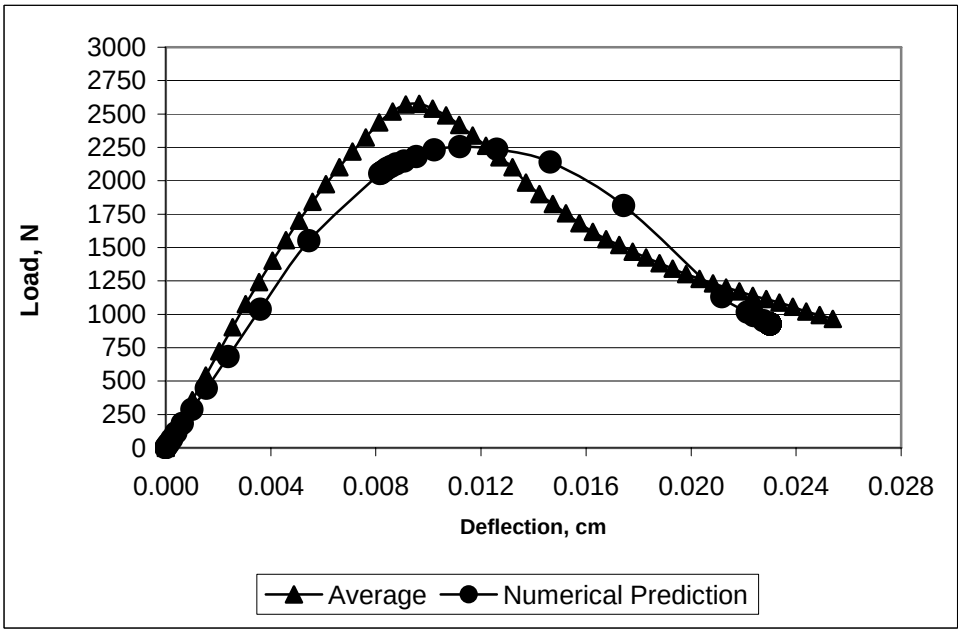

Figure 6-12 Comparison between average experimental results and numerical prediction for 28-day cured specimens

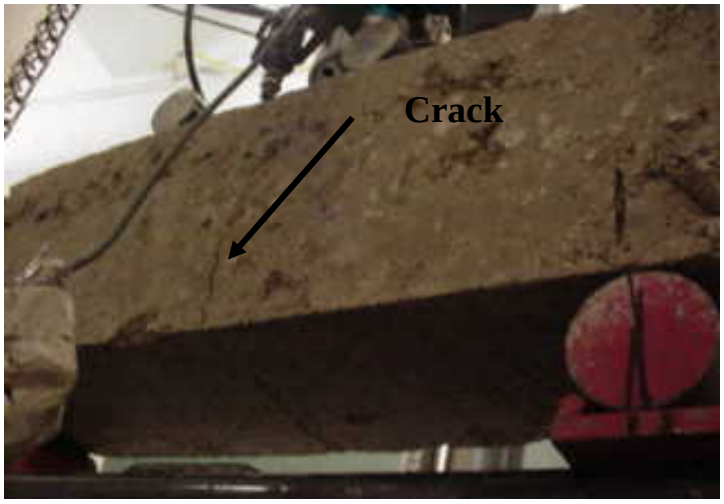

Figure 6-13 Crack propagation of un-notched stabilized beam during a flexural strength test

CHAPTER

7

SUMMARY AND RECOMMENDATIONS

7.1 Summary

The notion of durability of pavement materials induced by environmental factors such as freeze-thaw and wet-dry actions can have a major effect on the performance of a pavement structure. Variation in pavement performance due to these actions indicates possible changes in the engineering properties of pavement materials.

In this study, the effect of F-T and W-D cycles on the performance of stabilized aggregate bases was examined. Four aggregates commonly used in Oklahoma were utilized: (1) Meridian; (2) Richard Spur; (3) Sawyer; and (4) Hanson. Cylindrical specimens were prepared of aggregates mixed with different stabilizing agents (i.e., cement kiln dust (CKD), class C fly ahs (CFA), or fluidized bed ash) and water, followed by compaction. After compaction specimens were cured for 28 days, subjected to either W-D or F-T cycles prior to testing for resilient modulus. Results showed that the resilient modulus, in general, reduces as W-D cycles increase up to 30 cycles. However, the extent of reduction depends on the number of cycles, and on the stabilizing agents. For example, the effect of these cycles on CKD-stabilized specimens is more detrimental than CFA-stabilized specimens, followed by FBA-stabilized specimens. It was also found that the variation of M_r values correlate better

with amount of lime, SAF content, and optimum moisture content and maximum dry density. In addition, the M_r values of specimens subjected to F-T cycles exhibited a decrease as F-T increased up to 30 cycles. Such decreases can be explained by the amount of water absorbed by the specimens during the thawing process. The more the amount of water absorbed, the higher the distortion of specimens during the freezing phase due to formation of ice lenses. A relative comparison showed changes in resilient modulus is more vulnerable to F-T cycles than W-D cycles.

The effect of F-T cycles on the resilient modulus in flexural (M_{rf}) and modulus of rupture (MOR) was also observed on CFA-stabilized aggregate. It is due to the fact that stabilized aggregate bases are subjected to flexural stress under vehicular loading. Beam specimens were prepared by compacting aggregate mixed with 10% CFA and water. After compaction, specimens were cured for 1 hour, 3 days and 28 days prior to subjecting them for 0, 8 and 16 F-T cycles. After a specified number of F-T cycles, specimens were tested for M_{rf} and MOR. Results showed that both M_{rf} and MOR exhibited a decrease with the number of F-T cycles. The level of decrease depended on the curing time of the stabilized beam. It was also found that the beams that tested without any curing (1 hour) were more susceptible to reduction in M_{rf} than 3-day cured specimens, followed by 28-day cured specimens. The effect of stress ratio on the resilient modulus was also observed. Results showed that M_{rf} values decrease as the stress ratio increased up to 0.6, beyond which only a slight decrease was observed. Findings from this study help enrich the database on the durability of stabilized aggregate bases. Also, the test procedures employed in this study are expected to benefit future studies in this area.

Another contribution of this study is the implementation of various techniques, namely, X-ray diffraction (XRD), scanning electron microscopy (SEM) and energy dispersive spectrum (EDS), to the evaluation of the micro-structural developments in cementitiously stabilized aggregates. Materials passing US standard No. 40 sieve were stabilized with different stabilizing agents, namely, cement kiln dust, class C fly ash, and fluidized bed ash. The effect of curing time was also examined. From EDS and SEM, it was found that the presence of cementitious compounds was responsible for an increase in strength compared to raw specimens. However, the intensity of crystals increased with time and percentage of fly ash. EDS and SEM were used as qualitative techniques to examine the micro-structural developments, while XRD was used to semi-quantify these compounds using the RIR method. Cementing compounds such as ettringite, C-S-H, C-A-H and CASH were identified and their mass percent varied from one stabilized specimen to another. Correlations between the sum of cementing compounds (SCC) and UCS values showed a fairly consistent trend. The UCS values increased approximately linearly with SCC.

Numerical modeling of pavements using finite element method has advanced steadily with the advancement of computing power. Several computer programs, namely, ILLI-PAVE, MICH-PAVE and Kenpave, have been developed for the analysis of pavement structures. Most of these programs assume the stabilized base layer as an uncracked layer, thereby overestimating the overall stiffness of a pavement structure. Recent developments in finite element modeling and the availability of general purpose computer programs such as ABAQUS have significantly enhanced the treatment of cracks in numerical modeling of a stabilized

base layer.

In this study, the flexural behavior of stabilized aggregate base was examined by using a smeared crack model, available in ABAQUS. The stabilized base layer is treated as a simply supported beam. Meridian aggregate stabilized with 10% CFA was used to mold these specimens. Laboratory tests, namely, tensile strength, compressive strength, biaxial strength, and flexural strength, were performed to calibrate the employed model for CFA-stabilized aggregates. The load-deflection curves from the finite element simulations were compared with pertinent laboratory results. Results showed that the peak loads from the numerical simulation compared well with the experimental results. The postcracking behavior, on the other hand, exhibited some differences in the softening zone of the load-deflection curves. For 3-day cured specimens, the load-deflection trend showed a less stiff behavior than the experimental results, which could be attributed to the steep change in the tension-softening curve. Contrary to the 3-day cured specimens, the postcracking behavior of 28-day cured specimens was somewhat stiff, due to the bias the smeared crack approach introduces to the analysis. The smeared crack approach does not account for the crack propagation (vertical or curved), although this phenomenon is clearly evident in experimental results.

In an overall sense, it is evident that the smeared crack model can be useful in predicting the flexural behavior of stabilized aggregate beams. Implementation of smeared crack model can be pursued in the mechanistic-based approach in the pursuit of a new and better procedure for designing pavements in the 21st century.

7.2 Recommendations

Based on the observations from this study, the following recommendations are made for future studies:

1. The change in the percentage of stabilizing agents changes the performance of stabilized aggregate bases under the durability effect of W-D and F-T cycles. Therefore, future studies are recommended to evaluate the durability effect of aggregate stabilized with different amounts of stabilizing agents. Such knowledge is important particularly in terms of design applications.
2. The resilient modulus tests were performed on specimens at either wet (after W-D cycles) or thaw (after F-T cycles) state to simulate the worst case scenario in the field. It seems necessary to conduct future tests on specimens at freeze or dry states to get systematic data that would provide valuable information about the performance of an aggregate base during its design life. Also, in real life, a pavement structure is subjected to combined cycles of freeze-thaw and wet-dry. Therefore, it is important to pursue the combined effect of F-T cycles and W-D cycles on the performance of stabilized aggregate bases, in a future study.
3. Drainage of a base layer is one of the most important factors in designing a pavement structure. If not well designed, it causes damage to the overall performance of a pavement structure. This factor was not addressed in this study. It is recommended that future tests be conducted to evaluate the drainage characteristics of stabilized aggregate bases. Also, future studies addressing the effect of aggregate gradation on the permeability and resilient modulus of stabilized aggregates would be beneficial.

4. There is a need to understand the reactions, both short-term and long-term, of cementitously stabilized aggregate bases. This study employed a semi-quantification method, known as reference intensity ratio (RIR), to observe the micro-structural development in stabilized aggregate specimens. Other quantification techniques such as Rietveld method are recommended for future studies to determine the developments of cementing compounds of cementitiously stabilized aggregates. Such studies would add useful information on the mechanism that occurs in the stabilization process.

5. Non-destructive methods have become more acceptable and available techniques to evaluate the modulus of pavement materials in both the laboratory and the field. These techniques have the potential to provide reliable moduli of pavement materials compared with traditional methods (e.g., resilient modulus testing). These techniques can provide comparable results under similar conditions in the laboratory and the field. A future study is recommended to evaluate the seismic modulus of stabilized aggregates in the laboratory. It is also important to have a field study to evaluate the performance of a pavement structure with stabilized layer, by using non-destructive techniques in the fields such as falling weight deflectometer (FWD) and surface analysis of seismic wave (SASW). A comparison between the laboratory and field results would be beneficial in this research area.

6. Although this study addressed the capability of smeared crack modeling in evaluating the behavior of stabilized beams under flexural loading, it was limited only to 10% CFA stabilized beams. A future study using the same

approach can be pursued to evaluate the flexural behavior of CKD- and FBA-stabilized beams. It is also recommended that additional studies be conducted to model discrete cracks in stabilized aggregate beams, although it is very complex and rather impractical approach from an application point of view. These studies would be beneficial in the pursuit of a new and better procedure for designing future pavements with stabilized aggregate bases.

REFERENCES

American Association of State Highway and Transportation Officials (AASHTO) (2005), ″http://www.mrr.dot.state.mn.us/pavement/PvmtDesign/designguide.asp,″ accessed April 2005.

ABAQUS (2005), ABAQUS/CAE User's Manual, version 6.5.

AMIA (2003), ″Semi-Quantitative Analysis - using the RIR method,″ http://www.rigakumsc.com/contract/amia_res_TN-G03.htm, accessed July 2003.

Baghdadi, Z.A., Fatani, M.N. and Sabban, N.A. (1995), Soil Modification by Cement Kiln Dust, ASCE Journal of Materials in Civil Engineering, Vol. 7, No. 4, 1995.

Barstis, W.F. and Metcalf, J. (2005), ″A Practical Approach to Criteria for the Use of Lime-Fly Ash Stabilization in Base Courses,″ Transportation Research Board 2005 Annual Meeting (CD-ROM), Washington D.C., January 2005.

Bazant, P.Z. and Planas, J. (1998), Fracture and Size Effect in Concrete and Other Quasibrittle Materials, CRC Press, Washington D.C., USA, ISBN 0-8493-8284, 616 pages.

Berg, K.C. (1998), Durability and Strength of Activated Reclaimed Iowa Class C Fly Ash Aggregate in Road Bases, Master Thesis, Iowa State University, 1998.

Bergeson, K.L. and Barnes, A. (1998), ″Iowa Thickness Design Guide for Low Volume Roads Using Reclaimed Hydrated Class C Fly Ash Bases,″ Proceedings of Transportation Conference, 1998.

Bergeson, K.L. and Mahrt, D. (2000), ″Reclaimed Fly Ash as Select Fill under PCC Pavement, ″ Proceedings of MID-Continent Transportation Symposium, 2000, pp. 147-150.

Cavey, J.K., Krizek, R.J., Sobhan, K. and Baker, W.H. (1995), Waste Fibers in Cement-Stabilized Recycled Aggregate Base Course Material, Journal of Transportation Research Record, No. 1486, 1995, pp. 97-106.

Chen, W.F. and Saleeb, A.F. (1982), Constitutive Equations for Engineering Materials, Wiley-Interscience Publication, John Wiley & Sons, NewYork, USA, 1982, Volume 1, ISBN 0-471-09149-9, 580 pages.

Dempsey, B.J. and Thompson, M.R. (1973) Vacuum Saturation Method for Predicting the Freeze-Thaw Durability of Stabilized Materials, Highway Research Record, No. 442, 1973.

Federal Highway Administration (FHWA) (1982), Kiln Dust-Fly Ash Systems for Highway Bases and Subbase, FHWA-RD-82-167, 1982, Federal Highway Administration, Washington, D.C.

Griffith, A.A. (1921), The Phenomena of Rupture and Flow in Solids, Philosophical Transactions of the Royal Society of London, Series A 221, 1921, pp. 163-198.

Hillerborg, A. (1985), The Theoretical Basis of a Method to Determine the Fracture Energy G_F of Concrete, Materials Structure, No. 18, 1985, pp. 291-296.

Huang, Y.H. (2004), Pavement Analysis and Design, 2nd edition, Prentice Hall, Inc. Englewood liffs, New Jersey, 2004, ISBN 0-13-142473-4, 775 pages.

Ingraffea, A.R. (1977), Discrete Fracture Propagation in Rock: Laboratory tests and Finite Element Analysis, Ph.D. Dissertation, University of Colorado, Boulder, Co, 1977.

Ioannides, A.M. and Peng, I. (2004), ″Finite Element Simulation of Crack Growth in Concrete Slabs: Implications for Pavement,″ Proceedings of the Fifth International Workshop on Fundamental Modeling of Concrete Pavements, Istanbul, Turkey, April, 2004.

Irwin, G.R. (1948), Fracture Dynamics, American Society for Metals, Cleveland, OH, pp. 147-166.

Jacobs, M.M., Hopman, P.C. and Molenaar, A.A. (1996), ″Application of Fracture Mechanics in Principles to Analyze Cracking in Asphalt Concrete,″ Proceedings of the Association of Asphalt Paving Technologists, 1996, pp. 1-39.

Jade (1999), Manual, Materials Data, Livermore, CA, 94550, Copyrights, 1995-1999.

Kalankamary, G.P. and Davidson, D.T. (1963), Development of a Freeze-Thaw Test for Design of Soil-cement, Highway Research Board (HRB), No. 36, 1963, pp. 77-96.

Khalid, J. (1993), Resilient Modulus versus Strength of Cement Stabilized Base Courses, Master Thesis, University of Arkansas, Arkansas, December 1993.

Khoury, N.N. and Zaman, M.M. (2006), Durability of Flexural Behavior of Fly Ash Stabilized Limestone Aggregate, ASTM Journal of Testing and Evaluation Materials, Vol. 34, No. 3, 2006.

Khoury, N.N. and Zaman, M.M. (2005a), Influences of Various Cementitious Agents on the Performance of Stabilized Aggregate Bases Subjected to Wet-Dry Cycles, International Journal of Pavement Engineering, June 2005, pending.

Khoury, N.N. and Zaman, M.M. (2005b), Environmental Effects on Durability of Aggregates Stabilized with Cementitious Materials, ASCE Journal of Materials in Civil Engineering, in press.

Khoury, N.N., Zaman, M.M. and Laguros, J.G. (2005c), Semi-Quantification of Cementing Products of Stabilized Aggregate Bases Using X-Ray Diffraction Technique, Journal of X-Ray Science and Technology, accepted for publication.

Khoury, N.N., Zaman, M.M. and Laguros, J.G. (2005d), Finite Element Modeling of Cementitiously Stabilized Un-notched Beams Using a Smeared Fracture Approach, ASCE International Journal of Geomechanics, will be submit for possible publication, December 2005.

Khoury, N.N, Zaman, M.M. and Khoury, C.N. (2005) New Laboratory Procedure for Characterization of Compaction in Fine-Grained Soils, Journal of Testing and Evaluation, American Society for Testing Materials, May 2005, pending.

Khoury, N.N. and Zaman, M.M. (2002), Effect of Wet-Dry Cycles on Class C Fly Ash Aggregate Base, Transportation Research Record, Journal of the Transportation Research Board, Geomaterials, No. 1787, 2002, pp.13-21.

Khoury, N.N. (2001), The Effect of Freeze-Thaw and Wet-Dry Cycles on Resilient Modulus of Class C Fly Ash Stabilized Aggregate Base, Master Thesis, The University of Oklahoma, Norman, Oklahoma, Summer, 2001.

Khoury, N.N., Srour, C. and Zaman, M. (2004), ″Performance of Stabilized Aggregate Base Under Flexural and Compressive Cyclic Load,″ Proceedings of the Geo-Trans 2004 Conference, UCLA campus, Los Angeles, CA, USA, July 27-31 2004.

Kim, K.W. and El Hussein, H.M. (1995), ″Effect of Differential Thermal Contraction on Fracture Properties of Asphalt Materials at Low Temperature,″ Proceedings of the Association of Asphalt Paving Technologists, 1995, pp. 474-499.

Kim, D. and Siddiki, N.Z. (2003), ″Lime Kiln Dust and Lime-A Comparative Study in Indiana,″ Transportation Research Board 2004 Annual Meeting (CD-ROM), Washingtonc D.C., January 2003.

Kruger, R.A. (1990), The Chemistry of Fly Ash and the Pozzolanic Reaction," Chemsa, Vol. 16, No 11, 1990, pp. 301-303.

Kupfer, H.B. and Gerstle, K.H. (1973), Behavior of Concrete Under Biaxial Stresses, Journal of the Engineering Mechanics Division, Vo., 99, No. EM4, August 1973.

Laguros, L.G. and Zenieris, P. (1987), Feasibility of Using Fly Ash as a Binder and Fine Aggregates for Bases, FHWA/OK 86(8), ORA 155-04, Item 2125, June 1987, Oklahoma Department of Transportation, Oklahoma City, OK.

Lav, A.H. and Lav, M.A. (2000), Microstructural Development of Stabilized Fly Ash as Pavement Base Material, Journal of Materials in Civil Engineering, ASCE, Vol. 12, No. 2, May 2000.

Lea, F.M. (1971), The Chemistry of Cement and Concrete, 1st edition, 1971.

Little, D.N., Males, E.H., Prusinski, J.R. and Stewart, B. (2005), ″Cementitious Stabilization,″ http://gulliver.trb.org/publications/millennium/00016.pdf, accessed January 2005.

Livingston, R.A., Stutzman, P.E. and Schumann, I. (1998), Quantitative X-ray Diffraction Analysis of Handmolded Brick, Conservation of Historic Brick Structures, Donhead Publishing Ltd., Shafesbury, UK, 1998.

Lytton, R.L. and Zollinger, D.G. (1993), Modeling Reliability in Pavement, Transportation Research Borard 72nd Annual Meeting (CD-ROM), Washington, D.C., January 1993.

Majidzadeh, K. (1970), Analysis of Fatigue and Fracture of Bituminous Paving Mixtures," Final report of Project RF 2845. Phase I, 1970, Ohio State University Research Foundation.

Majidzadeh, K., Kauffman, E.M. and Ramsamooj, D.V. (1971), ″Application of Fracture Mechanics in the Analysis of Pavement Fatigue,″ Proceedings of the Association of Asphalt Paving Technologists, 1971, pp. 227-246.

Majko M.R. (2004), Fly Ash in Soil Stabilization and as an Engineered Construction Material. www.geocities.com/capecanaveral/launchpad/2095/soilstab.htm. Accessed Oct. 5, 2000.

Miller, G. A., Zaman, M.M., Rahman, J. and Tan, K.N. (1999), Laboratory and Field Evaluation of Soil Stabilization using Cement Kiln Dust, Item 2144, ORA 125-5693, February 1999, Oklahoma Department of Transportation (ODOT), Oklahoma City, OK.

Minnick, L.J. Webster, W.C. and Prudy, E.J. (1967), Prediction of Fly Ash Performance," Proceedings Fly Ash Utilization Conference, Bureau of Mines Information Circular 8488, 1967.

Misra, A. (1998), Stabilization Characteristic of Clays Using Class C Fly Ash, Journal of Transportation Research Record, No. 1611, 1998, pp. 46-54.

Mitchell, J.K. and Shen, C.K. (1967), Soil-Cement Properties Determined by Repeated Loading in Relation to Bases for Flexible Pavements, Proceedings of the Second International Conference on the Structural Design of Asphalt Pavements, University of Michigan, 7-11 August 1967.

Monismith, C.L., Hicks, R.G. and Salam, Y.M. (1971), Basic Properties of Pavement Components, FHWA report RD-72-19, 1971, Federal Highway Administration, Washington, D.C.

National Highway Research Program (NCHRP) (2004), Mechanistic-Empirical Pavement Design Guide, Project 1-37A, December 2004.

National Cooperative Highway Research Report (NCHRP). (1992). Calibrated Mechanistic Structural Analysis Procedures for Pavements, Final Report, Project 1-26, May 1992.

National Cooperative Highway Research Report (NCHRP) (1976), Lime-Fly Ash-Stabilized Bases and Subbases, NCHRP 37, 1976, Transportation Research Board, National Council, Washington, D.C.

Nunan, T. and Humphrey, D. (1990), A Review and Experimentation of Gravel Stabilization Method, Technical Report 90-2, 1990, Maine Department of Transportation.

Pan, C.L. (1997), Analysis of Bituminous Mixtures Stripping/Rutting Potential, Ph.D. Dissertation, Purdue University, West Lafayette, Indian, August 1997.

Pandey, K.K. (1996), ″Evaluation of Resilient Modulus and Layer Coefficient of a Coal Ash Stabilized Marginal aggregate Base for AASHTO Flexible Pavement Design,″ Ph.D. Dissertation, University of Oklahoma, Norman, Oklahoma, 1996.

Parsons, R.L. and Kneebone, E. (2004), ″Durability of Fly Ash Stabilized Subgrades,″ Transportation Research Board 2004 Annual Meeting CD-ROM, Washington D.C., January 2004.

Pirabarooban, S. (2002), Modeling of Rutting in Asphalt Mixes Using ABAQUS, Master Thesis, University of Oklahoma, Norman, Oklahoma, 2002.

Rashid, Y.R. (1968), Analysis of Pre-stressed Concrete Pressure Vessels, Nuclear Engineering and Design, 7(4), 1968, pp. 334-344.

RILEM (1991), Size-effect Method for determining Fracture Energy and Process Zone Size of Concrete, Materials and Structures, 23, 1991, pp. 461-465.

Road Information Program (RIP) (2005),
″http://www.tripnet.org/nationalfactsheet.htm,″ accessed April, 2005.

Shah, S.P. and McGarry, F.J. (1971), Griffith Fracture Criterion and Concrete, Journal of Engineering Mechanics, ASCE, 97(EM6),1971, pp. 1663-1676.

Seeds, S. (2005), ″Flexible Pavement Design,″ www.trb.org, accessed June 2005.

Soares, J.B. (1997), Concrete Characterization Through Fracture Mechanics and Selected Pavement Applications, Ph.D. Dissertation, Texas A&M University, Texas, December 1997.

Sobhan, K. (1997), Stabilized Fiber-Reinforced Pavement Base Course With Recycled Aggregate, Ph.D. Dissertation, Northwestern University, Evanston, Illinois, June, 1997, 303 pages.

Song, S.H., Paulion, G. and Buttlar, W.G. (2005), Cohesive Zone Simulation of Mode I and Mixed Mode Crack Propagation in Asphalt Concrete, Geotechnical Special Publication, Geo Frontiers, 2005, pp. 130-142.

Sukumaran, B., Chamala, N., Willis, M, Davis, J, Scott, J. and Vishal, K. (2004), ″Three Dimensional Finite Element Modeling of Flexible Pavements,″ Proceedings of the 2004 FAA Worldwide Airport Technology Transfer Conference, Atlantic City, New Jersey, USA, April, 2004.

Tjan, A. (1998), ″Fracture Mechanics Approach for Crack Propagation Modeling in Flexible Pavement Structures,″ Proceedings of Conference of the Australian Road Research Board, Transport, pp. 132-147.

Thompson, M.R. and Smith, K.L. (1990), Repeated Triaxial Characterization of Granular Bases, Transportation Research Board, No 1278, 1990, pp. 7-17.

Zaghloul, S.M. and White, T.D. (1993), Use of Three Dimensional Finite Element Program for Flexible Pavement, Journal of Transportation Research Record, No. 1338, 1993, pp. 60-69.

Zaman, M.M. and Khoury, N.N. (2003), ″Effect of Freeze-Thaw Cycles on Class C Fly Ash Stabilized Aggregate Base,″ Transportation Research Board 82nd Annual Meeting (CD-Rom), Washington D.C., 12-16 January 2003.

Zaman, M.M., Zhu, J. and Laguros, J.G. (1999), Durability Effects on Resilient Moduli of Stabilized Aggregate Base, Journal of Transportation Research Record, No., 1687, 1999, pp. 29-38.

Zaman M., Laguros J., Tian P., Zhu J. and Pandey K., (1998), Resilient Moduli of Raw and Stabilized Aggregate Bases and evaluations of Layer Coefficients for AASHTO Flexible Pavement Design," ORA 125-4262, Item 2199, August 1998, Department of Transportation, Oklahoma City, OK.

Wang, L., Roy, A., Tittsworth, R. and Seals, R. (2004), Mineralogy of Soil Susceptible to Sulfate Attack after Stabilization, Journal of Materials in Civil Engineering, Vol. 16, No. 4, 2004.

Wagoner, M.P., Buttlar, W.G. and Paulino, G.H. (2005), Development of a Single-Edge Notched Beam Test for the Study of Asphalt Concrete Fracture, Geotechnical Special Publication, Geo-Frontiers, 2005.

Witczak, M.W. and Root, R.E. (1974), Summary of Complex Modulus Laboratory Test Procedures and Results, American Society for Testing and Materials, STP 561, 1974, pp. 67-94.

Witczak, M.W. (2000), Harmonized Test Methods for Laboratory Determination of Resilient Modulus for Flexible Pavement Design, NCHRP 1-28A, Volume I, June 2000.